LA-10288-PR
Progress Report

Los Alamos National Laboratory is operated by the University of California for the United States Department of Energy under contract W-7405-ENG-36.

Applied Nuclear Science Research and Development Semiannual Progress Report

October 1, 1983–May 31, 1984

Los Alamos
Los Alamos National Laboratory
Los Alamos, New Mexico 87545

The four most recent reports in this series, unclassified, are LA-9468-PR, LA-9647-PR, LA-9841-PR, and LA-10069-PR.

This work was performed under the auspices of the US Department of Energy's Division of Reactor Research and Technology, Office of Basic Energy Sciences and Office of Fusion Energy.

LA-10288-PR
Progress Report

UC-34C
Issued: January 1985

Applied Nuclear Science Research and Development Semiannual Progress Report

October 1, 1983—May 31, 1984

Compiled by
E. D. Arthur
A. D. Mutschlecner

Los Alamos National Laboratory
Los Alamos, New Mexico 87545

CONTENTS

APPLIED NUCLEAR SCIENCE RESEARCH AND DEVELOPMENT
SEMIANNUAL PROGRESS REPORT

October 1, 1983 - May 31, 1984

Compiled by

E. D. Arthur and A. D. Mutschlecner

ABSTRACT

This progress report describes the activities of the Los Alamos Applied Nuclear Science Group for October 1, 1983, through May 31, 1984. The topical content is summarized in the Contents.

I. THEORY AND EVALUATION OF NUCLEAR CROSS SECTIONS

A. Spectra for the t-^{6}Li Reaction (G. Hale)

New measurements[1] of neutron spectra from the ^{6}Li(t,n)2α reaction have recently become available at Los Alamos. Experimental data for the reaction, which could be important in the blanket of a fusion reactor, have been widely discrepant.

A preliminary comparison of our three-body resonance model prediction for the spectra with the uncorrected data at E_t = 1.75 MeV, shown in Fig. 1, is encouraging. The calculation is taken essentially from parameters that describe the proton spectra from the ^{3}He-^{6}Li reaction reasonably well at energies below 2 MeV; it includes contributions from the ground state and first, third, and fourth excited states of ^{8}Be, as well as from the ground-state resonance in ^{5}He. These contributions are evident in Fig. 1 as well-defined peaks in the spectrum at E_n ~ 17.3, 14.5, 0.93, and 0.55 MeV, as well as a broad shoulder at E_n ~ 3 MeV. The energy shift between the calculation and the data for the two lowest energy peaks probably is due to the fact that energy loss in the target-foil system degraded the triton energy from 1.750 to 1.638 MeV. Differences between

calculated and measured peak widths, especially for the ground-state peak at 17.3 MeV, are due to experimental resolution effects, which are not included in the calculations. Particularly encouraging is the agreement in scale between the calculations and absolute measurements, indicating that charge-symmetric consistency with the ^{3}He-^{6}Li data obtains.

We expect to see improved agreement as the calculations and measurements are refined to correspond more closely (e.g., removing resolution effects, detector cutoff distortion, multiple scattering and contaminant corrections, etc.). Especially at higher energies, these corrections to the data are expected to be linked strongly to the calculated predictions, which in turn will be improved by comparisons with these measurements and others done at Bruyères-le-Châtel in France.

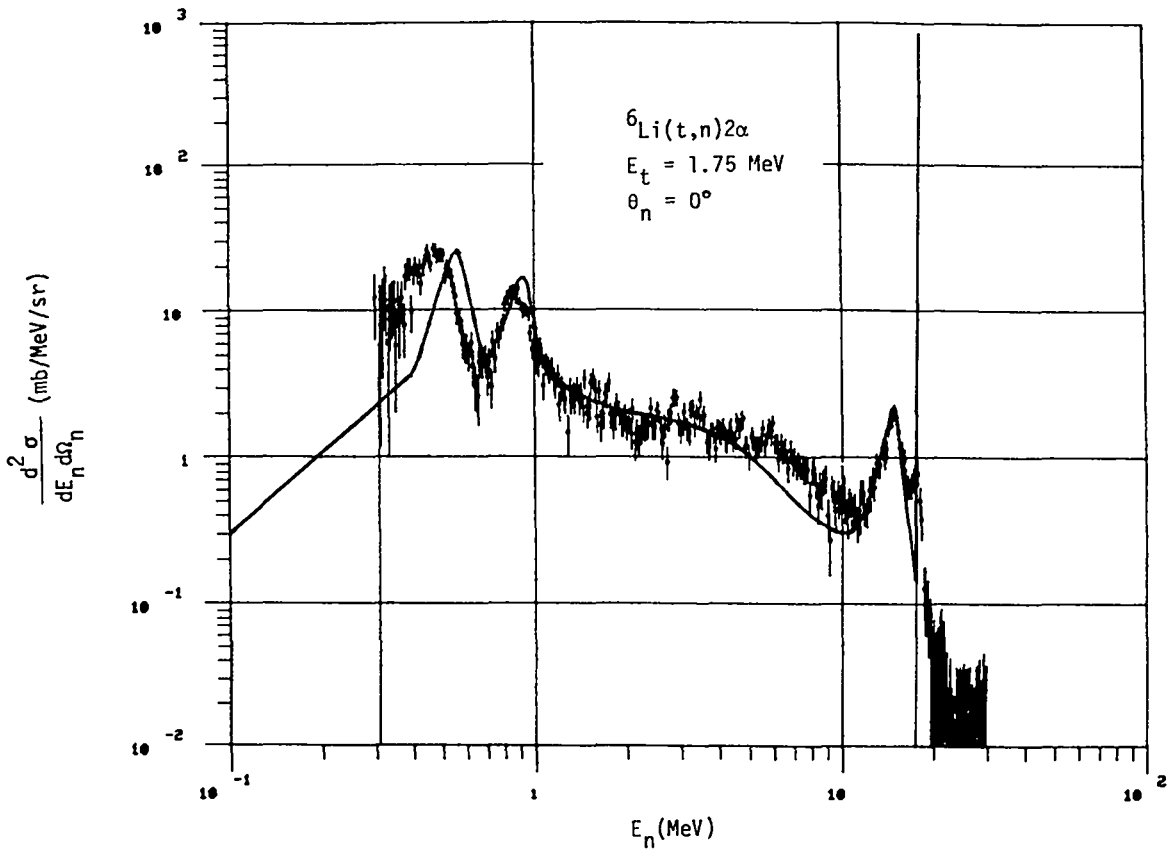

Fig. 1. Absolute laboratory neutron spectra for the $^{6}Li(t,n)2\alpha$ reaction at 0° for E_t = 1.75 MeV. The solid curve is a three-body resonance-model calculation and the data are measurements of Lisowski et al.[1]

B. Cross Sections and Maxwellian Reaction Rates for Polarized Fusion [G. Hale, G. Doolen (X-5), P. W. Keaton (P-DO)]

The work reported last quarter on polarized $\vec{d}+\vec{d}$ reactions has been written up and circulated as a Los Alamos report.[2] In the meantime, a microscopic calculation of the d+d reactions[3] that takes into account d-wave contributions to the bound trinucleon clusters in the final state confirms our result that the $^5S_2$ d-d partial wave is important in the low-energy region, with the result that the $\vec{d}+\vec{d}$ reactions are not strongly suppressed when the deuterons are polarized spin-parallel.

Continuing interest in this area has prompted us to write a two-part paper,[4] to be submitted to Physical Review, dealing with the formalism for calculating cross sections and reaction rates for polarized-particle interactions and giving our numerical results for $\vec{d}+\vec{t}$ and $\vec{d}+\vec{d}$.

C. ^{28}Si Level Density Calculations [B. Strohmaier (T-2 Collaborator, on Leave from Institut für Radiumforschung und Kernphysik, U. of Vienna)]

Spectral distribution calculations of the level density for ^{28}Si are being performed based on the strength-function method. Paralleling this work are continuing studies on the method itself. Both these efforts are part of a collaboration among Ohio University, Lawrence Livermore National Laboratory, and the University of Vienna.

D. Calculation of Neutron and Gamma-Ray Emission Spectra Produced by p +^{27}Al Reactions (E. D. Arthur)

Preliminary calculations of neutron and gamma-ray spectra induced by proton reactions on aluminum have been made to provide data required for shielding design for a proposed proton linear accelerator. The nuclear models used in this study were the preequilibrium and Hauser-Feshbach models as embodied in the GNASH program.[5] This nuclear model code has been used in the past to successfully investigate higher energy ($E \leq 50$ MeV) neutron and proton interactions with nuclei in the structural materials region.[6]

Because this study was of an exploratory nature, we did not attempt to optimize input parameters but instead relied upon global sets, especially for optical parameters. In particular, for neutrons we chose the Wilmore-Hodgson parameter set[7] after confirmation of its suitability through comparison to n+^{27}Al total cross-section data between 0.5 and 60 MeV. Agreement with the

data on the level of 5-10% occurred. Comparisons were also made to measured nonelastic data for incident energies between 10 and 60 MeV. Again, there was generally good agreement although there was some tendency to overpredict such data for incident neutron energies below several MeV. For protons we found the Becchetti-Greenlees[8] parameter set reproduced nonelastic data recently measured by McGill et al.[9] Finally, for alpha particles we used the parameters of Ref. 10.

Gamma-ray production measurements[11] for p+^{27}Al reactions for the energy range of interest here (10-50 MeV) were published during the 1960's. For neutron-induced reactions, similar gamma-ray production data are valuable in determining how well an overall description of the reaction process the nuclear model provides. Thus, for this case we sought to provide as detailed a description as possible of the major reaction paths to insure that major production and deexcitation processes were included. Unfortunately, for higher energy p+^{27}Al reactions (E_p 50 MeV), the number of reaction channels and the fact that charged-particle reaction paths contribute significantly add to the complexity of the calculations. For the present calculations, this meant inclusion of more than 35 reaction paths.

From examination of 17.5 MeV ^{27}Al(p,p') data,[12] we found direct-reaction contributions to inelastic scattering were also important. In order to include such direct effects in the GNASH calculations, we employed the distorted wave Born approximation (DWBA). These results were normalized to the data of Ref. 12 and were included for the first six excited states of ^{27}Al.

A comparison of the calculated gamma-ray production spectra with the measurements of Ref. 11 appears in Fig. 2 for a proton energy of 16 MeV. Unfortunately, this comparison suffers because of the poor quality of the data that is due to use of thick targets and poor resolution detectors. There is, however, qualitative agreement between the calculation and the experimental data. A similar comparison for a proton energy of 50 MeV is shown in Fig. 3. Again, qualitative agreement occurs. Finally, Fig. 4 illustrates neutron emission spectra calculated at incident proton energies of 16, 33, and 50 MeV. In this case, no data exist for comparison.

In spite of the preliminary nature of these calculations and the absence of reasonable quality experimental data, these results should be useful in the shielding design for proton linear accelerators.

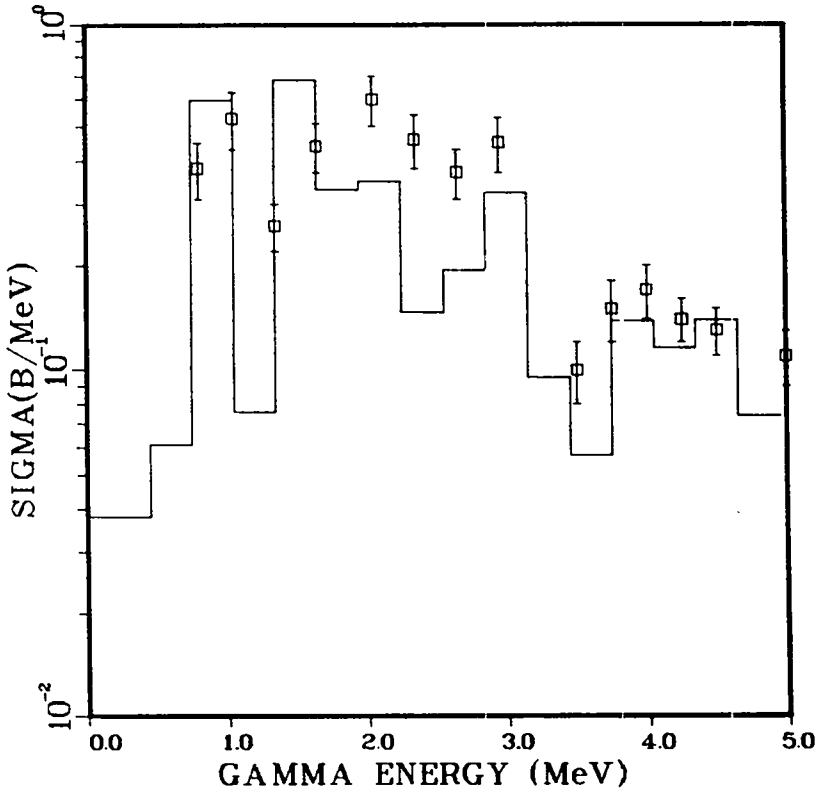

Fig. 2. The calculated gamma-ray production spectrum for 16 MeV p+^{27}Al interactions is compared with the data of Ref. 11.

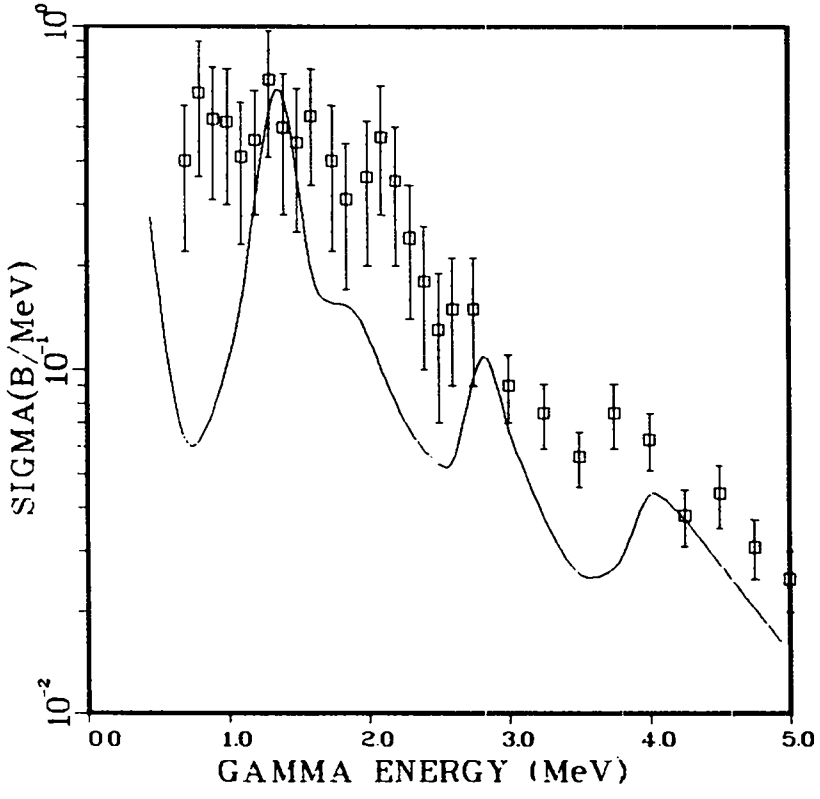

Fig. 3. The calculated gamma-ray production spectrum for Ep = 50 MeV p+^{27}Al interactions is compared with the data of Ref. 11.

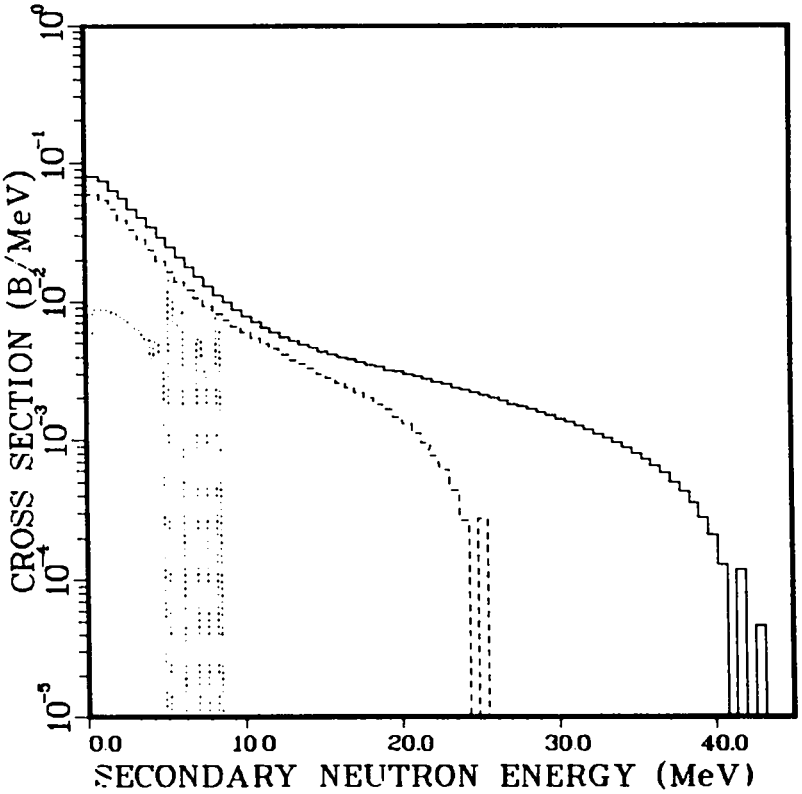

Fig. 4. Calculated neutron emission spectra for E_p = 16, 33, and 50 MeV (dotted, dashed, solid histograms, respectively).

E. Calculation of $^{235}U(n,f)$ Cross Sections Using Fission Probability Data (E. D. Arthur)

On page 19 of Ref. 13, I have described the development of theoretical approaches that would allow one to better use fission probability data, P_f, to predict or to aid in calculations of (n,f) cross sections. Such an approach takes into account explicit differences occurring in spin distributions populated in neutron-induced reactions and those occurring in direct-reaction data that are generally used to determine fission probabilities. The model provides a consistent analysis of both data types rather than the use of the following simple relationship between σ_{nf} and P_f

$$\sigma_{nf}(E_n) \simeq P_f(E_n+B_n)\sigma_{CN}(E_n) \quad . \tag{1}$$

Instead, the model analysis allows one to determine a fission probability that depends explicitly upon compound nucleus spin and parity, which can then be related back to measured fission probability data, $P_f(E)$.

$$P_f(E) = \sum_{J\Pi} P_f(EJ\Pi)\ \alpha\ (EJ\Pi) \tag{2}$$

Here $\alpha(EJ\Pi)$ represents the compound-nucleus spin distribution that for direct reactions can be determined from distorted wave Born approximation calculations.

To further investigate these techniques, fission probability data from the $^{234}U(t,pf)^{236}U$ reaction[14] were fit, as shown in Fig. 5. The resulting fission parameters for the ^{236}U compound system should be directly applicable to $n+^{235}U$ fission calculations. To do this the parameters determined from such a fit were used to determine spin and parity dependent partial fission widths, which should have effects resulting from the initial spin population distribution removed. This information was then combined with compound-nucleus formation cross sections determined from $n+^{235}U$ coupled-channel calculations to predict values for $^{235}U(n,f)$.

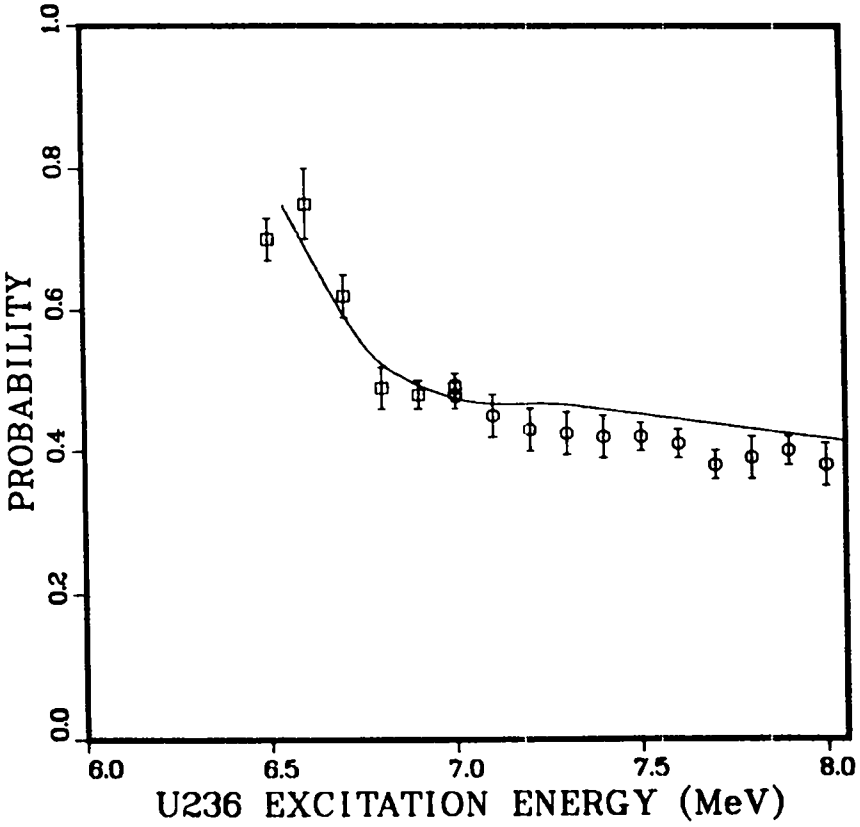

Fig. 5. Fit to the $^{234}U(t,pf)^{236}U$ P_f data of Ref. 14.

Figure 6 compares the results of this technique to evaluated $^{235}U(n,f)$ cross sections appearing in the current ENDF/B-V library. The data points represent ENDF/B-V while the curve is the "predicted" $^{235}U(n,f)$ based on the analysis of the $^{234}U(t,pf)$ P_f data described above. The agreement is within 7% or less, which is approximately the accuracy of the P_f data. The dashed curve shows the predicted (n,f) cross section obtained by simply multiplying the P_f data of Fig. 5 by a compound-nucleus formation cross section. In spite of the fact that the compound-nucleus formation cross sections used were determined from realistic coupled-channel calculations, the spin population effects discussed lead to significant disagreements with both ENDF/B-V $^{235}U(n,f)$ data as well as the more realistic calculations shown by the solid curve.

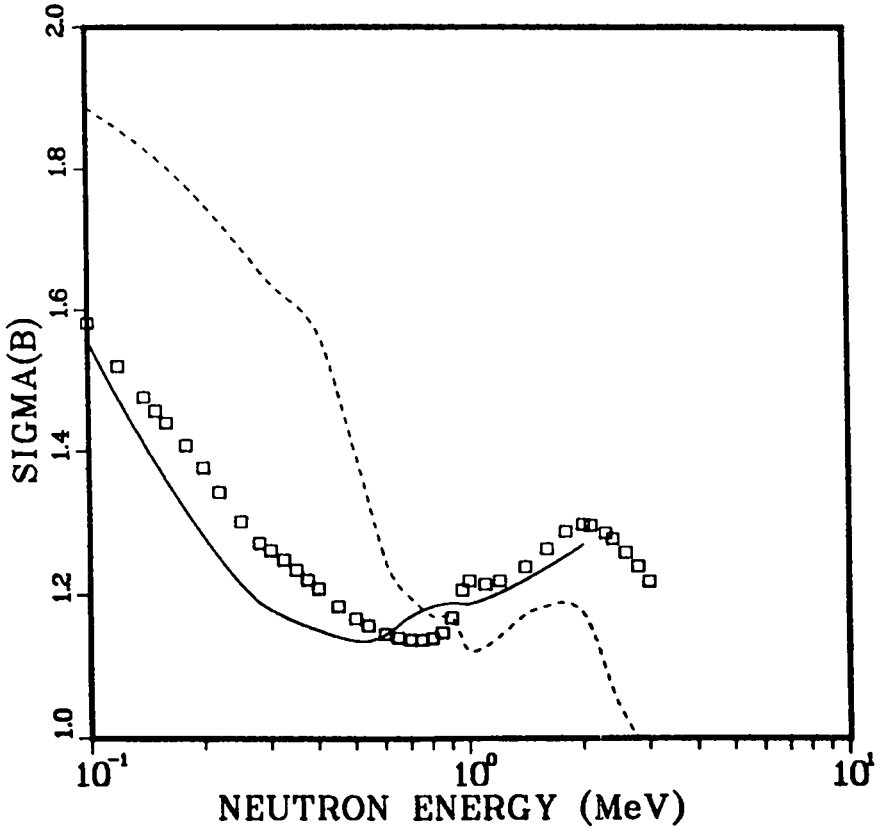

Fig. 6. Predicted $^{235}U(n,f)$ cross sections based on the P_f data of Ref. 14. The solid curve shows results obtained when such data are analyzed in the manner described in the text, i.e., spin population distributions are explictly accounted for. The dashed curve shows the results when such P_f data are simply multiplied by a compound-nucleus formation cross section. The data points represent evaluated data appearing in ENDF/B-V.

F. Calculation of (n,n') Excitation Functions for Higher-Lying Levels in ^{238}U (E. D. Arthur)

In 1981 and 1982 I reported calculations[15,16] of cross sections for neutron inelastic scattering to higher-lying levels (vibrational band members) in ^{238}U. These calculations concentrated primarily on compound nucleus contributions that were determined using the COMNUC[17] Hauser-Feshbach statistical model code. Fission competition was accounted for via a realistic fission model based on a coupled oscillator barrier representation. Even though these calculations addressed primarily compound-nucleus contributions to inelastic scattering, some attention was paid to the amount of direct-reaction contributions one could expect for scattering from states lying above the ground-state rotational band. In Ref. 16 such direct-reaction contributions for scattering from the 3^- 0.73 MeV octupole state in ^{238}U were determined from distorted wave Born approximation (DWBA) calculations. These results were then normalized through use of $B(E\ell)$ values determined from charged-particle reactions via the expression

$$B(E\ell) = (\tfrac{3}{4}\pi Z e R^{\ell} A^{\ell/3})^2 \beta_{\ell}^2 \quad . \tag{3}$$

Through use of a B(E3) value[18] for this state equal to $0.5e^2b^3$, the calculated direct reaction contribution to inelastic scattering was on the order of 5-10 mb over the neutron energy range from 2-4 MeV. This result was in apparent disagreement with direct-reaction contributions deduced from $^{238}U(n,n'\gamma)$ determinations of inelastic scattering[19] as well as other theoretical analyses.[20]

Recently, pertinent experimental data[21] have become available from the University of Lowell that are based on direct measurements of inelastic neutron scattering from ^{238}U. These measurements extend to incident energies of 2.2 MeV and allow one to reach some conclusions concerning direct-reaction contributions to scattering from states occurring in higher-lying vibrational bands.

With the advent of these data, I have extended the investigation of such direct-reaction components in ^{238}U to states extending up to excitation energies of 1.169 MeV. Of the 20 states that are members of higher lying vibrational bands, seven have $B(E\ell)$ values that have been determined from Coulomb scattering results. Furthermore, the strengths of the 1^- 0.68 MeV and the 5^- 0.827 MeV states of the octupole vibrational band can be determined from (p,p')

and (d,d') scattering data[22,23]) by comparisons with known cross sections for excitation of ground-state band members. Table I summarizes B(Eℓ) data[18] available for higher-lying ^{238}U levels.

TABLE I

MEASURED B(Eℓ) VALUES FOR ^{238}U STATES LYING ABOVE THE G.S. ROTATIONAL BAND

E_x (MeV)	J^π	B(Eℓ)
0.68	1^-	see text
0.73	3^-	0.5
0.87	5^-	see text
0.927	0^+	——
0.931	1^-	——
0.966	7^-	——
0.9663	2^+	0.017
0.993	0^+	——
0.9975	3^-	0.22
0.9983	2^+	0.002
1.0373	2^+	0.063
1.055	4^+	——
1.06	2^+	0.13
} 8 states with no B(Eℓ) data		
1.169	3^-	0.25

To compute direct-reaction components, DWBA calculations were performed using the spherical iteration of the Madland-Young actinide optical model potential for neutrons[22] along with a complex form factor. The resulting DWBA cross sections were normalized using values calculated from Eq. (3) that were based on the B(Eℓ) data presented in Table I. The direct reaction cross sections for the 0.68 and 0.83 MeV states were normalized as described above. Finally, these direct reaction components were combined incoherently with compound-nucleus results previously calculated in 1981.

Figure 7 compares the calculated results for the excitation function for scattering from the 3^- 0.73 MeV level to the recent data of Shao.[21] The solid curve represents the sum of compound nucleus (CN) and direct interactions (DI)

while the dashed curve represents only the DI contributions computed as described above. Also shown on the figure are data from (n,n'γ) measurements of Olsen.[19] At energies above 2 MeV these data are in substantial disagreement with the directly measured (n,n') data of Shao and with the present calculations.

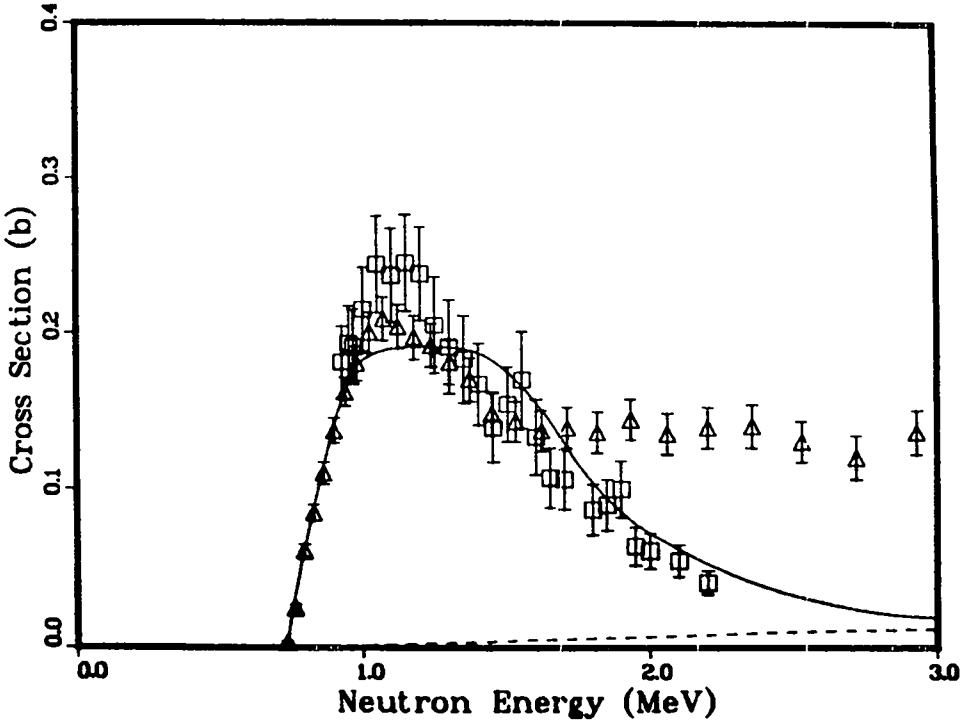

Fig. 7. The present calculations (solid curve) for excitation of the 3^- 0.73 MeV state in ^{238}U are compared with new measurements of Shao.[21] Shown by triangles are cross sections deduced from the (n,n'γ) values of Olsen.[19] The dashed curve represents the DI contribution calculated as described in the text.

Figure 8 compares this same calculation to a similar one by Chan et al.[20] that employed combined statistical and coupled-channel models. In particular, their coupled-channel calculations included explicit coupling between ground-state band members (generally 0^+ and 2^+ states) and states lying in higher vibrational bands. In these calculations the relative band coupling strengths were treated as an adjustable parameter. They used as a guide in determination of such strengths inelastic results deduced from the ^{238}U(n,n'γ) measurements of Ref. 23. This approach led to too large a direct-reaction contribution, as illustrated by the dotted curve. Such large DI components appear to be inconsistent with the new data of Shao[21] and with DI contributions that are determined from charged-particle data as described here. This problem occurs for several other such levels that are members of ^{238}U vibrational bands.

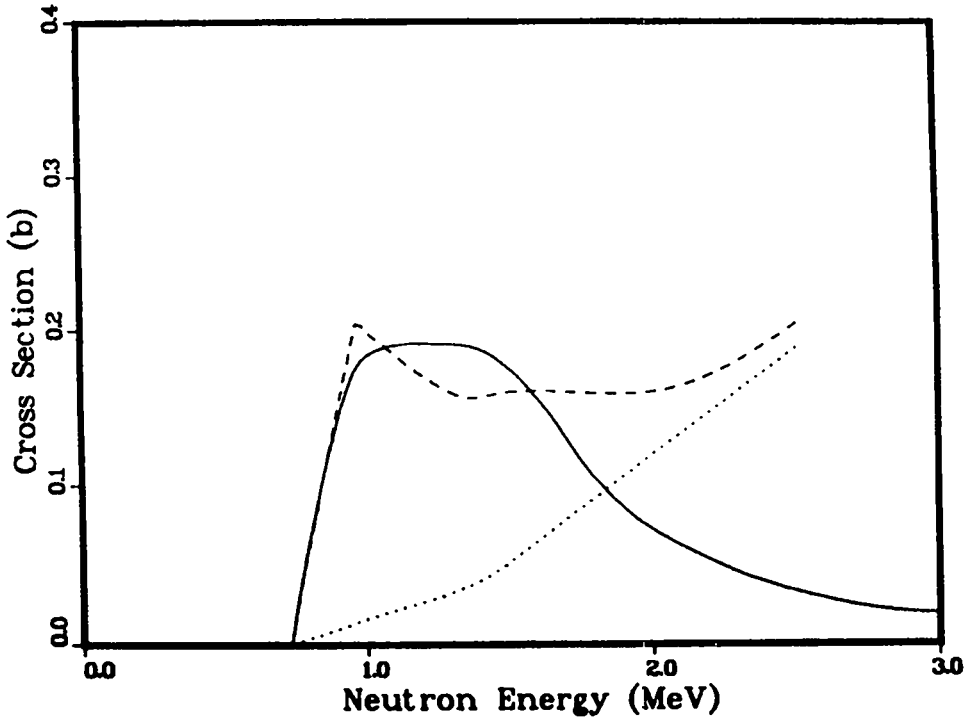

Fig. 8. The present calculations for (n,n') scattering from the 0.73 MeV state (solid curve) are compared with similar results by Chan et al.[20] (dashed curve). The dotted curve represents the amount of direct-reaction contributions calculated in Ref. 6.

Unfortunately, the new measurements of Shao[21] do not extend to as high an energy as one would like to reach definite conclusions concerning the role of direct-interactions in the excitation functions of other levels. For this, one would prefer to have such data extending to incident neutron energies of 3 MeV or higher. These measurements do allow, however, statements to be made concerning the shape and magnitude of the excitation function of several other levels. Figure 9 shows such an example for scattering from the 4^+ 1.055 MeV and 2^+ 1.06 MeV states. The directly measured (n,n') data of Shao are shown by the squares while cross sections deduced from the (n,n'γ) measurements of Olsen are represented by the triangles. The solid curve illustrates the present calculations and is composed of the sum of compound-nucleus and direct-interaction contributions for the 1.06 MeV 2^+ state along with compound-nucleus contributions for the 1.055 MeV 4^+ and 1.059 MeV 3^+ states. The theoretical calculations and the data of Shao are in reasonable agreement while the (n,n'γ)-based results of Olsen disagree, indicating possible problems in the treatment of gamma-ray branching processes. Again, for the calculated curve, the DI component is on the order of 10 mb or less for incident energies below 2.5 MeV. The cross section at these energies is thus still dominated by compound-nucleus contributions, a result that disagrees with conclusions one might reach from consideration of (n,n'γ) data only.

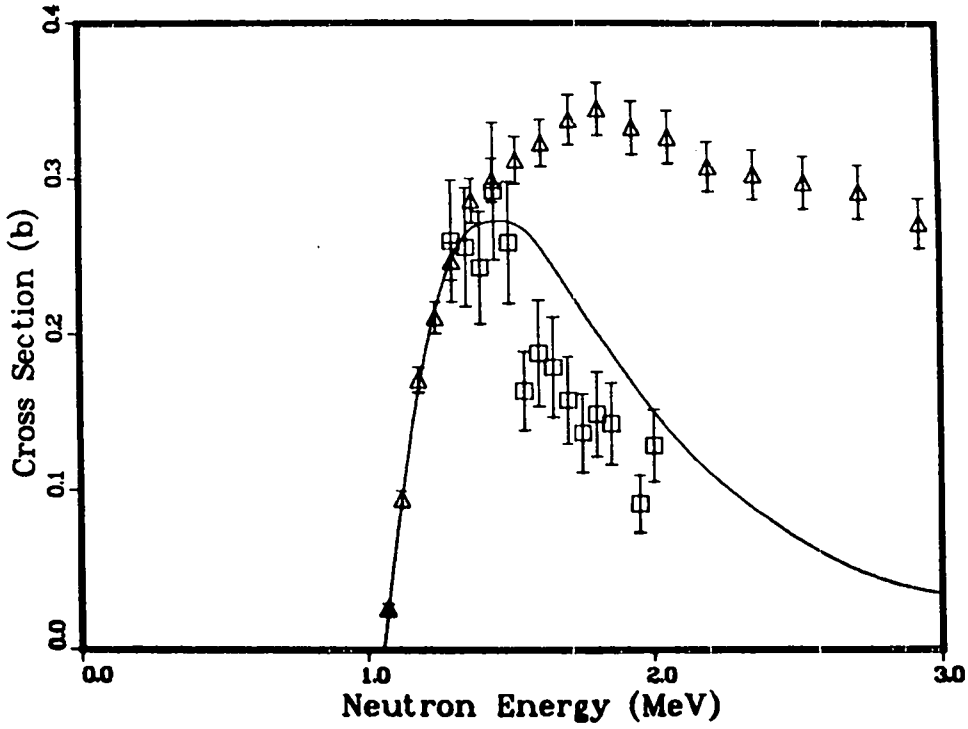

Fig. 9. Calculations of the excitation function for scattering from the 4^+ 1.055, 3^+ 1.059, and 2^+ 1.06 MeV states in ^{238}U are compared with Shao's data (squares). These calculations include both DI and CN contributions for the 2^+ 1.06 MeV state whereas for the others only CN contributions were assumed. The triangles are based on the (n,n'γ) data of Olsen.

G. Calculation and Evaluation of n + ^{237}Np Cross Sections (E. D. Arthur, D. G. Madland, and P. G. Young)

Knowledge of the production of ^{236}Pu is important in the fabrication of fuel for fast reactors because of the hard (2.6 MeV) gamma rays emitted by its daughter product, ^{208}Tl. The principal process for ^{236}Pu production is via $^{237}Np(n,2n)^{236}Np(\beta^-)^{236}Pu$ for which data are sparse and the existing ENDF/B evaluation may be discrepant by almost a factor of two. A method that could aid in the solution of such problems is calculation of the $^{237}Np(n,2n)$ cross section using the GNASH preequilibrium-statistical model code[5] (see p. 15 of Ref. 24) in a manner similar to our calculations for $^{239}Pu(n,2n)$. The GNASH code employs a realistic fission description so that the major competition from (n,xf) reactions can be modeled correctly. Also the code allows one to produce reasonable calculations of isomer ratios to enable meaningful comparisons to available data to be made.

To prepare for such an effort we have made preliminary calculations of n+^{237}Np reactions with particular emphasis on inelastic scattering. We have included the results of the calculations in a revision to the current ENDF/B-V ^{237}Np evaluation that covers the incident energy range up to 5 MeV. Additionally we have taken this opportunity to incorporate improvements to other data, particularly those for (n,γ), (n,f), $\bar{\nu}_p$, and prompt fission neutron spectra.

As described on page 50 of Ref. 24, we initially used the Madland-Young optical model parameters[22] in coupled-channel calculations to generate direct-reaction components for the $7/2^+$ and $9/2^+$ first- and second-excited states. These coupled channel calculations were also used to produce neutron transmission coefficients for Hauser-Feshbach statistical model calculations of compound elastic and inelastic scattering reactions.

Such calculations were made with the COMNUC[17] code and, while they were generally satisfactory, we found we did not reproduce measured ^{237}Np(n,γ) cross sections at energies below 0.1 MeV as well as we would like. Additionally, the s-wave strength function values calculated using these parameters lay about 30% higher than the experimental data of Mewissen et al.[25]

In an attempt to eliminate these low energy difficulties, we also made calculations using optical model parameters based on analyses made at Bruyeres-le-Chatel[26] but with the β_2 and β_4 deformation parameters originally specified by Madland in Ref. 22. These appear in Tables II and III along with calculated resonance parameter data (S_0, S_1, R'). The calculated s-wave strength function value S_0 lies close to the experimental value of 0.994 ± 0.12.[25] Furthermore, as illustrated by the solid curve in Fig. 10, these parameters produce better agreement with the ^{237}Np(n,γ) data of Weston et al.[27]

TABLE II

NEUTRON OPTICAL PARAMETERS FOR ^{237}Np COUPLED-CHANNEL CALCULATIONS[a]

	r	a
$V = 46.2 - 0.3E$	1.26	0.63
$W_{SD} = 3.6 + 0.4E$	1.24	0.52
$V_{SO} = 6.2$	1.12	0.47
$\beta_2 = 0.214$ $\beta_4 = 0.074$		

[a] Well depths in MeV; geometrical parameters in Fermis.

TABLE III

CALCULATED ^{237}Np RESONANCE DATA

	Theory	Exp. (Ref. 25)
S_0 ($X10^4$)	1.04	0.994 ± 0.012
S_1 ($X10^4$)	2.02	1.82 ± 0.2
R' (fm)	9.03	9.54 ± 0.5

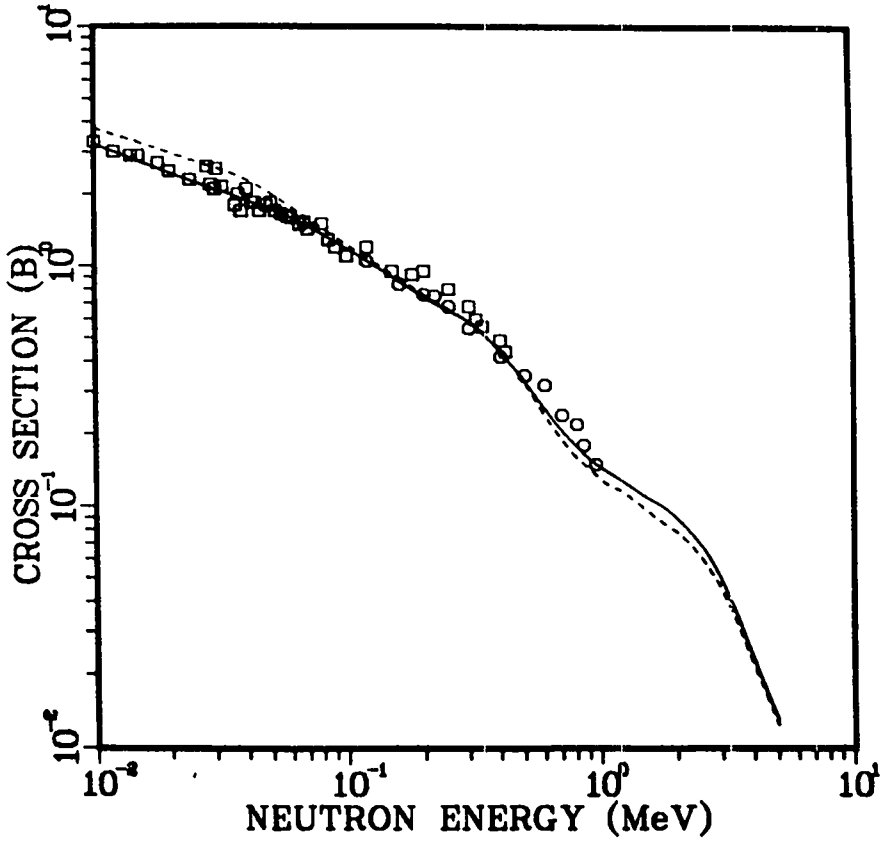

Fig. 10. Comparison of (n,γ) calculations with the data of Weston et al.[27] The solid curve employed Bruyeres-le-Chatel based optical parameters for neutron transmission coefficients while the dashed curve was calculated using Madland-Young optical model results.

Although ^{237}Np is a threshold fissioner, the (n,f) cross section presents a sizable competition to inelastic scattering for neutron energies above several hundred kilovolts. To describe the fission process, we used the coupled oscillator representation in COMNUC along with a fairly rapid damping term. Thus the representation at higher incident energies quickly approached that of two uncoupled oscillators. The fission transition state spectrum was assumed to be identical at each barrier and was constructed by taking known (or calculated) energy levels in ^{238}Np and compressing their spacing by a factor of

two. The resulting barrier parameters appear in Table IV and are compared there to values deduced from other analyses.[28,29] Also given are factors that were used to multiply the phenomenological level density computed for ^{238}Np in its ground state deformation. These factors take into account enhancements in the fission transition-state density occurring at a barrier that results from increased asymmetry conditions. These factors agree qualitatively with enhancements deduced by Bak et al.[28] in that their level density determined for barrier A was substantially greater than that for the ground state deformation. Likewise, their state density for the outer barrier B was also greater than for the ground state deformation but less than for barrier A.

TABLE IV

BARRIER PARAMETERS FOR THE ^{238}Np COMPOUND NUCLEUS

	This Work	Ref. 28	Ref. 29
E_A (MeV)	5.87	5.94	6.19
$\hbar\omega_A$ (MeV)	0.31	0.52	0.65
E_B (MeV)	5.4	5.8	5.99
$\hbar\omega_B$	0.36	0.4	0.45

DENSITY ENHANCEMENTS

Barrier A	4.0
Barrier B	2.0

Figure 11 compares the excitation functions calculated for scattering from the first excited state to results occurring in the current ENDF/B evaluation (dashed curve) and to results from a recent French evaluation by Derrien et al.[30] (data points). Both our present calculations and those of Derrien are in reasonable agreement but differ significantly from the ENDF values. The ENDF data obviously suffer from an unphysical shape as well as apparent neglect of direct-reaction contributions.

In spite of our concerns about optical model parameters, the results calculated for the total inelastic cross section using the Madland-Young or Bruyeres-le-Châtel optical parameters do not differ appreciably from each other. As Fig. 12 shows, they generally agree to within 10% except at energies below 300 keV. Here the effects we discussed earlier that are related to calculated s-wave strength function differences cause a larger deviation. Also shown on the figure by the data points are total inelastic cross sections

obtained in the recent Derrien evaluation. We observe some differences in magnitude with these results.

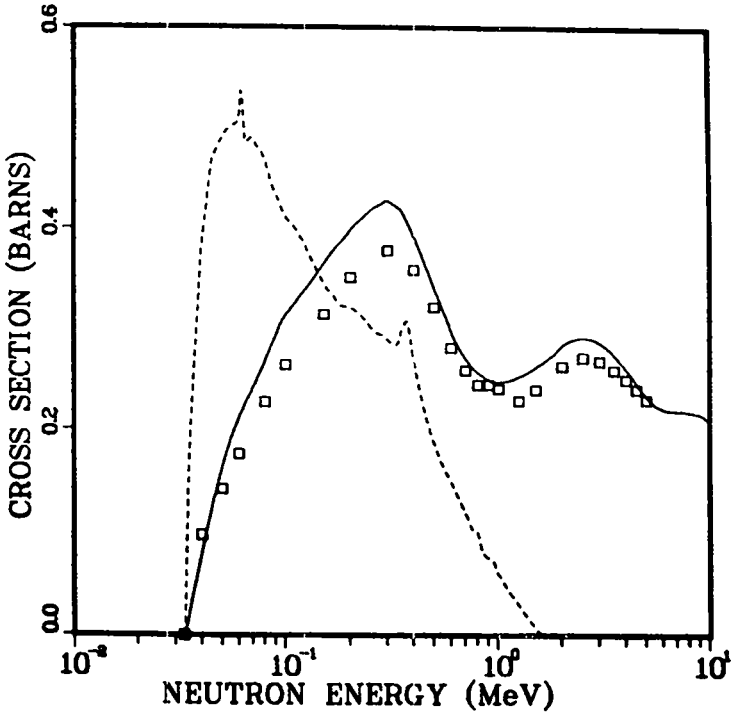

Fig. 11. Comparison of our calculated excitation function (solid curve) for scattering from the first excited state in ^{237}Np with ENDF/B-V results (dashed curve). The data points represent results from a recent evaluation by Derrien et al.[30]

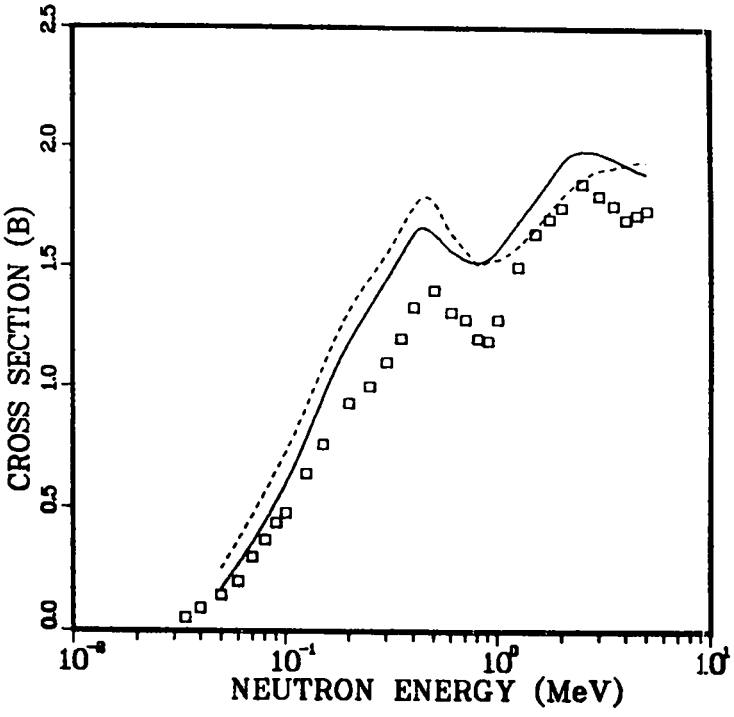

Fig. 12. Comparison of the total inelastic scattering cross section calculated using optical parameters of Table II (solid curve) with that resulting from use of the Madland-Young optical parameters. Both these calculated results agree well with each other except at lower energies (see text for discussion). Both disagree somewhat with total inelastic values appearing in the Derrien evaluation (data points).

These calculated results have been incorporated into a temporary revision of the current ^{237}Np ENDF/B evaluation. We have also improved other evaluated data particularly those for $\bar{\nu}_p$, fission neutron spectra, (n,γ), and (n,f). For

$\bar{\nu}_p$ and fission neutron spectra, we implemented the Madland-Nix results from p. 42 of Ref. 31. We updated (n,γ) cross sections to agree with our calculations as well as the data of Weston.[27] For the (n,f) cross section we adopted the evaluation of Derrien for neutron energies below 0.9 MeV. This resulted in a lowering of the fission cross section in this energy range by 5-25% over values occurring in the ENDF/B-V file. For the (n,f) cross section between E_n = 0.9 and 5 MeV we retained the current ENDF/B values because they agree closely with ^{237}Np ^{235}U fission ratios recently measured by Meadows.[32] Figure 13 shows the comparison between these data and ratios based on the Derrien evaluation (dashed curve) as well as results from ENDF/B (solid curve) that we incorporated.

The next step in this effort is extension of the calculations to higher energies with particular emphasis on description of competing (n,nf) and (n,2nf) reaction channels. This will require determination of fission barrier parameters for the ^{237}Np and ^{236}Np compound systems, which we plan to do through a consistent analysis of fission probability data.

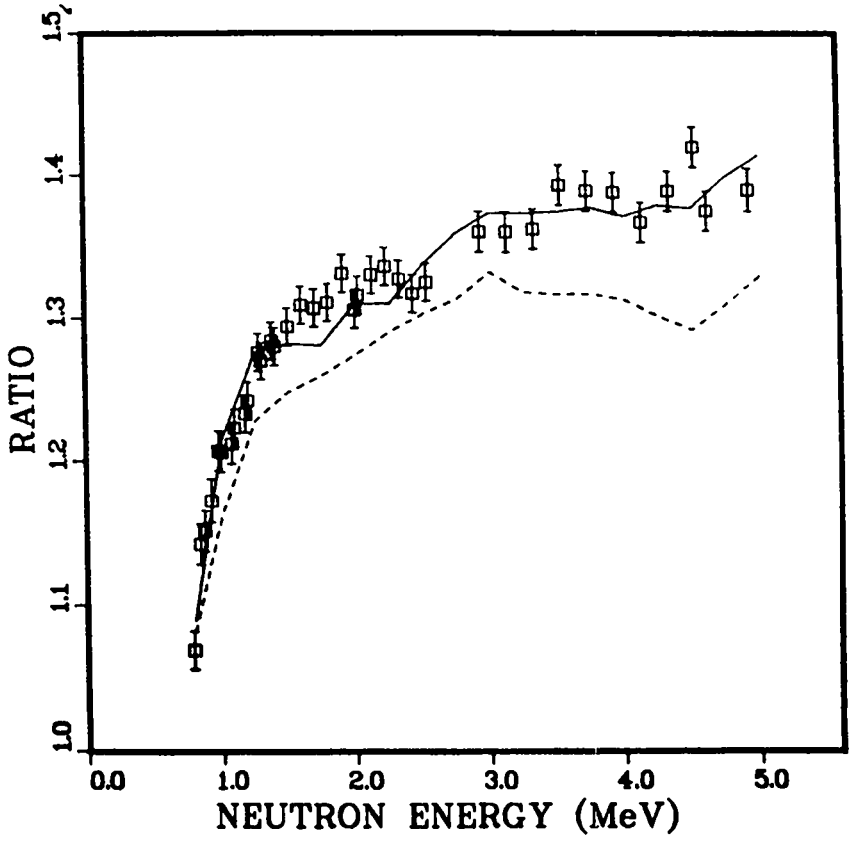

Fig. 13. A comparison of evaluated data for ^{237}Np ^{235}U fission ratios with the measurements of Meadows.[32] The dashed curve is the ratio resulting from the Derrien evaluation while the solid curve represents ENDF/B-V values that have been retained in our ^{237}Np revision.

H. Calculation of Gamma-Ray Emission from 14-MeV Neutron Interactions with ^{14}N (P. G. Young)

In an earlier analysis, total and elastic neutron cross-section measurements on ^{14}N for neutron energies between 0.1 and 16 MeV were fit with a spherical optical model (Arthur and Young, Pg. 6 of Ref. 24). The resulting parameters were used to calculate all significant neutron reactions with ^{15}N over the energy range 5.4-20 MeV, including gamma-ray emission spectra (Young and Arthur, Pg. 9 of Ref. 24). In order to further test those parameters for applicability with both ^{14}N and ^{15}N, we have calculated gamma-ray emission spectra for 14-MeV neutrons on ^{14}N and compared the results with experimental data from the Oak Ridge Electron Linear Accelerator (ORELA).[33]

The Hauser-Feshbach statistical theory calculations were performed with the GNASH[5] nuclear model code. Transmission coefficients for protons and alphas were calculated using the optical model parameters of Perey[34] and Lessor and Schenter.[35] As was the case with neutrons, these are the same parameters used in the earlier ^{15}N calculations. Similarly, the level density formulations,[36,37] discrete levels,[38,39] and gamma-ray strength functions from the ^{15}N analysis[24] are also employed here.

The major processes resulting in production of gamma rays from 14-MeV neutrons incident on ^{14}N are the (n,n'γ), (n,αγ), (n,pγ), (n,npγ), and (n,2nγ) reactions. The calculated gamma-ray spectrum is compared to the measurement of Dickens et al.[33] in Fig. 14. The agreement with experiment appears quite reasonable, especially considering that no data of this type were involved in determining any of the model parameters. These results and those of the earlier comparisons[24] indicate that the models used here can be employed with some confidence in calculations of neutron reactions on ^{14}N and ^{15}N.

I. Conversion of the GNASH Code to the CRAY Computer [K. Witte (C-3)and P. G. Young]

The standard Los Alamos version of the GNASH code,[5] operational on the CDC-7600 computers has been converted to the CRAY. A series of test calculations for n+^{197}Au and n+^{239}Pu reactions were run to ensure that identical results were obtained from both the 7600 and CRAY versions. The CRAY version will be expanded to permit calculation of much larger problems than are possible with the 7600 version.

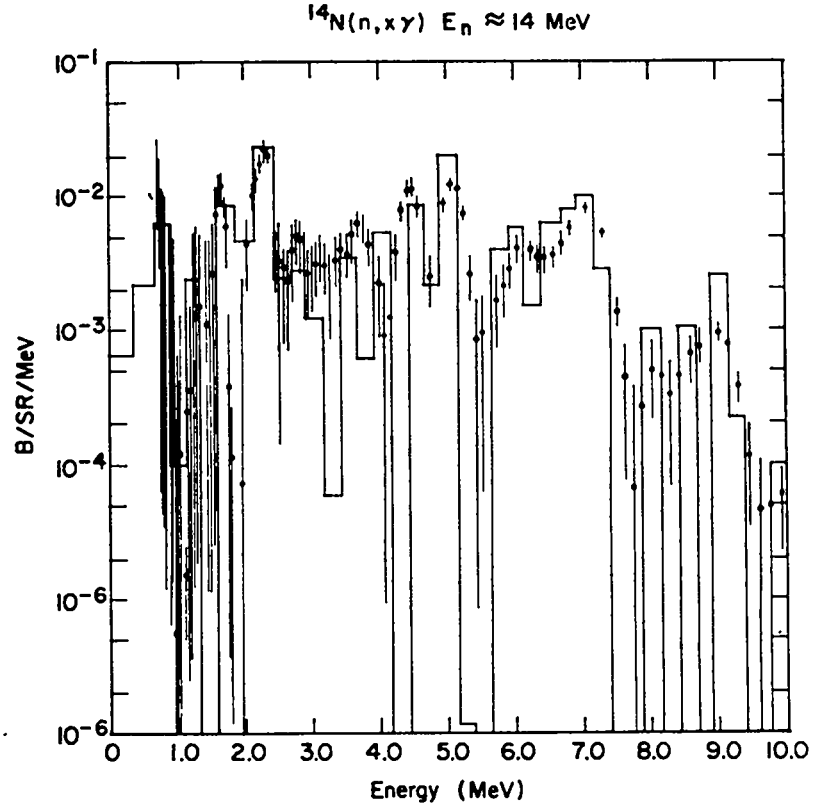

Fig. 14. Comparison of the calculated gamma-ray emission spectrum for 14-MeV neutrons on ^{14}N with the experimental data of Dickens et al.[33]

J. Neutron-Induced Cross Sections for ^{197}Au Between 0.005 and 20 MeV (P. G. Young and E. D. Arthur)

The analysis of n+^{197}Au reactions described in our previous progress report (Young and Arthur, Pg. 12),[31] has been completed over the neutron energy range 0.005-20 MeV. A covariance analysis that merges the coupled-channel optical model calculations with experimental data was performed for the ^{197}Au total cross section, and comparisons of the calculations with the extensive gamma-ray emission spectrum measurements of Morgan and Newman[40] were carried out.

The covariance analysis of the total cross section utilized the GLUCS code system developed by Hetrick and Fu,[41] which employs Bayes' theorem for simultaneous evaluation of reaction cross sections. Covariance data were estimated for all the ^{197}Au total cross-section measurements in the literature that at least contain standard deviations for the experimental cross sections.[42] In most cases generic assumptions were required to obtain the desired correlation

matrices for the experiments. For the two most recent measurements[43,44] and one extensive older measurement,[45] however, adequate information was available to reliably determine the correlations. In the case of the Larson et al.[44] data, a correlation matrix was provided directly by the authors.

The deformed optical model calculations[31] of the total cross section were used as the "prior" or starting point for the analysis. An overall error of ±10% was arbitrarily assumed for the total cross section, with systematic error such that a long range correlation of 25% was maintained, with higher correlations occurring for nearby energies. Because the errors on the most accurate measurements (for example, Refs. 43-45) are much smaller than ±10%, the main effect of the prior set is to preserve the general shape of the optical model calculations in energy regions where the measurements are less dense.

The smoothed results of this analysis (solid curve) are compared in Figs. 15-18 with the experimental data base and with the ENDF/B-V evaluation (dashed curve). The overall error on the resulting evaluated total cross section is generally less than ±1% except for the lowest energies where the error increases to ±7%.

The unadjusted optical model calculation (dashed curve) is compared with the results of the analysis and with ENDF/B-V (dotted curve) in Fig. 18. The plus symbols are the direct results from the GLUCS analysis and, with the associated covariances, represent (on a 49-point grid) a composite of the experimental data base and the prior optical model calculations. Over most of the energy range, the adjustment of the prior cross section was less than ±5%. (The solid curve is a smoothed representation of the GLUCS results.)

The calculations of the ^{197}Au(n,γ) and ^{197}Au(n,n'γ) reactions were carried out using slightly different values for the E1 gamma-ray strength function to obtain optimum agreement with experiment. The difference in the two strength functions is small, however, and the same general shape is maintained. The (n,γ) calculations are described in some detail in our previous progress report.[31]

Comparisons of the present calculations with the gamma-ray emission spectrum measurements of Morgan and Newman[41] are shown at two incident neutron energies in Figs. 19 and 20. Reasonable agreement with the measurements was also obtained at other energies used in the experiment.

The results of the present analysis were merged with the ENDF/B-V evaluation[46] at lower energies to produce an evaluated data set covering the incident neutron energy range from 10^{-5} eV to 20 MeV. The present results are included

in the evaluation down to an energy of 5 keV for all major reactions except capture, for which the ENDF/B-V evaluation is used up to 1 MeV because of its status as a standard. The new analysis will be available for the next issue of the ENDF/B data files.

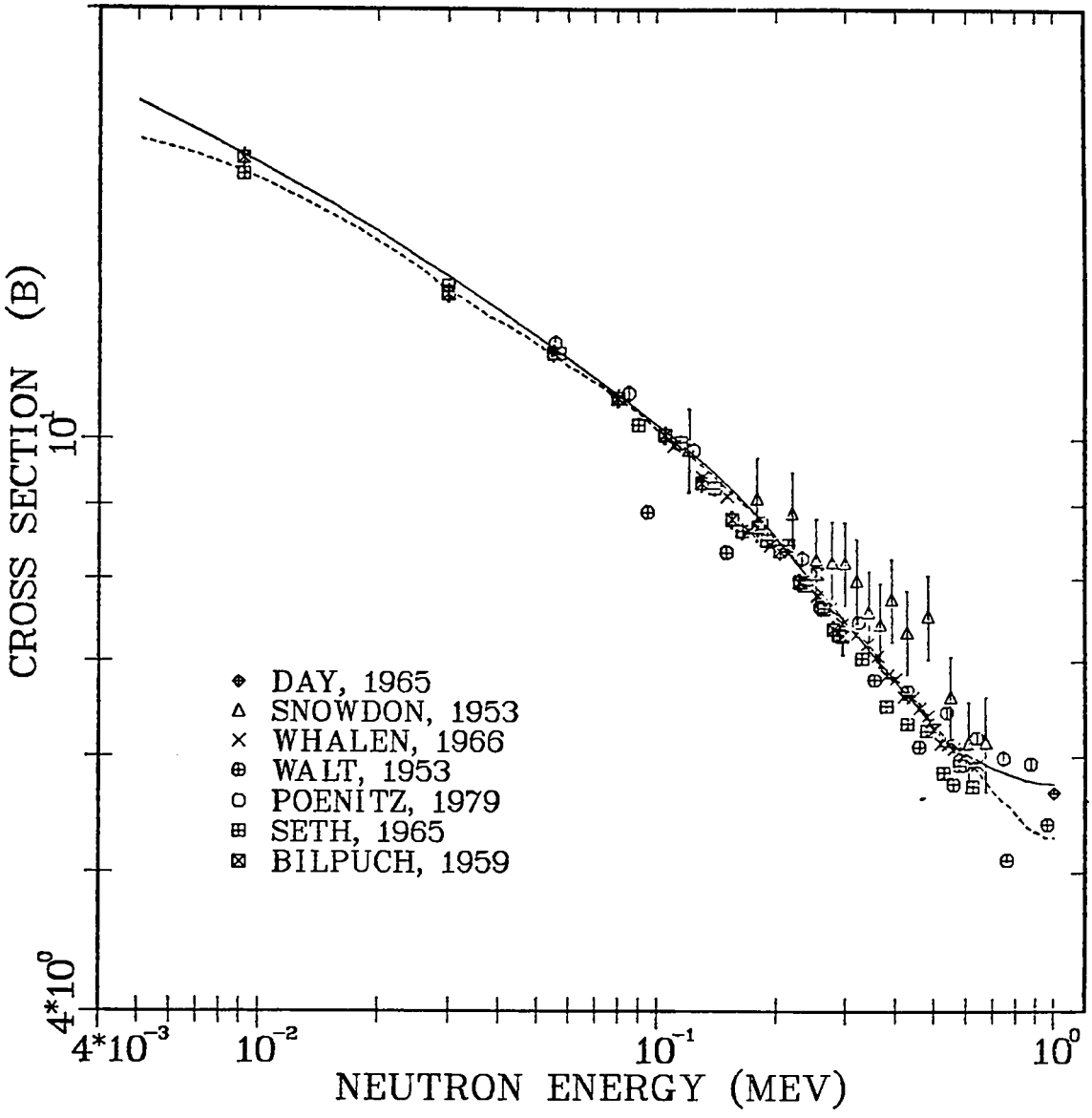

Fig. 15. Measured and evaluated neutron total cross section for ^{197}Au from 0.005 to 1.0 MeV. The solid curve is the present evaluation and the dashed curve is ENDF/B-V.

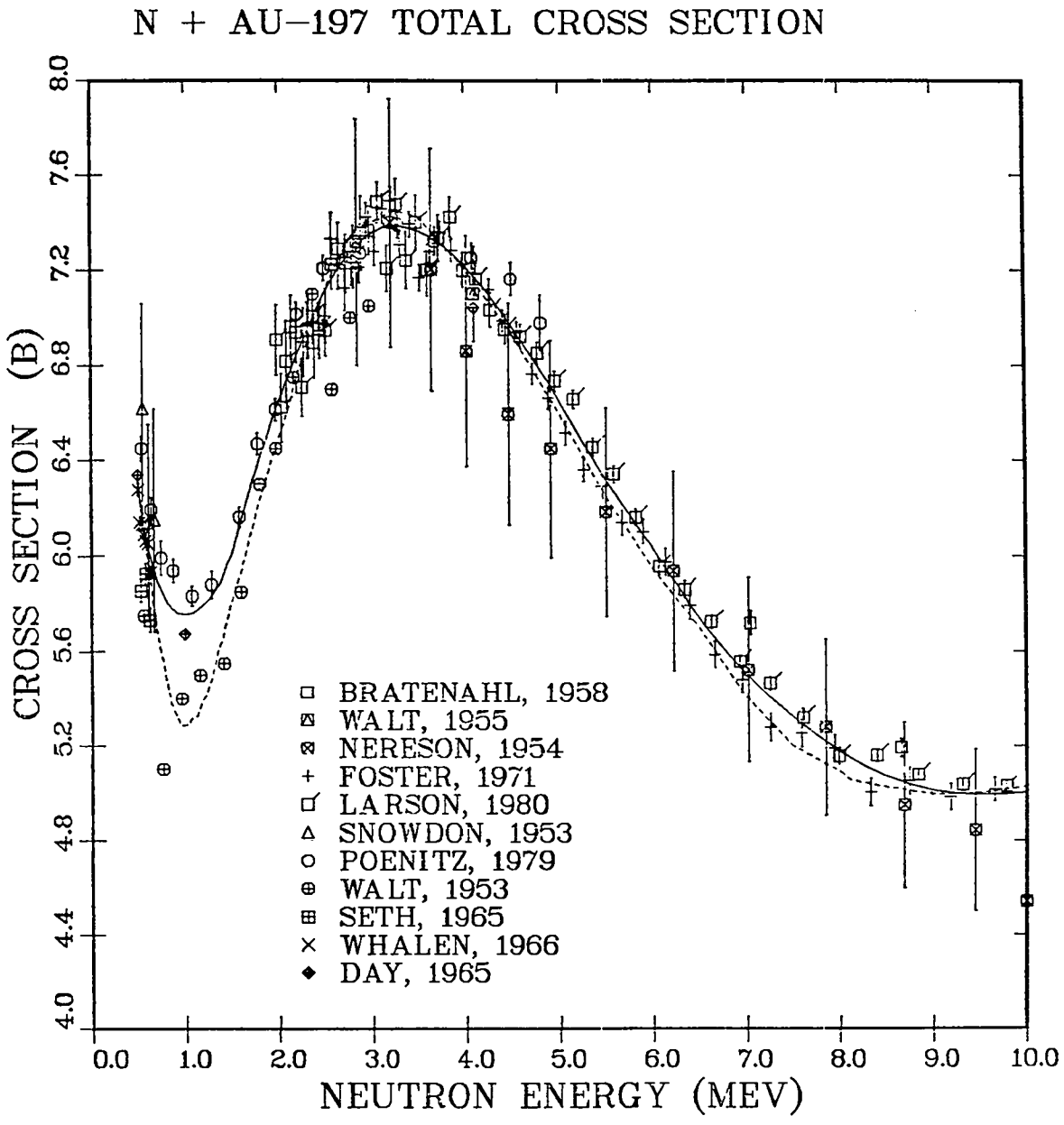

Fig. 16. Measured and evaluated and evaluated neutron total cross section for ^{197}Au from 0.5 to 10.0 MeV. The solid curve is the present evaluation and the dashed curve is ENDF/B-V.

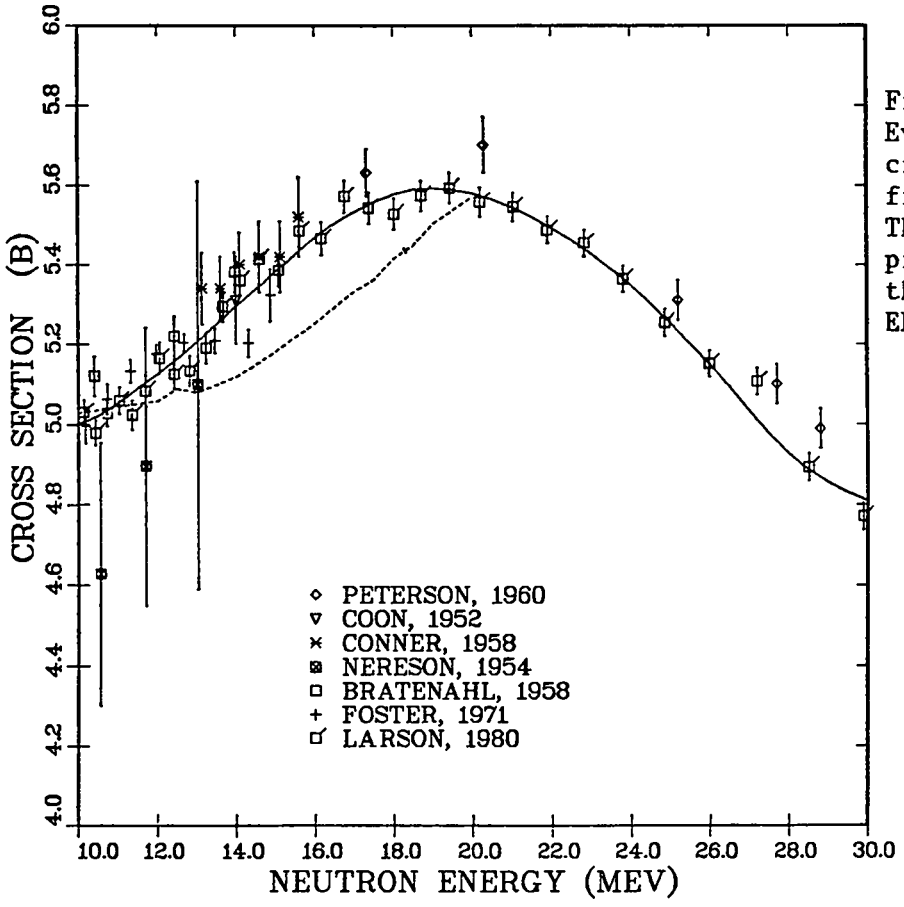

Fig. 17. Measured and Evaluated neutron total cross section for ^{197}Au from 0.5 to 10.0 MeV. The solid curve is the present evaluation and the dashed curve is ENDF/B-V.

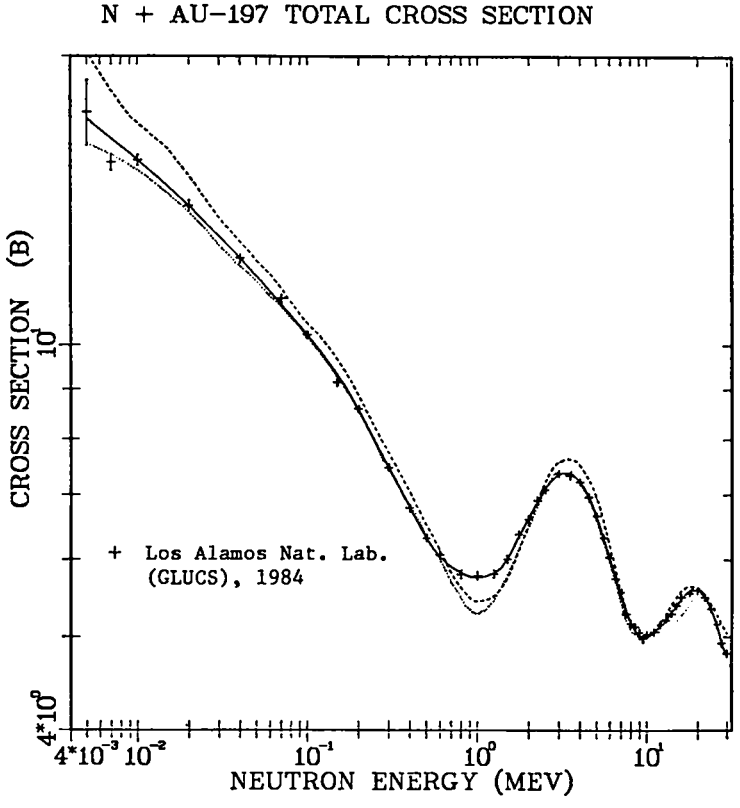

Fig. 18. Comparison of the n+^{197}Au total cross section calculated with a deformed optical potential (dashed curve), ENDF/B-V (dotted curve), and the evaluated results. The direct results of the GLUCS analysis are given by the plus symbols, and the solid curve is a smoothed version of these results.

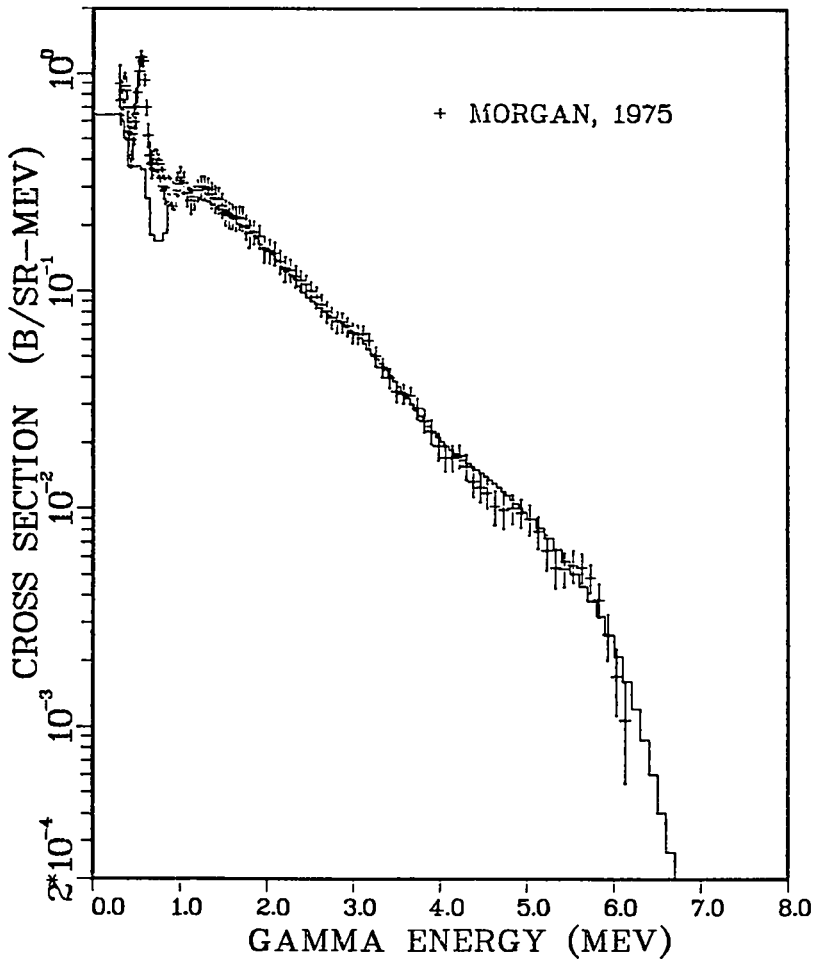

Fig. 19. Measured and calculated gamma-ray emission spectra from bombardment of ^{197}Au with neutrons in the energy range of 6-7 MeV.

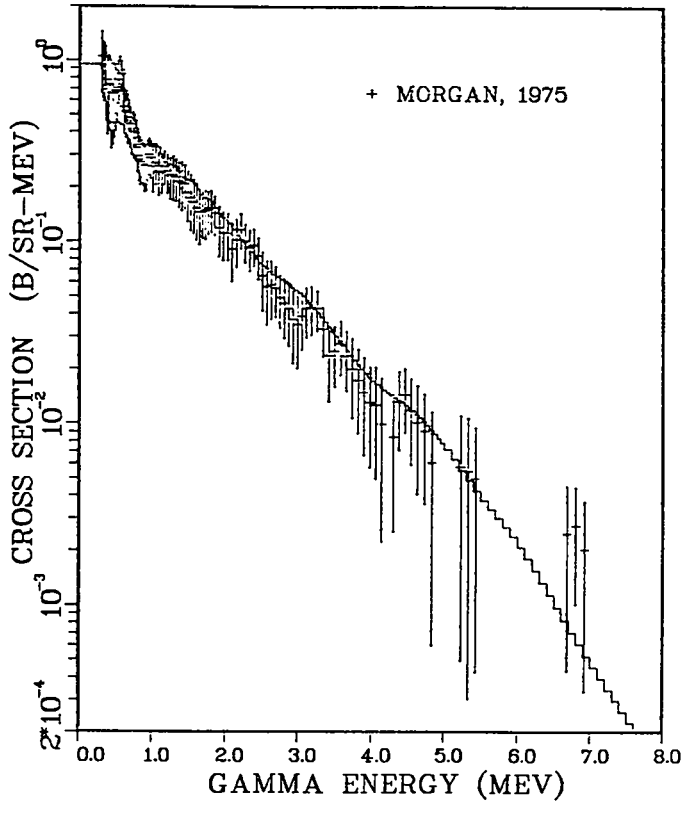

Fig. 20. Measured and calculated gamma-ray emission spectra from bombardment of ^{197}Au with neutrons in the energy range 14-17 MeV.

K. Search for a Suitable Isomer for the GRASER Program (D. G. Madland)

Fairly simple considerations of nuclear level densities, residual neutron-proton forces and coupling in odd-odd nuclei, and shell-model predictions of the occurrence of isomerism have led to the following first guess (Table V) as to where to concentrate efforts on the search for a suitable nucleus for the gamma-ray laser.

TABLE V

PLACES TO LOOK FOR GRASER CANDIDATES - FIRST GUESS

1. Rare Earth Nuclei $150 \leq A \leq 190$
   a. odd Z-odd N nuclei
   b. odd A nuclei

2. Actinide and Transactinide Nuclei $A > 220$
   a. odd Z-odd N nuclei
   b. odd A nuclei

3. Nuclei with $39 \leq Z \leq 49$, $57 \leq N \leq 65$
   a. odd Z-odd N nuclei
   b. odd A nuclei

L. Calculation of Average Pairing Gaps [D. G. Madland and J. R. Nix (T-9)]

We have begun a study of average pairing energies for neutrons, Δ_n, protons, Δ_p, and nucleons, Δ, to obtain their dependencies on mass number A and asymmetry parameter (N-Z)/A.

A Fortran code PAIR has been written to calculate Δ_n, Δ_p, and Δ using second-, third-, or fourth-order difference equations. The pairing energies are calculated using either experimental or calculated masses. Our equations include a term δ that accounts for the observation that the separation between the odd and odd-A mass surfaces is slightly smaller than the corresponding separation between the even and odd-A mass surfaces. Magic number crossings in both neutron number and proton number can either be deleted or included in the calculations. Also, a linear least-squares adjustment option can be used to test various model parameterizations of the pairing energies.

Standard parameterizations have already been tested and some new approaches are currently under study.

M. Medium Energy Proton-Nucleus Scattering Calculations (D. G. Madland)

Preliminary calculations have been performed for the scattering of medium-energy protons by a wide range of nuclei. Using available phenomenological proton-nucleus optical model potentials,[8,47] the total, reaction, elastic, differential elastic, and Rutherford cross sections were calculated as well as the polarization and the scattering S matrix. The calculations were performed for proton energies E_p in the range $10 \leqq E_p \leqq 200$ MeV and target mass numbers in the range $27 \leqq A \leqq 238$. The code SNOOPY-VIII was used to perform these preliminary calculations.*

We illustrate some of our results in Figs. 21-27. Figures 21 and 22 show the dependence of the elastic scattering angular distribution on the proton bombarding energy for a light (^{27}Al) and a heavy (^{238}U) target nucleus, respectively. Doubling the proton energy three times clearly demonstrates, for both cases, the increasing extent to which the elastic scattering is forward directed. Shown for comparison are the corresponding 14-MeV neutron elastic angular distributions calculated using the neutron optical-model potential of Ref. 8. Figures 23 and 24 show the dependence of the elastic scattering angular distribution on the target mass for a low (25-MeV) and a high (200-MeV) proton bombarding energy, respectively. Approximate doubling of the target mass three times shows, as expected, that the elastic scattering is larger for larger targets, but that for fixed energy, the shapes of the angular distributions are very crudely (to within two orders of magnitude) the same. A more detailed examination of these shapes is seen in Figs. 25 and 26, which are identical to Figs. 23 and 24 except for normalization to the Rutherford scattering cross section. Figure 25 shows that the elastic scattering can be approximated by the Rutherford cross section to within an accuracy of about ± one order of magnitude, for $E_p = 25$ MeV, while Fig. 26 shows that the Rutherford approximation cannot be used to anywhere near this accuracy for $E_p = 200$ MeV.

We conclude from Figs. 21-26 that accuracy requirements on elastic proton scattering angular distribution of, say 50%, for the energy range illustrated here, will require a separate calculation for each case. Figure 27 shows the calculated total reaction cross section as a function of proton bombarding energy for the same four target nuclei. At low energies, the reaction cross

*This code was provided by P. Schwandt, Indiana University, Bloomington, Ind., April 1984.

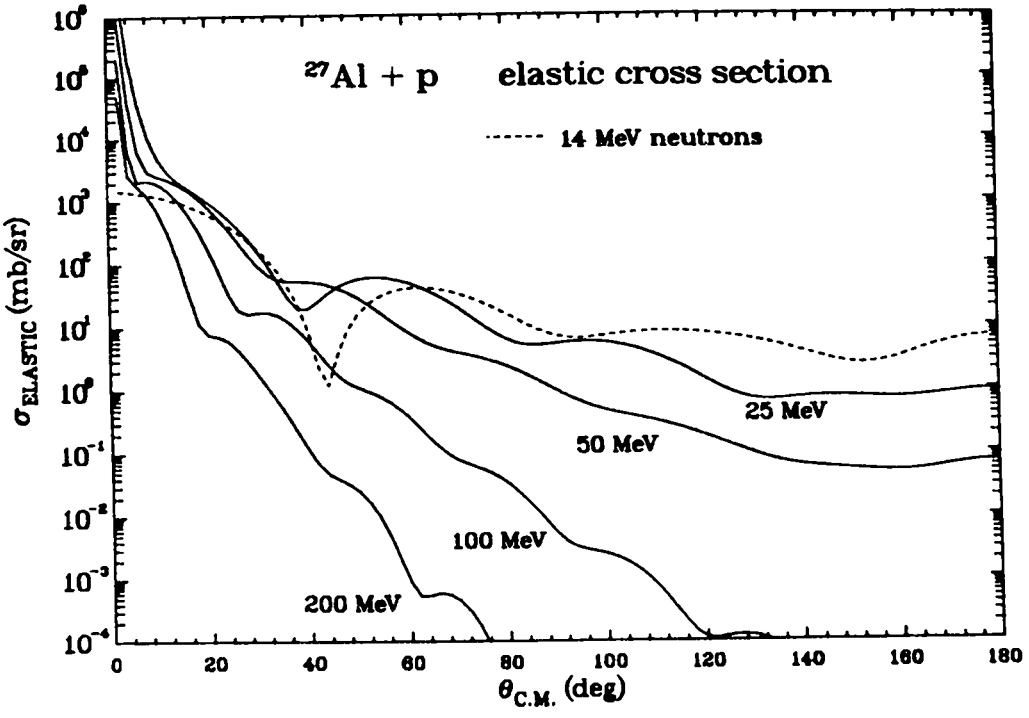

Fig. 21. Calculated differential cross sections for the elastic scattering of 25, 50, 100, and 200-MeV protons and 14-MeV neutrons by ^{27}Al.

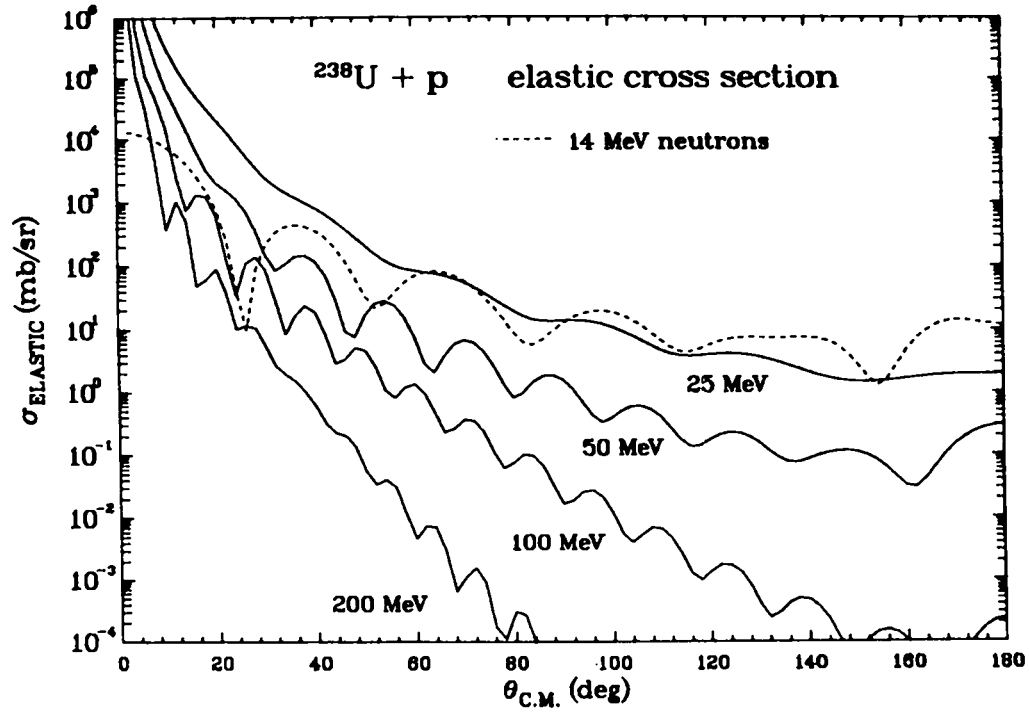

Fig. 22. Identical to Fig. 21 except that the target nucleus is ^{238}U.

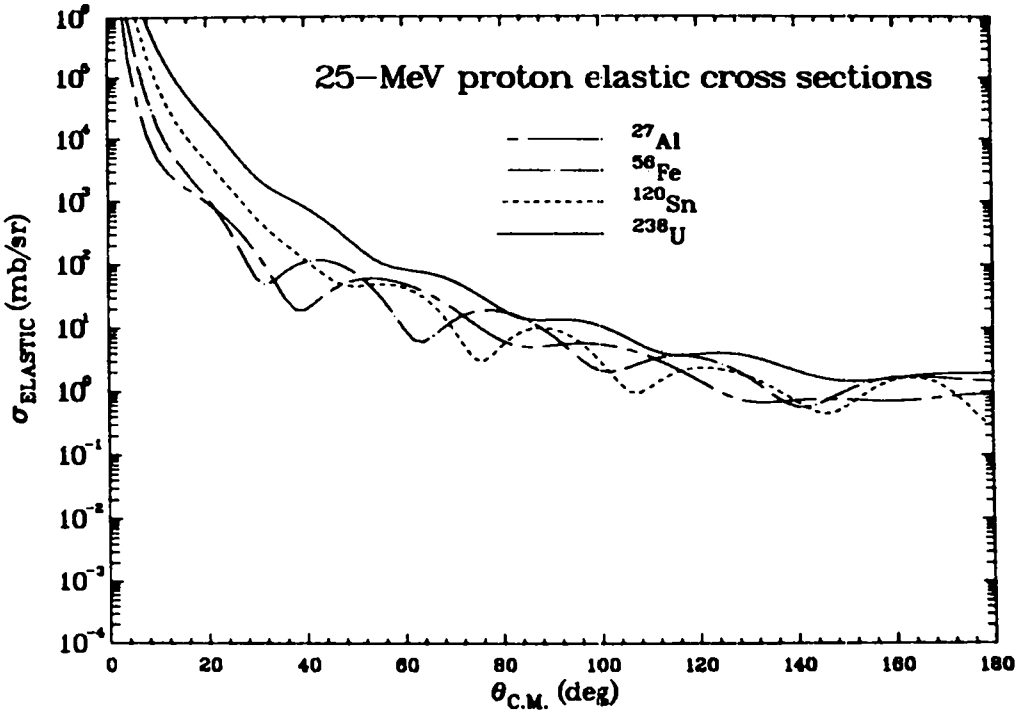

Fig. 23. Calculated differential cross sections for the elastic scattering of 25-MeV protons by ^{27}Al, ^{56}Fe, ^{120}Sn, and ^{238}U.

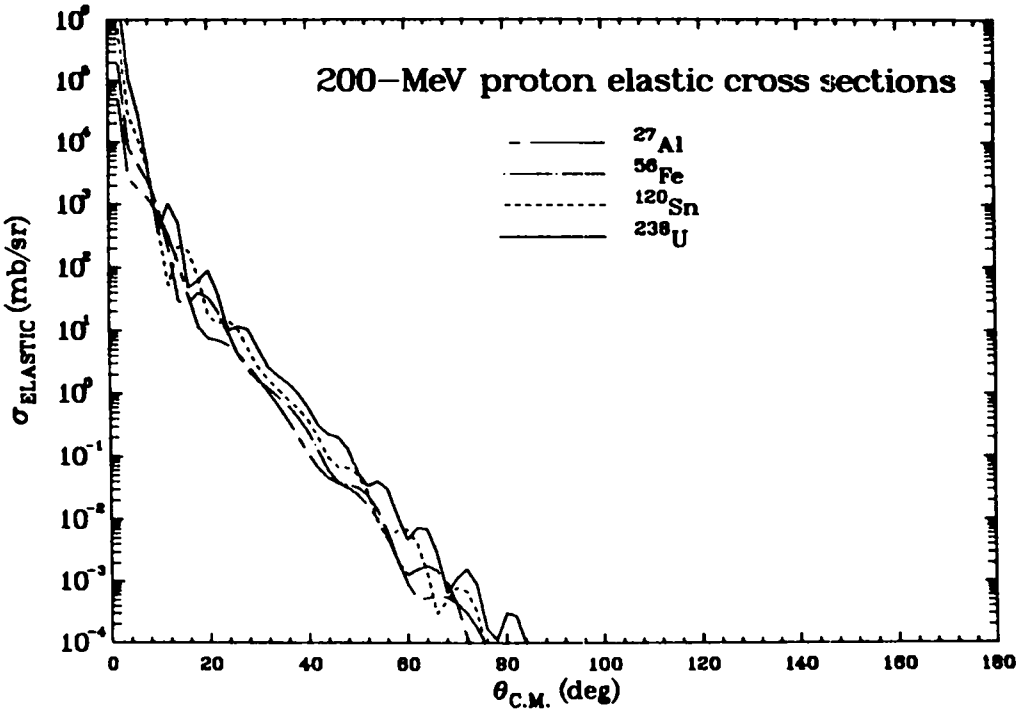

Fig. 24. Identical to Figure 23 except that the proton bombarding energy is 200 MeV.

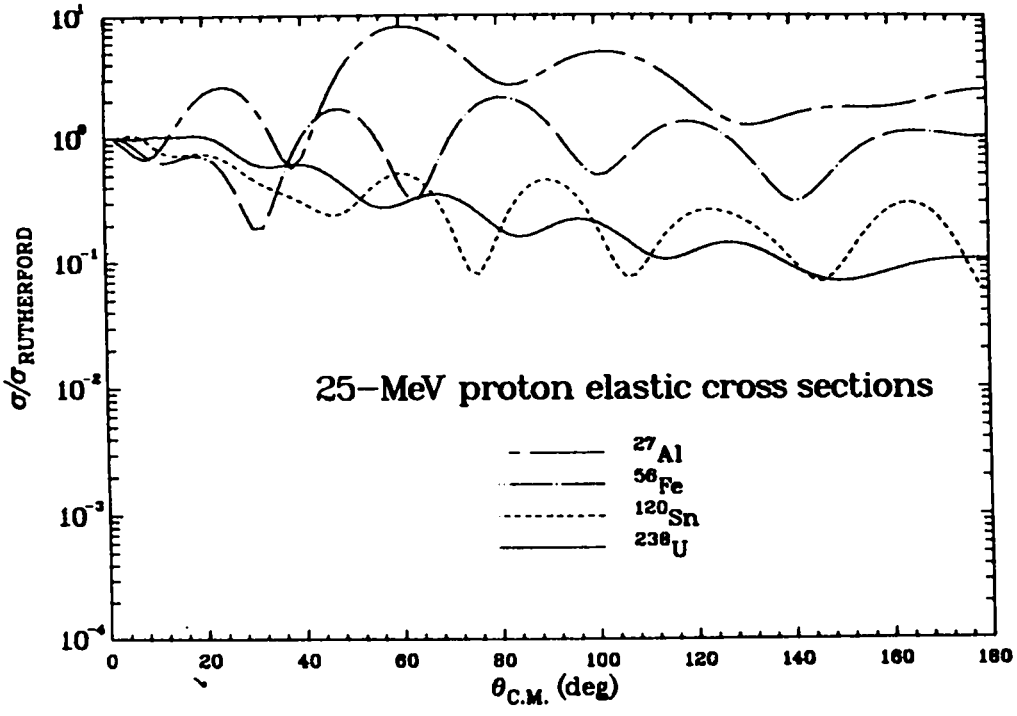

Fig. 25. Identical to Figure 23 except that the ratio to Rutherford scattering is shown.

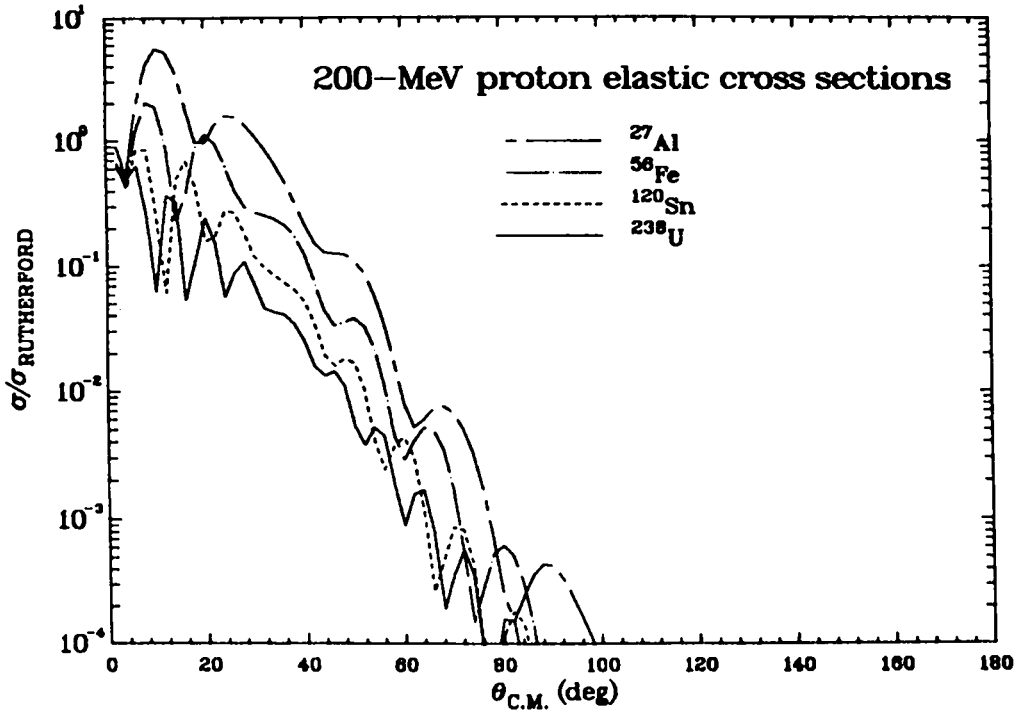

Fig. 26. Identical to Fig. 24 except that the ratio to Rutherford scattering is shown.

sections are decreasing with decreasing energy because of the Coulomb barrier, whereas at higher energies they are roughly constant with energy and scale approximately at $A^{2/3}$ as expected. Note that the calculated reaction cross sections agree reasonably well with the experimental values (not shown here) and that the optical-model potentials of Refs. 47 and 8 are determined primarily from elastic scattering angular distribution and polarization measurements, which they, of course, optimally reproduce.

Alternatives to the phenomenological relativistic Schrödinger equation approach are currently under study for purposes of greater predictive power and higher accuracy, especially for the reaction cross section and the S matrix.

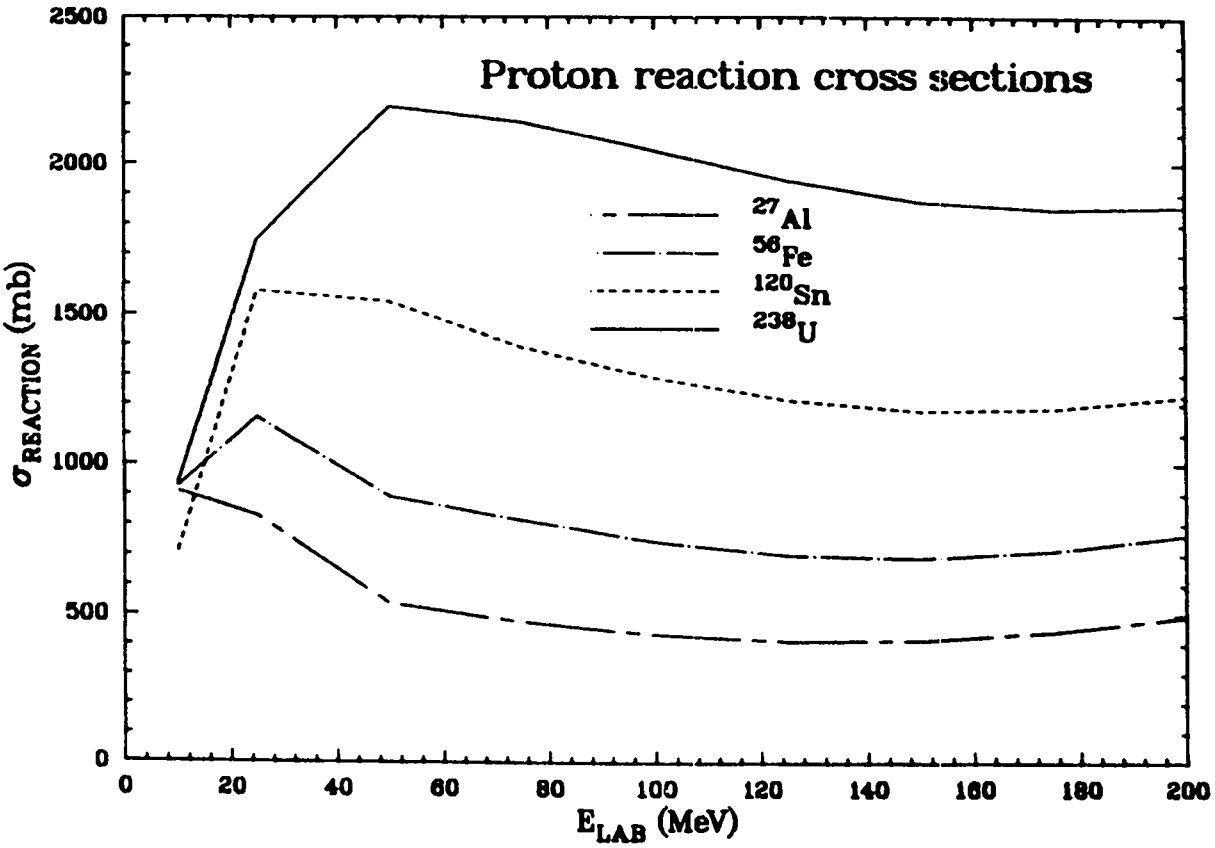

Fig. 27. Calculated total reaction cross sections for the scattering of protons by ^{27}Al, ^{56}Fe, ^{120}Sn, and ^{238}U as functions of the proton bombarding energy.

N. Medium Energy Scattering Codes (D. G. Madland)

Three nuclear reaction scattering codes[48-50] have been made operational for medium energy calculations. These are:

1. SNOOPY-VIII for the nuclear optical-potential analysis of the elastic scattering of projectiles of spin 0, 1/2, and 1 by nuclei with spin 0. Relativistic kinematics and/or a relativistic form of the Schrödinger wave equation are options. The optical potential may be generated phenomenologically or microscopically in (1) the impulse approximation or (2) the relativistic Dirac-Hartree model. The total, reaction, elastic, and differential elastic cross sections are calculated together with the polarization and the scattering S matrix. The code is described in detail in Ref. 48.

2. ECIS-78 for the coupled-channel optical-model analysis of the elastic and direct inelastic scattering of projectiles of spin 0, 1/2, and 1 by vibrational and deformed nuclei with arbitrary spin. Relativistic kinematics are now a working option. The total, reaction, elastic, differential elastic, direct inelastic, and differential direct inelastic cross sections are calculated together with the polarization, inelastic asymmetry, and scattering S matrix. This code is described in detail in Ref. 49.

3. RELOM for the nuclear optical-potential analysis of the elastic scattering of projectiles of spin 0 or 1/2 by nuclei with spin 0, at relativistic and non-relativistic energies.[50] The optical potential may be generated phenomenologically or read-in externally. The reaction and differential elastic cross sections are calculated as are the polarization and scattering S matrix. Several potential options exist.

Each of these codes possesses search options on experimental data for determining a best-fit phenomenological optical-model potential.

O. Verification of the Los Alamos Theory of the Prompt Fission Neutron Spectrum (D. G. Madland and R. J. LaBauve)

In our previous papers on this subject,[51-53] we have demonstrated the validity of the Los Alamos (Madland-Nix) fission spectrum theory[54] by comparisons of integral and microscopic measurements with calculation for the thermal-neutron-induced fission of ^{235}U and ^{239}Pu and for the spontaneous fission of ^{252}Cf. Our results[51,52] for the ^{235}U thermal fission spectrum remain unchanged as of this date. These showed that, on the basis of experimental evidence then available, the agreement between experiment and theory was especially good in the case of the Los Alamos exact[54] energy-dependent cross-section calculation. We know of no new experiments to affect this agreement.

Similarly, our results[52] for the ^{239}Pu thermal fission spectrum remain unchanged. Very good agreement with experiment was obtained for both the Los Alamos exact and approximate[54] calculations by adjusting the nuclear level-density parameter to optimally reproduce the Grundl integral experiment[55] while maintaining good agreement with the microscopic measurements of Abramson and Lavelaine.[56] Again, we know of no new experiments to affect this agreement. However, the Cross Section Evaluation Working Group (CSEWG), while choosing the Madland-Nix approximate formalism for the ^{239}Pu ENDF/B-V: Revision 2 evaluation,[57] has required[58] that the average energy <E> of the thermal spectrum be identical to that of the original ENDF/B-V evaluation. This decision produces a significant departure from the Grundl experiment, namely, the average C/E (calculation/experiment) value is now 1.048, with an extremum of 1.176, whereas the values inferred from Table I of Ref. 52 are, respectively, 1.003 and 1.014.

Two new ^{252}Cf spontaneous fission experiments have been performed since our previous work[53] on this nucleus, namely, the microscopic measurement of the $^{252}Cf(sf)$ spectrum by Poenitz and Tamura* (Ref. 59) and the integral measurements of 12 reactions by Kobayashi et al.[60] Least-squares adjustments of the Los Alamos exact spectrum and a Maxwellian spectrum fit to the Poenitz and Tamura experiment are described in Ref. 61. The final values of the two parameters of adjustment are, respectively, $a = (A/9.15)\ MeV^{-1}$ for the nuclear level density and $T_M = 1.429$ MeV for the Maxwellian temperature. The χ^2_{min} value for the best-fit Los Alamos exact spectrum is a factor ~ 2.2 better than that of the best-fit Maxwellian spectrum. In fact, the ratios of the Los Alamos exact

*The experimental spectrum was provided by W. P. Poenitz, Argonne National Laboratory West, Idaho Falls, Idaho, in April 1983.

spectrum and the experimental spectrum to the Maxwellian spectrum, shown in Fig. 28, clearly indicate that the Los Alamos spectrum is in uniformly better agreement with the experiment.

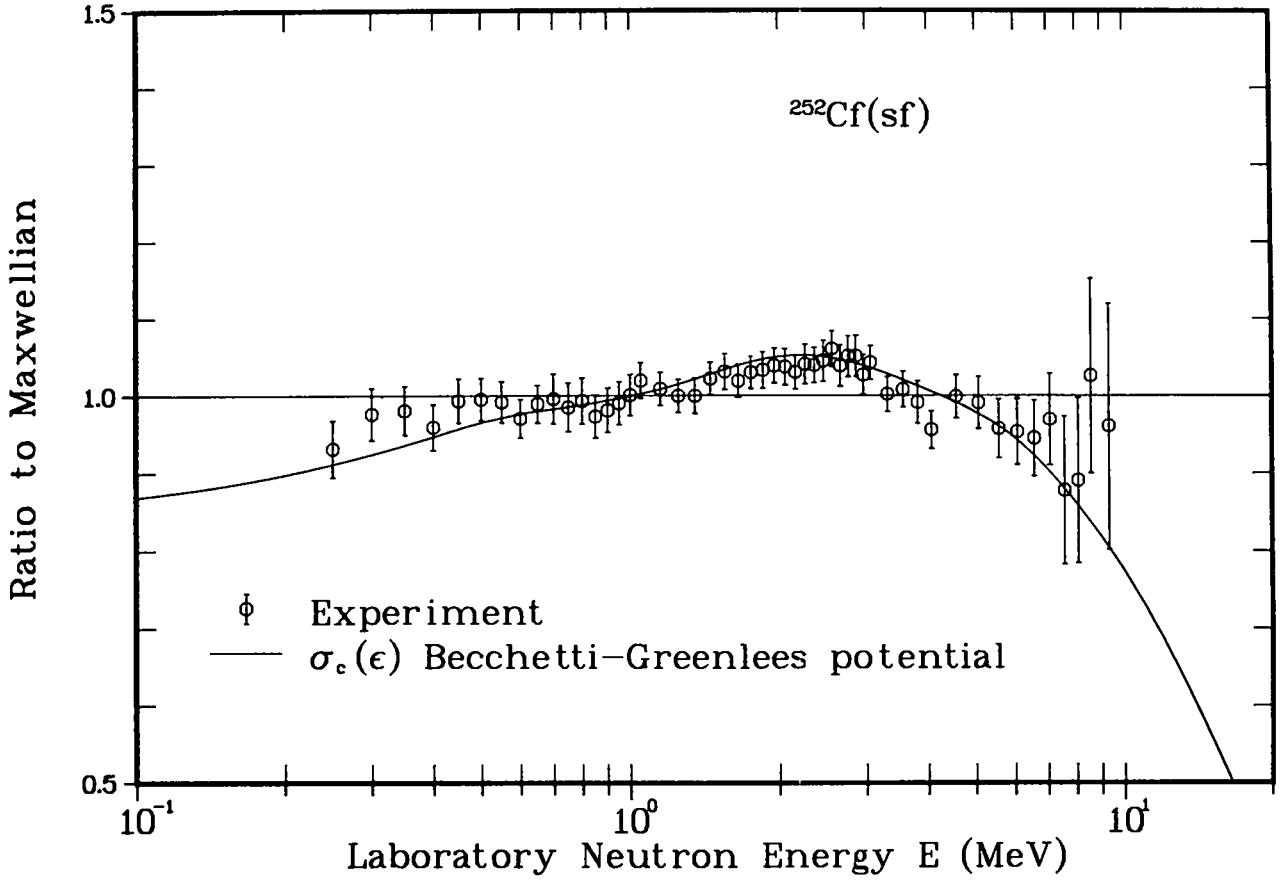

Fig. 28. Ratio of the best-fit Los Alamos exact-dependent cross-section spectrum, calculated using the Becchetti-Greenlees potential[8] and the experimental spectrum of Poenitz and Tamura[59] to the best-fit Maxwellian spectrum.

Using these two spectra, we have calculated 10 of the 12 integral cross sections measured by Kobayashi et al.[60] for which ENDF/B-V microscopic cross sections exist, together with the normalizing ^{27}Al(n,α) integral cross section. Our calculated results are compared to the experiment in Cols. 4 and 7 of Table VI. We include in Table VI the same integral cross sections calculated using three spectra that we have previously studied.[53] These are the Los Alamos exact spectrum (Col. 5) and Maxwellian spectrum (Col. 8) obtained by performing least-squares analyses of the Boldeman et al. microscopic measurement* (Ref. 62),

*The experimental spectrum was provided by J. W. Boldeman, Australian Atomic Energy Commission, Lucas Heights, N.S.W., Australia, in May 1983.

and the piecewise continuous NBS spectrum obtained by fitting the integral measurements of Grundl and Eisenhauer[63] (Col. 6). Inspection of the table (two-sigma uncertainties and average C/E values) shows that

a. the two Los Alamos exact spectra agree best with the experiment,

b. the two Maxwellian spectra agree worst with the experiment, and

c. the NBS spectrum is intermediate.

We therefore conclude on the basis of the evidence summarized here that the Los Alamos (Madland-Nix) exact energy-dependent cross-section calculation is the preferred prompt fission neutron spectrum representation.

TABLE VI

CALCULATED INTEGRAL CROSS SECTIONS FOR SEVERAL REPRESENTATIONS OF THE ^{252}Cf SPONTANEOUS FISSION NEUTRON SPECTRUM[a]

Reaction	Effective Threshold (MeV)	Measured Value (Per Cent Error)	Los Alamos Poenitz Exp. Calc. (C/E)	Los Alamos Boldeman Exp. Calc. (C/E)	NBS Grundl Exp. Calc. (C/E)	Maxwellian Poenitz Exp. Calc. (C/E)	Maxwellian Boldeman Exp. Calc. (C/E)
$^{24}Mg(n,p)$	6.08	1.9400(4.6)	2.0633(1.06)	2.0526(1.06)	2.0495(1.06)	2.0247(1.04)	2.0264(1.04)
$^{27}Al(n,p)$	3.35	4.8900(3.7)	5.1372(1.05)	4.9380(1.01)	4.8795(1.00)	4.5272(0.93)[b]	4.5574(0.93)
$^{27}Al(n,\alpha)$	6.25	1.0060(2.2)	1.0060(1.00)	1.0060(1.00)	1.0060(1.00)	1.0060(1.00)	1.0060(1.00)
$^{32}S(n,p)$	2.01	72.5000(4.1)	74.1156(1.02)	69.5397(0.96)	67.8264(0.94)	61.1978(0.84)[b]	61.8790(0.85)[b]
$^{51}V(n,p)$	3.98	0.7130(8.3)	0.5376(0.75)[b]	0.5221(0.73)[b]	0.5181(0.73)[b]	0.4907(0.69)[b]	0.4930(0.69)[b]
$^{54}Fe(n,p)$	1.89	87.6000(5.0)	91.3475(1.04)	85.8621(0.98)	83.8696(0.96)	75.7705(0.86)[b]	76.5887(0.87)[b]
$^{56}Fe(n,p)$	5.20	1.4400(4.9)	1.3675(0.95)	1.3476(0.94)	1.3442(0.93)	1.3018(0.90)	1.3049(0.91)
$^{58}Ni(n,p)$	1.39	118.0000(3.4)	117.9435(1.00)	110.7150(0.94)	108.1203(0.92)[b]	97.5994(0.83)[b]	98.6783(0.84)[b]
$^{59}Co(n,\alpha)$	5.68	0.2180(6.4)	0.2068(0.95)	0.2060(0.94)	0.2060(0.94)	0.2043(0.94)	0.2045(0.94)
$^{115}In(n,n')$	0.76	201.0000(4.0)	192.3775(0.96)	177.3204(0.88)[b]	172.7176(0.86)[b]	153.9558(0.77)[b]	156.2215(0.78)[b]
$^{197}Au(n,2n)$	8.31	5.2700(4.4)	5.1429(0.98)	5.3021(1.01)	5.3639(1.02)	5.7414(1.09)[b]	5.7136(1.08)
		Average C/E	0.98	0.95	0.94	0.90	0.90
		Spectrum <E>	2.134	2.168	2.120	2.144	2.136

[a] Normalized to the $^{27}Al(n,\alpha)$ measured value and expressed in millibarns.

[b] Calculation outside two-sigma measurement uncertainty.

P. Coupled Energy-Angle Distributions of Recoiling Nuclei (D. G. Foster, Jr. and R. E. MacFarlane

We have almost completed development of a code system for calculating the coupled energy spectra and angular distributions of the various residual nuclei produced by bombarding nuclei with neutrons having energies up to about 40 MeV. Such information is needed, for example, to calculate the neutron-induced first-surface spallation and interior damage to the walls of proposed fusion reactors.

The calculations begin with the GNASH[5] code and are followed by two new codes, RECOIL and MAKE6. In recent years, we have routinely stored the output from GNASH calculations in standardized files. RECOIL reads these files, which are very detailed, and uses the particle-emission data to identify the residual nucleus created by each multistep decay of the initial compound nucleus. Using the angular-distribution systematics dictated by an input parameter (the options are isotropic or some version of the Kalbach-Mann formalism),[64] RECOIL averages over all possible sequences of directions in space to determine the angular distribution of each final residual nucleus as a function of the corresponding recoil energy. These distributions, which retain the axial symmetry dictated by the direction of the original incoming neutron, are expressed as energy-dependent Legendre expansions in the center-of-mass system of the original compound nucleus.

The angular-distribution calculation for one-step reactions is straightforward, and is performed separately by RECOIL. The code for multistep reactions is fully recursive and can accommodate up to six reaction steps. One of these steps can be photon emission, if it is followed by emission of another type of particle. If the GNASH data call for another photon, it is sent directly to the ground state. We were surprised to discover empirically that major energy imbalance can occur if such intermediate-photon emission is not included. We have also learned empirically that most of the recoil angular distributions are almost isotropic. In those that are markedly anisotropic, the normalized Legendre moments for $\ell = 1$ and $\ell = 2$ are frequently of the same order of magnitude. We have not yet encountered a need for $\ell > 2$.

The principal output from RECOIL is a file of ENDF/B fragments, which are labelled to go into FILES 3, 6, 12, or 15. These fragments are the input to

MAKE6, which sorts through them repeatedly to construct the four ENDF/B files in the appropriate sequences of primary and secondary energies. MAKE6 takes full advantage of the new FILE 6 formats that permit all products of a reaction, whether particle or recoil, to be included in a single section under a single group of formats. For particles, only the spectrum and preequilibrium fraction are given, since the angular distributions will use the Kalbach-Mann formalism. The recoil angular distributions are automatically suppressed unless either the $\ell = 1$ or the $\ell = 2$ Legendre coefficient exceeds a fixed threshold (typically 0.1) for at least one secondary energy in the record for that primary energy.

The extensive multistep averaging in RECOIL makes it comparatively expensive to use. Consequently RECOIL includes provisions for adjusting the number of angle bins (both polar and equatorial) that are used for averaging each step in a multistep reaction. Coarser meshes degrade the quality of both the recoil spectrum and its corresponding angular distribution. Since most of the effect of recoils occurs in the first few emissions, it is also possible to decrease the computer time with minimal loss of accuracy by restricting the angular averaging to the first few steps. Accordingly, RECOIL accepts as an input option the maximum number of steps to be included.

We have applied RECOIL and MAKE6 to the GNASH data calculated[66] for the ENDF/B version 4 evaluation for ^{56}Fe, for incident-neutron energies between 5.25 and 36 MeV. An unrestricted calculation at 14 MeV using a 12 x 12 averaging mesh at every step required 18 minutes of CDC-7600 computer time. A similar calculation using a 5 x 5 mesh at 24 MeV required 80 minutes, which was reduced to 31 minutes by restricting the angular averaging to one-step and two-step reactions. Under the latter restriction, a calculation for an incident energy of 36 MeV on a 2 x 2 averaging mesh required 216 minutes. We conclude that it is impractical to use RECOIL on a 7600 computer above 40 MeV.

II. NUCLEAR CROSS-SECTION PROCESSING AND TESTING

A. TRANSX-CTR (R. E. MacFarlane)

A version of the TRANSX code especially adapted to fusion systems analysis has been released through the Radiation Shielding Information Center (RSIC) at the Oak Ridge National Laboratory. A report is now available (Ref. 66).

TRANSX-CTR reads multigroup data in MATXS format and prepares it for use in a variety of transport codes. Options include neutron, photon, or coupled sets; direct or adjoint tables; collapse; micro or macro cross sections; self-shielding; mix and energy-dependent fission spectra; and flexible response edits. The last capability is important for fusion work, and it allows easy access to heating, damage, and gas production response functions.

Cross section libraries available for TRANSX-CTR include a compact 30-neutron by 12-photon group library for general use, an 80 x 24 library for fast breeder reactor (FBR) and fusion blanket work, a 69-group thermal library useful for pressurized water reactor (PWR) calculations, and a 187 x 24 shielding library. Versions of both codes and data are available on the Magnetic Fusion Energy (MFE) computing network.

B. The COVFILS-2 Library of Neutron Cross Sections and Covariances for Sensitivity and Uncertainty Analysis (D. W. Muir)

As a contribution to the US/Japan cooperative program in fusion neutronics, we have prepared a library of multigroup neutron cross sections, scattering matrices, and covariances (uncertainties and their correlations). This 74-group library, called COVFILS-2, is being used at Los Alamos and at the University of California at Los Angeles in the sensitivity and uncertainty analysis of the Li_2O integral experiment recently performed at the Fast Neutron Source (FNS) in Japan. Another intended use of this library is in the estimation of the uncertainty in key performance parameters (such as breeding ratio) of conceptual fusion reactors. The 14 materials included in the first version of COVFILS-2 are H, ^{6}Li, ^{7}Li, Be, C, N, O, Na, Al, Si, Cr, Fe, Ni, and Pb.

Like the earlier COVFILS 30-group library (Ref. 66), COVFILS-2 was produced using modules of the NJOY nuclear data processing system (Refs. 67 and 68). COVFILS-2 is largely based on data evaluations from the ENDF/B-V library, although some minor corrections and improvements are incorporated. In cases where the covariance evaluation is missing (as in the case of Be) or judged to

be inadequate, private Los Alamos evaluations (such as Ref. 69) are employed. The COVFILS-2 74-group structure, Table VII, was chosen for compatibility with the extensive, general-purpose MATXS8 187-group library, also produced with NJOY. COVFILS-2 contains full (P_0 - P_3) transfer matrices for all neutron scattering reactions for which covariance evaluations are available. This is a useful feature, because some basic data evaluations provide the uncertainty in special sums of cross sections, called "lumped" partial cross sections. Important examples can be found in the most recent ENDF/B evaluations for ^{7}Li (MAT1397) and natural iron (MAT1326). Cross sections and transfer matrices for these special "lumped" partials may not be easily available from other data libraries. All data in COVFILS-2 are written in the highly compressed BOXER format,[70] which typically achieves data compression factors of 10 or more, relative to the previous COVFILS format. Even with this compression COVFILS-2 is large, containing over 40 000 BCD card images.

TABLE VII

ENERGY BOUNDARIES AND GROUP-INTEGRATED WEIGHT FUNCTION FOR COVFILS-2

GROUP NO.	LOWER ENERGY	GROUP FLUX	GROUP NO.	LOWER ENERGY	GROUP FLUX
1	1.0000E-05	6.3540E+03	38	3.0197E+05	3.2657E+05
2	7.6022E-04	1.1870E+06	39	3.8774E+05	1.9125E+05
3	1.2395E-02	5.5633E+06	40	4.3937E+05	2.1268E+05
4	4.2755E-02	4.0997E+06	41	4.9787E+05	2.3232E+05
5	8.1968E-02	1.8615E+06	42	5.6416E+05	2.4872E+05
6	1.5230E-01	1.1480E+06	43	6.3928E+05	2.6625E+05
7	4.1399E-01	8.6592E+05	44	7.2440E+05	2.8502E+05
8	8.7642E-01	2.8838E+05	45	8.2085E+05	5.9106E+05
9	1.1254E+00	5.7659E+05	46	1.0540E+06	2.9571E+05
10	1.8554E+00	8.6549E+05	47	1.1943E+06	2.9610E+05
11	3.9279E+00	2.8877E+05	48	1.3534E+06	5.4009E+05
12	5.0435E+00	5.7808E+05	49	1.7377E+06	2.3460E+05
13	8.3153E+00	8.6718E+05	50	1.9691E+06	2.1369E+05
14	1.7603E+01	8.6648E+05	51	2.2313E+06	1.8707E+05
15	3.7267E+01	8.6609E+05	52	2.5284E+06	1.5676E+05
16	7.8893E+01	2.8864E+05	53	2.8650E+06	1.2948E+05
17	1.0130E+02	5.7727E+05	54	3.2465E+06	1.0509E+05
18	1.6702E+02	8.6556E+05	55	3.6788E+06	8.2106E+04
19	3.5358E+02	8.6537E+05	56	4.1686E+06	6.1472E+04
20	7.4852E+02	8.6617E+05	57	4.7237E+06	4.5989E+04
21	1.5846E+03	8.6684E+05	58	5.3526E+06	3.4425E+04
22	3.3546E+03	8.6679E+05	59	6.0653E+06	2.5494E+04
23	7.1017E+03	2.8872E+05	60	6.8729E+06	1.8676E+04
24	9.1188E+03	5.7730E+05	61	7.7880E+06	1.3525E+04
25	1.5034E+04	5.7704E+05	62	8.8250E+06	9.6781E+03
26	2.4788E+04	5.7637E+04	63	1.0000E+07	6.7773E+03
27	2.6058E+04	8.6554E+04	64	1.1000E+07	7.3272E+03
28	2.8088E+04	1.4426E+05	65	1.2000E+07	9.8326E+03
29	3.1828E+04	2.8866E+05	66	1.3000E+07	9.6750E+03
30	4.0868E+04	2.8883E+05	67	1.3500E+07	1.0203E+04
31	5.2475E+04	2.8899E+05	68	1.3750E+07	1.4358E+04
32	6.7379E+04	2.8901E+05	69	1.3940E+07	2.8447E+04
33	8.6517E+04	2.8888E+05	70	1.4200E+07	1.4356E+04
34	1.1109E+05	2.8870E+05	71	1.4420E+07	4.9247E+03
35	1.4264E+05	2.8863E+05	72	1.4640E+07	3.0677E+03
36	1.8316E+05	2.8982E+05	73	1.5000E+07	2.6164E+03
37	2.3518E+05	2.9254E+05	74	1.6000E+07	3.7170E+03
				-1.7000E+07	

Both to save space and to facilitate the application of these data to uncertainty analyses, "redundant" reactions are omitted from COVFILS-2. Redundant reactions are reactions such as the total cross section (MT=1), the total nonelastic (MT=3), and (in some cases) the total inelastic (MT=4), which are merely sums of other reactions already present in the covariance library. In modern covariance evaluations, the well-known total cross section, for example, nearly always is used as a constraint in the evaluation of the covariances of the component partial reactions. When this is done, there is no difference between the covariances specified for MT=1 in the evaluation and the implied covariances in the sums of the partials. An advantage of eliminating redundant reactions is that, in expressions such as the familiar propagation-of-errors formula,

$$\Delta R = \sum_{i,j} \frac{\partial R}{\partial \sigma_i} \frac{\partial R}{\partial \sigma_j} \operatorname{cov}(\sigma_i, \sigma_j) \quad ,$$

one can let the index i range over all energy groups and over all reactions present in the library for the material of interest. This clearly simplifies the retrieval and summation algorithms.

A suite of subroutines called COVARD2 has been added to the SENSIT and SENSIT-2D sensitivity and uncertainty analysis codes[71,72] to retrieve data in BOXER format directly from the COVFILS-2 library. Upon initialization, COVARD2 makes a pass through the entire COVFILS-2 library, preparing tables of summary information and writing the scattering data to a separate binary disk file for later access by the sensitivity subroutines. On later calls, the covariance matrix for a requested reaction pair, as well as the associated cross-section and standard-deviation vectors, is read from the library and reconstructed in full matrix form (including zeroes) and stored in fast memory.

A special index at the beginning of COVFILS2 is read on each call to COVARD2, but an actual search and retrieval operation is conducted only for reaction pairs that are indicated in the index to have non-zero covariances in the library. This is an important time-saving feature, because there are presently 201 different nuclear reactions in the library. In principle, there could exist over 20 000 distinct covariance matrices giving correlations among these 201 reactions. In fact, however, covariances are given for only 748 reaction pairs, and time is spent reading through the main body of the library

only for these "active" pairs. For the materials selected for this first version of the library, the ENDF/B evaluators have supplied no cross-material covariances, such as the covariances of ^{1}H elastic scattering with $^{27}Al(n,\alpha)$. However, the structure of the library and the coding in COVARD2 are designed to allow the easy addition of such data in the future. A stand-alone version of COVARD2 is available from the Los Alamos Applied Nuclear Science Group.

The treatment of inelastic scattering covariances varies considerably from one evaluation to another, and thus there is variation from one material to another in COVFILS-2. This variation is detailed in Table VIII, which also lists the MAT and ENDF/B-V, Rev. 2, tape numbers of the evaluations employed. For ^{1}H, there is no inelastic scattering. For ^{6}Li, the covariance evaluation does not assign uncertainties to these reactions. For most other materials, little or no detailed uncertainty information is provided by the evaluators for individual discrete levels, but uncertainties are given for the total inelastic cross section MT=4. For Cr, uncertainties are given for every discrete level (all 40 of them) plus continuum inelastic scattering. At 14 MeV, continuum inelastic is 74% of the total inelastic for this material so it was decided that the cost of processing and storing all of the low-lying discrete-level information is, at least for fusion applications, probably not justified. Hence, only MT=4 is included. A very similar situation exists for both Ni and Na.

For Fe, both a fine-detail and a coarse treatment are provided. In MAT=1326, the full details of 28 inelastic reactions (26 discrete levels, one lump of 14 levels, and continuum inelastic scattering) are provided. On the other hand, in MAT=1300 (which is, in all other respects, the same as MAT=1326), only MT=4 is given. For Fe, then, one can test whether or not the detailed treatment is necessary in a given application. Similarly, for Be (Ref. 70) in the energy range up to 17 MeV, P. G. Young provides uncertainties in 27 "pseudo-levels," which describe both the cross sections and energy-dependent secondary energy spectra for the (n,2n) reaction. Unlike the other evaluations discussed above, here correlations are provided for every possible pair of levels. Because of the importance of this nuclide for certain fusion systems, in MAT=2104 this information is preserved in full detail. Again, as a tool for testing the importance of such fine detail, we provide in MAT=2101, 2102, and 2103 alternative data sets that result from grouping these 27 reactions (MT=51-77) into 1, 3, and 9 "lumps," respectively. As shown in Table VIII, special MT numbers in the 600-series are used to identify these special groupings.

TABLE VIII

CONTENTS OF COVFILS-2

Nuclide	ENDF/B-V, Rev. 2 or Los Alamos (*) MAT/TAPE Number	Number of Inelastic[a] "Lumps"
^{1}H	1301/511	—
^{6}Li	1303/511	—
^{7}Li	1397/561	7
^{9}Be	2101 (*)	1 (MT=4)
	2102 (*)	3 (MT=610-612)
	2103 (*)	9 (MT=601-609)
	2104 (*)	27 (all)
^{nat}C	1306/556	15 (all)
^{14}N	1275/505	1
^{16}O	1276/551	1
^{23}Na	1311/556	1
^{27}Al	1313/506	1
^{nat}Si	1314/556	1
^{nat}Cr	1324/557	1
^{nat}Fe	1300 (*)/557	1
	1326/557	28 (all)
^{nat}Ni	1328/554	1
^{nat}Pb	1382/558	1

[a]For ^{9}Be all of the lumps are actually parts of the (n,2n) reaction.

C. Data Testing of ENDF/B-V Revision 2 [R. E. MacFarlane, D. W. Muir, G. E. Hansen (Q-2)]

One important feature of the new revision of Version V of the Evaluated Nuclear Data Files (ENDF) is the evaluation for ^{239}Pu contributed by Group T-2. Preliminary testing of this evaluation has been reported elsewhere.[73] These tests used the small Los Alamos critical assemblies as described in the ENDF

Benchmark Specifications.[74] However, the experimental results for these assemblies have been revised recently by the Los Alamos Advanced Nuclear Technologies Group (Q-2), taking into account a new National Bureau of Standards normalization of the fission deposits in the detectors used. In addition, some of the experimental numbers have been further refined by careful double-ratio work. Recently, E. Arthur has performed new statistical-model calculations of inelastic scattering in ^{237}Np using the same advanced methods used in the ^{239}Pu evaluation.[73] The availability of new experimental numbers for the critical assemblies and new ^{237}Np cross sections has led us to repeat and refine our previous data testing results.[75] Calculational details of the new central-worth calculations are discussed in Ref. 76. Our data-testing results (C/E ratios) are summarized in Table IX. Some of the new (preliminary) experimental values are given in Tables X and XI.

TABLE IX

LOS ALAMOS DATA TESTING RESULTS: 1981-1984
(C/E RATIOS ONLY)

Assembly Parameter	ENDF/B-V 1981 C/E	ENDF/B-V Recalc. 83-84 New E	Revision 2 1983-84 New ^{239}Pu	1984 New ^{237}Np
JEZEBEL				
k_{eff}	1.0068	1.0068	0.9982	
f28/f25	0.917	0.919	0.960	
f37/f25	0.989	0.966	0.979	.973
f49/f25	0.972	0.963	0.966	
w28/235	0.924	0.932	1.083	
w37/w25	1.073	1.074	1.100	1.070
w49/w25	0.995	0.994	0.984	
FLATTOP-PU				
k_{eff}	1.0093	1.0108	1.0050	
f28/f/25	0.941	0.937	0.973	
f37/f25	1.014	0.989	0.998	0.990
w28/w25	1.538	1.014	1.159	
w37/w25	1.027	1.010	1.031	0.999
w49/w25	1.028	1.005	1.001	

f/f = fission ratio
w/w = worth ratio

TABLE IX (Cont.)

Assembly Parameter	ENDF/B-V 1981 C/E	ENDF/B-V Recalc. 83-84 New E	Revision 2 1983-84 New ^{239}Pu	1984 New ^{237}Np
GODIVA				
k_{eff}	0.9989	0.9990		
f28/f25	1.037	1.037		
f37/f25	1.064	1.044		1.035
f49/f25	0.994	0.985	0.985	
w28/w25	1.024	1.024		
w49/w25	1.020	1.019	1.011	
FLATTOP-25				
k_{eff}	1.0067	1.0067		
f28/f25	1.038	1.033		
f37/f25	1.087	1.054		1.044
f49/f25	1.001	0.990	0.990	
w28/w25	1.013	1.059		
w37/w25	1.142	1.139		1.078
w49/w25	1.023	1.020	1.015	
JEZEBEL-PU				
k_{eff}	0.9980	0.9980	0.9917	
f28/f25	0.923	0.918	0.953	
f37/f25	1.017	0.998	1.009	
THOR				
k_{eff}	1.0266	1.0228	1.0070	
f28/f25	0.918	0.895	0.942	
f37/f25	0.962	0.923	0.948	
ZPR-6/7				
k_{eff}		0.9956	0.9958	
f25/f49		1.018	1.018	
f28/f49		1.010	1.020	
c28/f49		1.078	1.077	

TABLE X

PRELIMINARY MODIFICATIONS OF EXPERIMENTAL FISSION RATIOS FOR LOS ALAMOS CRITICALS

Assembly	f28/f25	f/37/f25	f49/f25
JEZEBEL	0.2133 ± 0.0023	0.9835 ± 0.014	1.4609 ± 0.013
GODIVA	0.1643 ± 0.0018	0.8516 ± 0.012	1.4152 ± 0.014
JEZEBEL-23	0.2131 ± 0.0026	0.9970 ± 0.015	
BIG TEN	0.03739 ± 0.00034	0.3223 ± 0.0039	1.1936 ± 0.0084
JEZEBEL-PU	0.2071 ± 0.0021	0.9365 ± 0.013	
FLATTOP-25	0.1492 ± 0.0016	0.7804 ± 0.010	1.3847 ± 0.012
FLATTOP-PU	0.1799 ± 0.0020	0.8561 ± 0.012	
FLATTOP-23	0.1916 ± 0.0021	0.9103 ± 0.013	
THOR	0.1962 ± 0.0022	0.9419 ± 0.010	1.429 ± 0.021

f/f = fission worth

TABLE XI

EXPERIMENTAL WORTH RATIOS

Assembly	w28/w25	w/37/w25	w49/w25
JEZEBEL	0.1390 ± 2.0%	1.030 ± 6.0%	1.996 ± 1.4%
GODIVA	0.1606 ± 2.2%		1.914 ± 1.4%
FLATTOP-25	0.1238 ± 4.1%	0.856 ± 0.7%	1.900 ± 0.7%
FLATTOP-PU	0.0940 ± 3.8%	0.944 ± 1.1%	1.934 ± 1.1%

w/w = worth ratio

Note that the results for the plutonium assemblies (JEZEBEL, FLATTOP-PU, JEZEBEL-PU, THOR) are rather consistent, all suggesting that the ^{235}U fast fusion cross section is slightly (~ 3%) too large. The results for the ^{235}U-fueled assemblies (GODIVA, FLATTOP-25) are also consistent with each other; they seem to suggest that the calculated neutron spectrum is somewhat too hard. Thus, the highest priority for future work seems to be a modern re-evaluation of ^{235}U. As discussed in Ref. 76, the low-energy (0.1-0.5 MeV) ^{238}U cross sections also deserve further scrutiny.

D. ENDF/B-VI Format Proposals [R. E. MacFarlane and L. Stewart (X-Consultant)

The Evaluated Nuclear Data Files (ENDF/B) have proven very successful, and their format is being adopted throughout the world for the exchange of evaluated data. However, these formats have always found it possible to grow to meet new requirements. We have been engaged in an attempt to extend the current formats to allow for coupled energy-angle distributions and incident charged particles. In collaboration with C. Dunford at the National Nuclear Data Center (NNDC) at Brookhaven National Laboratory, we have completed a massive rewrite of the format manual,[77] which accomplishes these two goals and makes numerous other improvements.

These changes were coordinated with the international community at an "IAEA Specialists Meeting on Format for the Exchange of Neutron Nuclear Data," held in Vienna on 2-4 April 1984. Preliminary approval from the Cross Section Evaluation Working Group (CSEWG) was received at the May meeting.

The proposals are now receiving final corrections and will soon be distributed to the CSEWG community in preparation for the ENDF/B-VI evaluations.

E. ENDF Thermal Photon Production (R. E. MacFarlane)

As discussed in the previous progress report,[31] several isotopes and elements from the current revision of ENDF/B-V show significant energy-balance errors for thermal neutrons. Except for Cl and K, the photon production for these materials is represented by a yield in MF=12, MT=102 and a normalized photon spectrum in MF=15, MT=102. The energy balance is checked by computing the average energy for the spectrum, multiplying by the yield, and comparing the result to the Q value given in MF=3, MT=102. Photon production for Cl and K is represented by giving energy-dependent yields for a number of discrete photons. Energy balance is checked by adding the products of yield times photon energy, and comparing the results with Q. Table XII gives the observed errors greater than 1% in descending order.

We have examined the sources of these errors. In several cases the problems arise from errors in transcribing the data from the tabulations in Ref. 78 (hereafter referred to as Orphan et al.). Other differences are more fundamental and would require some evaluation to correct.

TABLE XII

THERMAL PHOTON PRODUCTION ERRORS FOR ENDF/B-V.2

Material	% Error	Material	% Error
Mn55	53.7	Co59	8.0
Cl	-21.7	Ta181	3.6
W	-21.1	Ga	-3.3
Mo	20.9	Nb93	1.4
K	-17.7	Cu	-1.3
Bi209	-10.5		

Mn55 As shown in Figure 29, the spectrum is similar to Orphan et al., but shifted. This is clearly a mistake. In addition, the yield in MF=12, MT=102 is too large by about 50%. These problems can be easily repaired.

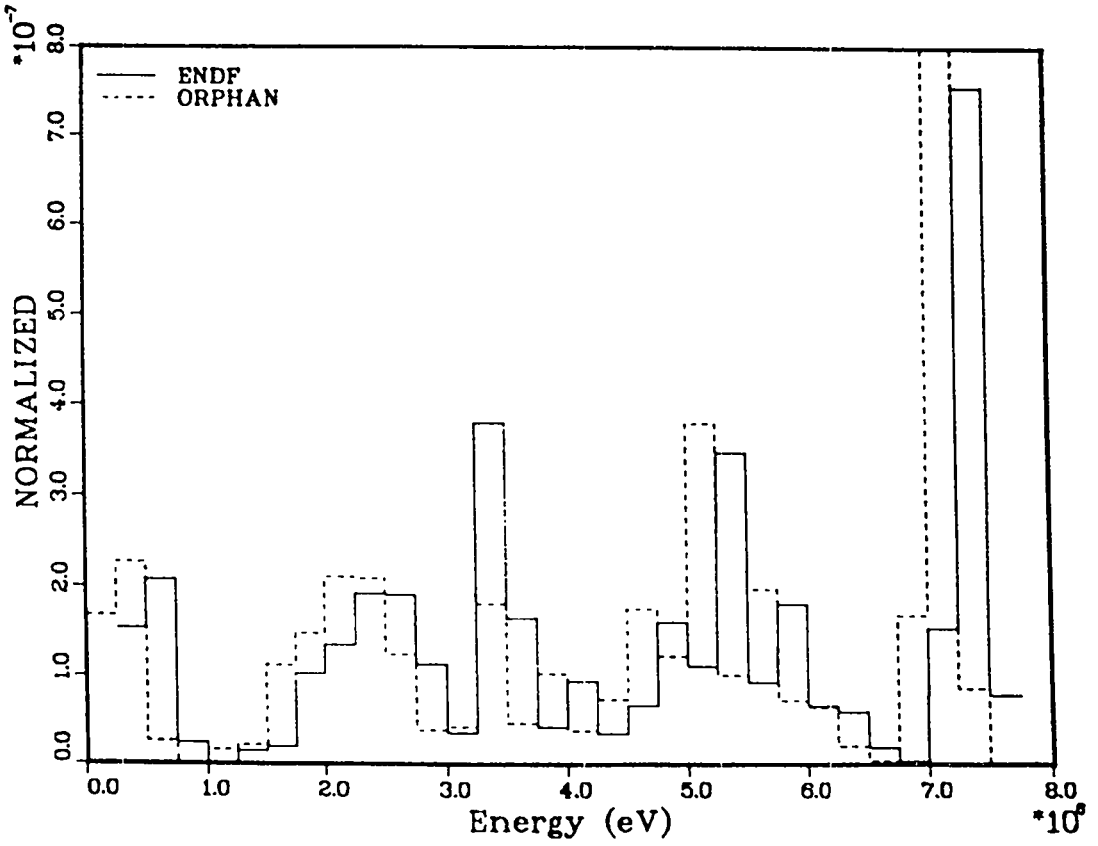

Fig. 29. Comparison of ENDF/B-V capture photon production for ^{55}Mn with data of Orphan et al.[78] showing apparent displacement.

Cl and K These evaluations were originally made before Orphan et al. appeared. Some of the gamma rays look reasonable, but many are simply missing. These missing lines seem to explain the ~ 20% of the binding energy not accounted for in the evaluations. These materials will have to be re-evaluated.

W The yield and spectrum were correctly derived from the isotopic evaluations, but the Q-value in MF=3, MT=102 was entered incorrectly. It should be changed to 5.8456 MeV.

Mo The yield and spectrum are from Orphan et al. To get proper agreement, the Q-value must be changed to 8.752 MeV.

Bi209 Spectrum is from Orphan et al., but the yield given is for the unnormalized spectrum. It should be multiplied by 1.117 for consistency with File 15. However, Orphan et al. only observed 72.6% of the binding energy, and a simple normalization may not be entirely appropriate. Re-evaluation may be necessary.

Co59 Spectrum is from Orphan et al., but the yield must be changed from 2.6416 to Orphan's value of 2.45 (better yet, use 2.4462).

Ta181 In the evaluation, an attempt was made to add internal-conversion effects to Orphan's spectrum. The apparent error may represent the energy of the electrons. This is not a simple "clerical" problem.

Ga Spectrum and yield are from Orphan et al. Either change the Q-value to Orphan's 6.970 MeV, or readjust the yields to correspond to a better $\bar{Q}$, if another value can be justified.

Nb93 The spectrum was derived from Orphan et al. by linearization and renormalization, as shown in Fig. 30. This resulted in a slight shift in the average energy, and the yield should be readjusted to match (2.85 changes to 2.8104).

Cu The spectrum and Q-value agree with Orphan et al. The yield should be changed from 1.957 to 1.980.

Most of these materials have other energy-balance errors at higher energies. However, making these simple changes reduces the number of materials with important thermal discrepancies to three (or four): Cl, K, and Ta181 (and possibly Bi209).

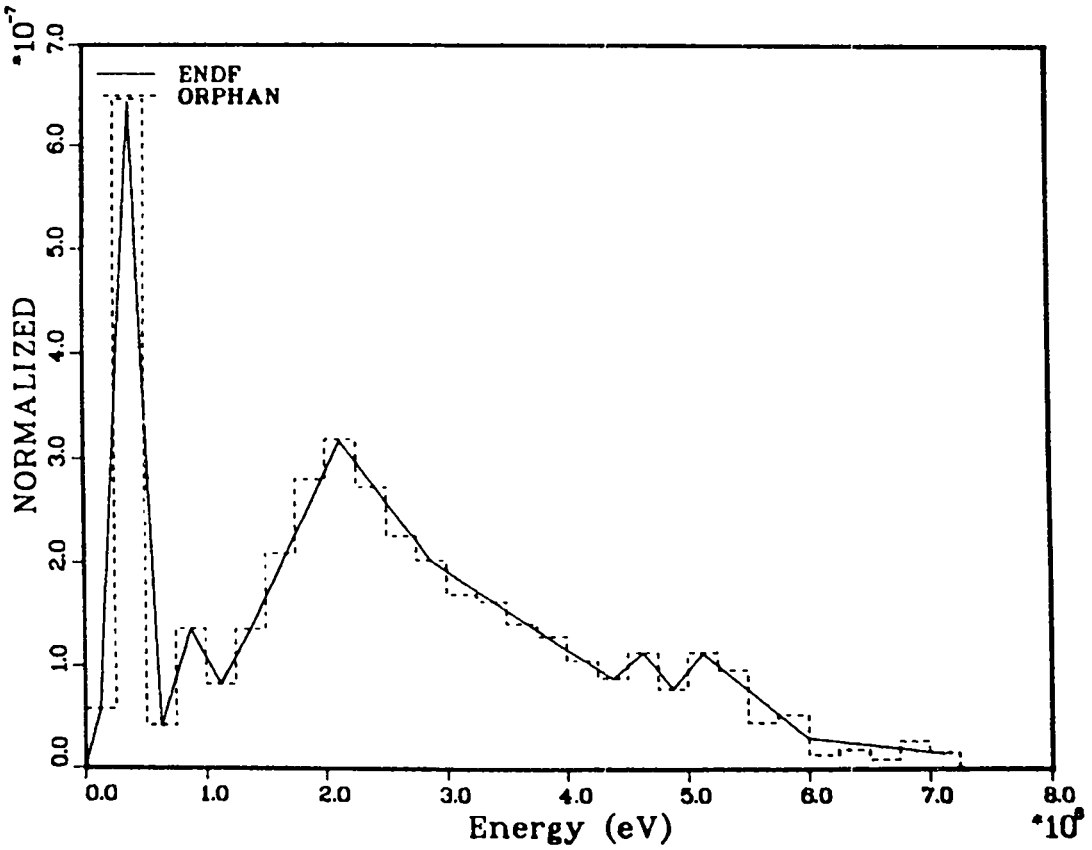

Fig. 30. Comparison of ENDF/B-V Capture Photon Production for ^{93}Nb with data of Orphan et al.[78]

F. Kinematic Kerma Factors (R. E. MacFarlane)

The HEATR module of NJOY computes heat production by energy-balance (usually); that is, it assumes that the energy available for charged-particle emission and nuclear recoil can be obtained from the available energy (E + Q) minus the energy carried away by neutrons (E_n) and the energy carried away by photons ($\bar{E}_\gamma$). If there are errors in either $\bar{E}_n$ or $\bar{E}_\gamma$, the local heating will be incorrect. In a large enough system, this heating error will be exactly compensated for by photon energy deposition, and the correct result for total heating will be obtained.

However, in very small systems where most of the photons escape, the local heating can have very large errors resulting from a lack of energy conservation in the nuclear data evaluation.[79] Accurate values for this local heating can be computed for some reactions by kinematics (radiative capture, elastic and inelastic neutron scattering). Reactions that emit charged particles are more difficult because the ENDF/B files do not contain the required particle spectra or angular distributions. Nevertheless, it is possible to establish an upper limit for the "kinematic kerma" factor by assuming that such reactions emit no photons.

The HEATR module has been modified to add kinematic kerma factors computed in this way to the NJOY calculational path. This means that they are available for either multigroup or Monte Carlo processing. Some examples are shown in Figs. 31 and 32.

Figure 31 shows an example in which too much photon energy is included between 100 keV and 1 MeV. This drives the energy-balance kerma strongly negative. The kinematic kerma is positive in this range. However, it is too large because the momentum of the photon field is too large. Above 16 MeV, the energy-balance result is too large.

The upper part of Fig. 32 shows very large errors for the important material chromium, but the lower half of the figure shows that iron is much better.

The ultimate solution to errors such as these is to re-evaluate the material with closer attention to energy balance (nuclear model codes help to accomplish this). A short-range solution for the user is to select energy-balance values for large systems and kinematic values for small ones.

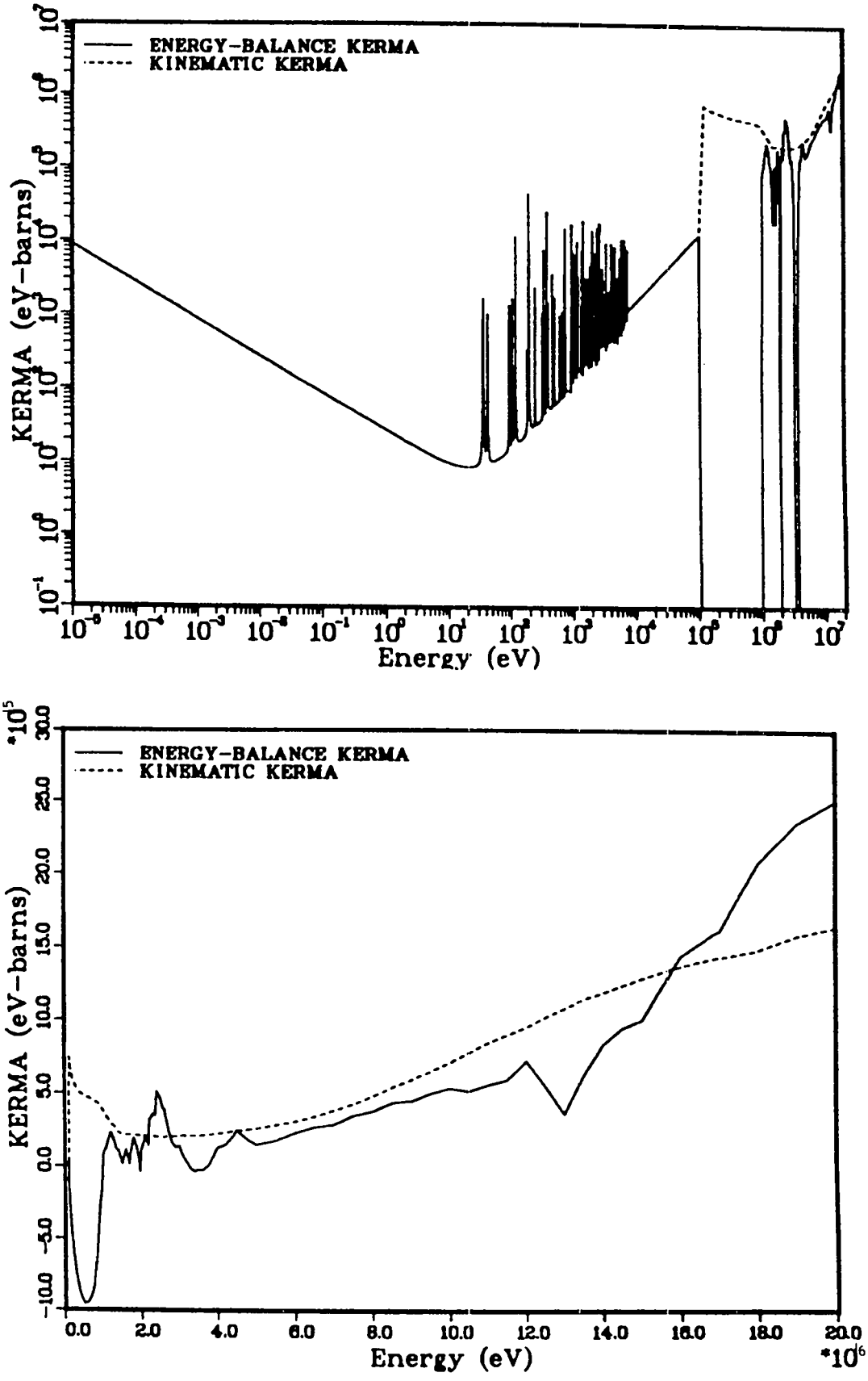

Fig. 31(a and b). Comparison of energy-balance and kinematic kerma factors for ^{93}Nb from ENDF/B-V.

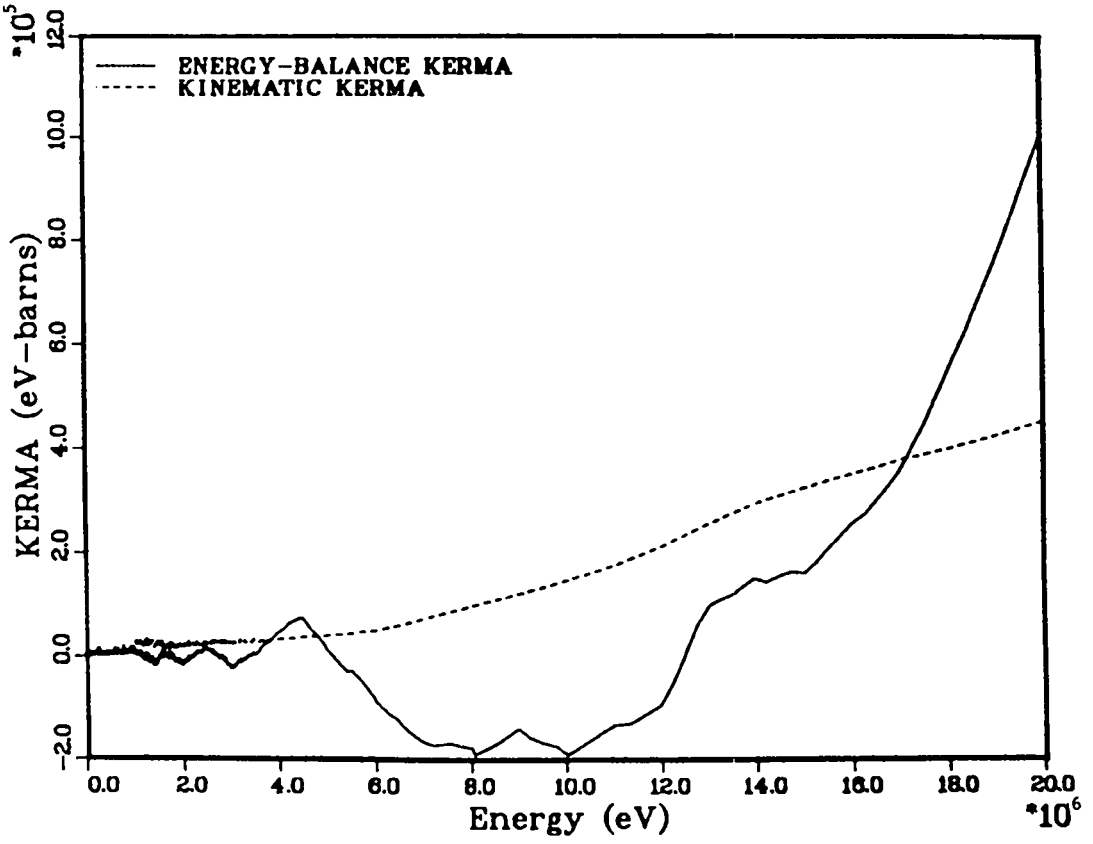

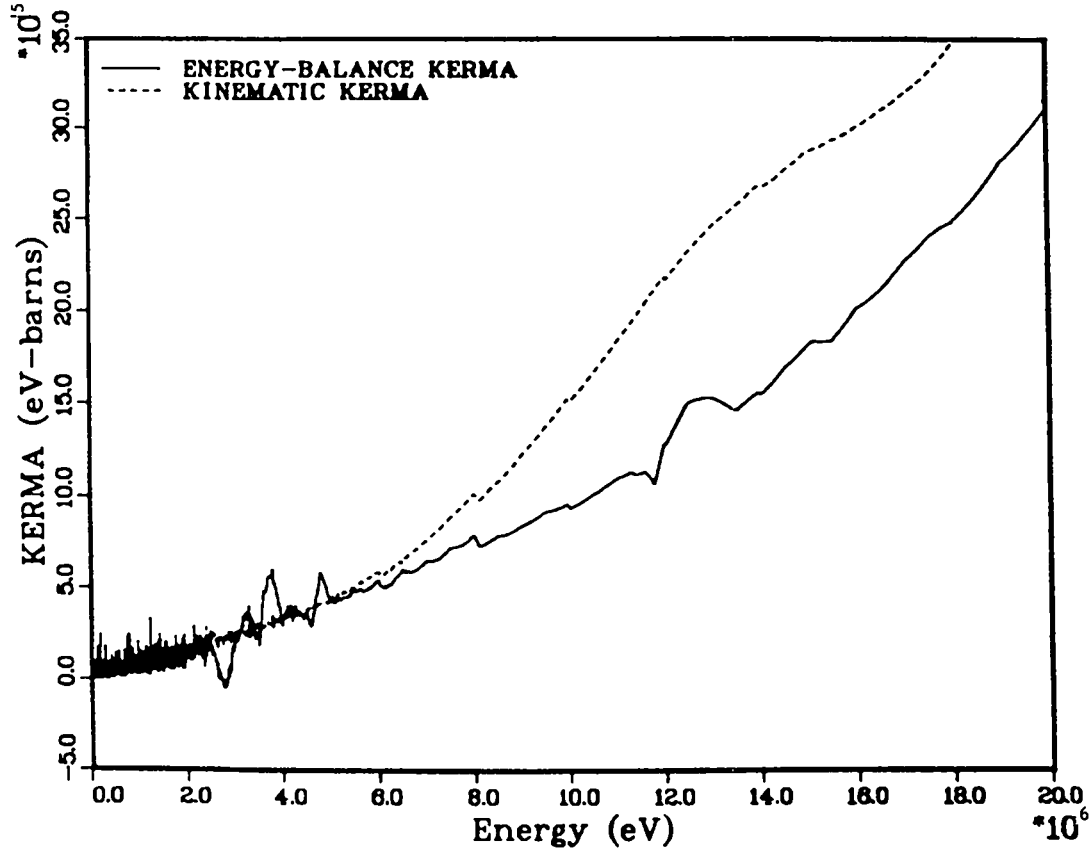

Fig. 32 (a and b). Comparison of energy-balance and kinematic kerma factors for the two important structural materials chromium (top) and iron (bottom). Note that the kinematic value for iron is an overestimate, as expected, because of photon emission from charged-particle emitting reactions.

III. NEUTRON ACTIVATION, FISSION PRODUCTS, AND ACTINIDES

A. ENDF/B-V Fission-Product and Actinide Data Summary Document [T. R. England, W. B. Wilson, R. E. Schenter (HEDL), and F. M. Mann (HEDL)]

A summary document of the fission-product and actinide data contained in ENDF/B-V data files was completed.[80] All fission products (877) and actinides (60) in Rev. "0" were included. Appendices contain additional augmentation of these data along with a presentation of probable data changes, errors, and existing revisions to date. These result largely from our experience with ENDF/B-V data testing and comparisons with other international evaluations. The main text identifies data that are commented upon in the Appendices, but otherwise it consists of Rev. "0" data. (In the case of group cross sections processed from Rev. "0," error corrections are discussed in the main text.) Mass chain yields, decay parameters (half-lives, branchings, beta, gamma, and alpha energies), processed one-group cross sections for fast reactor spectra, four-group cross sections for thermal reactors, and the resonance integrals and 2200 m/s cross sections are included, as well as other information pertinent to the ENDF/B-V files. The extensive decay spectra, charge distribution of mass chain yields, and energy-dependent cross sections are not included; such inclusion would require over 4000 pages. Rather, the document was prepared to serve as a relatively concise source for the most frequently requested data and as a convenient reference for the fission-product and actinide data contained in ENDF/B-V. Chain schematics are included. The additional augmentation of these data, relegated to the appendices, should add to the utility of this document as a general reference.

B. Nuclides Having ENDF/B-V Questionable Data or Errors [T. R. England, W. B. Wilson, R. E. Schenter (HEDL), and F. M. Mann (HEDL)]

All of the ENDF/B fission-product and actinide data have been incorporated into summation codes, including decay spectra, and aggregate comparisons were made with available measurements. Additional comparisons of many individual cross section and decay parameters with measurements and other evaluations have been made, and various consistency checks (e.g., the comparisons between average energies and values derived from spectra) have been made. Based on these comparisons and tests, we itemize here those nuclides and their parameters that should be reviewed for the next version of ENDF/B or before using the current Version-V data.

Table XIII provides a list of nuclides having questionable ENDF/B-V Rev. "0" data or data errors.

The so-called "Pandemonium Nuclides" are listed in Table XIV; average beta- and gamma-energies from ENDF/B-IV, -V, and the Japanese values are also included. This list consists of those nuclides identified by C. W. Reich, Idaho National Engineering Laboratory.

TABLE XIII

LISTING OF NUCLIDES HAVING ENDF/B-V QUESTIONABLE DATA OR ERRORS[a]

No.	Nuclide	MAT	Comment
6	31-Ga- 72m	9035	Q-value error. (Q=0.05MeV should be 0.12 MeV)
22	34-Se- 74	9089	Cross section interpolation error INT=2 should be INT=5
22	34-Se- 74	9089	Negative elastic scattering cross section
99	33-As- 83	9080	Half life to be reviewed (6.5s should be approx. 13.45s)
107	33-As- 84	9081	Half life error (0.3s should be 5.3s)
113	38-Sr- 84	9179	Cross section interpolation error INT=2 should be INT=5
117	34-Se- 85	9104	Q value error. (Q=14.0MeV should be 6.1 MeV)
122	38-Sr- 85	9180	Half life error (0.56+6s should be 0.56+7s)
221	44-Ru- 96	9325	Cross section interpolation error INT=2 should be INT=5
231	44-Ru- 97	9326	Review beta energy--some refs. do not use 0.0
241	44-Ru- 98	9327	Cross section interpolation error INT=2 should be INT=5
278	46-Pd-102	9379	Cross section interpolation error INT=2 should be INT=5
306	45-Rh-105	9355	Error in cap. cross sec. at E=0.5eV (change 360. to 3600.)
318	48-Cd-106	9440	Cross section interpolation error INT=2 should be INT=5
380	45-Rh-112	9367	Half life error (1.5s should be 4.6s)1.5s
384	50-Sn-112	9513	Cross section interpolation error INT=2 should be INT=5
375	48-Cd-111m	9446	Q value error (Q=0.05 MeV should be 0.396 MeV)
407	50-Sn-114	9516	Cross section interpolation error INT=2 should be INT=5
452	49-In-118n	9486	Spectra energies need to be reviewed
463	50-Sn-119m	9523	Spectra energies need to be reviewed
463	50-Sn-119m	9523	Q values need to be reviewed--some refs differ.
473	52-Te-120	9576	Cross section interpolation error INT=2 should be INT=5
485	52-Te-121m	9578	Review beta energy--some refs differ from 0.0
505	52-Te-123	9580	Negative elastic scattering cross section
528	54-Xe-125	9631	Review beta energy--some refs differ from 0.0
529	54-Xe-125m	9632	Review beta energy--some refs differ from 0.0
607	53-I -133	9614	Beta decay branching needs to be reviewed
667	53-I -140	9624	Review Q value--some refs differ
708	60-Nd-144	9765	Negative elastic scattering cross section
709	62-Sm-144	9803	Cross section interpolation error INT=2 should be INT=5
718	62-Sm-145	9804	Q value and ave. energies in error (Q value=6.15 MeV should be 0.615 MeV)
741	60-Nd-148	9769	Negative elastic scattering cross section
737	56-Ba-148	9701	Halflife needs review (3.325s is 0.55s in tab of isotopes)
825	62-Sm-158	9817	Halflife needs review (2640s recently reported as 330s)
854	66-Dy-162	9866	Negative elastic scattering cross section
876	68-Er-167	9876	Negative elastic scattering cross section
901	93-Np-237	1337	Thermal cross sections updated on second release, 6/83
912	95-Am-241	1361	Fast capture cross section needs review
919	95-Am-243	1363	Fast capture cross section updated on second release, 6/83
921	94-Pu-244	8444	X-ray energy and other spectral errors, corr. on second rel. 6/83
928	96-Cm-248	8648	X-ray energy and other spectral errors, corr. on second rel. 6/83
936	98-Cf-253	8853	X-ray energy and other spectral errors, corr. on second rel. 6/83

[a]The x-ray energy and spectral errors do not affect the average energies in ENDF/B-V. Spontaneous fission energy is not included in the average alpha energy, as is required by the ENDF/B-V formats manual. See also Tables XIV and XV. Table XV lists nuclides having spectra that do not reproduce one or more average energies as listed in the spectral files.

TABLE XIV

NUCLIDES TO BE EXAMINED FOR PANDEMONIUM EFFECT AND ENERGY COMPARISON WITH JNDC FILES[a]

Nuclide	MAT	Halflife(s)	Q(MeV)	ENDF/B-IV Beta	ENDF/B-IV Gamma	ENDF/B-V Beta	ENDF/B-V Gamma	JAPAN Beta	JAPAN Gamma
33-As 80	9076	1.650+01	6.000	2.523	0.607	2.455	0.610	2.478	0.259
33-As 82	9078	2.100+01	7.200	3.211	0.288	3.155	0.400	1.990	2.954
33-As 82m	9079	1.300+01	7.200	1.819	2.995	1.808	3.100	1.954	2.763
35-Br 87	9125	5.570+01	6.840	2.136	1.726	2.496	1.554	1.813	2.410
35-Br 88	9126	1.600+01	8.600	3.067	1.881	2.540	3.000	2.454	3.210
36-Kr 91	9152	8.570+00	6.120	2.578	0.724	1.941	1.733	2.055	1.617
36-Kr 92	9153	1.840+00	5.970	2.403	0.752	2.368	0.752	2.262	1.078
37-Rb 92	9169	4.530+00	7.770	3.459	0.261	3.481	0.261	2.856	1.566
36-Kr 93	9154	1.289+00	7.510	2.758	2.040	2.336	2.240	2.727	2.757
37-Rb 93	9170	5.860+00	7.360	2.027	1.415	2.605	1.320	2.147	2.675
39-Y 96	9213	6.000+00	6.500	2.408	1.461	3.147	0.003	3.024	0.000
39-Y 96m	9214	1.000+01	7.000	0.000	0.000	1.107	4.031	1.124	4.031
38-Sr 97	9194	4.000-01	7.400	2.350	1.838	2.620	1.490	2.603	1.501
39-Y 97	9215	3.700+00	6.670	2.162	0.935	2.154	1.800	2.472	1.231
39-Y 97m	9216	1.110+00	7.337	0.000	0.000	2.423	1.821	2.683	1.472
38-Sr 98	9195	6.500-01	5.810	1.690	1.496	2.527	0.176	2.139	1.051
39-Y 98	9217	2.000+00	7.300	2.845	1.943	1.806	3.151	3.216	2.041
39-Y 98m	9218	6.500-01	7.300	0.000	0.000	2.983	0.814	2.989	2.596
41-Nb 98	9258	2.860+00	4.585	1.865	0.140	1.959	0.080	1.965	0.080
39-Y 99	9219	1.400+00	6.390	2.092	1.647	2.606	0.611	2.375	1.147
40-Zr 99	9238	2.100+00	4.445	1.621	0.794	1.487	0.823	1.463	0.823
41-Nb101	9264	7.000+00	4.570	1.901	0.330	1.848	0.317	1.686	0.720
43-Tc102	9307	5.280+00	4.500	1.509	0.464	1.700	0.469	1.952	0.579
43-Tc102m	9308	2.610+02	5.000	0.720	2.547	0.940	2.377	0.855	2.430
43-Tc104	9310	1.092+03	5.400	1.193	1.448	1.582	1.940	1.244	2.678
44-Ru107	9336	2.520+02	3.150	1.238	0.251	1.250	0.180	1.212	0.241
45-Rh108	9360	1.680+01	4.500	1.828	0.709	1.800	0.347	1.813	0.338
45-Rh108m	9361	3.540+02	4.500	0.804	2.440	0.780	2.500	0.789	2.272
45-Rh110	9364	2.850+01	5.400	1.346	2.268	1.182	2.480	2.202	0.486
45-Rh110m	9365	3.000+00	5.400	2.481	0.056	2.367	0.056	2.237	0.777
49-In120	9489	3.080+00	5.400	1.039	3.060	2.258	0.331	2.228	0.331
49-In120m	9490	4.440+01	5.300	2.472	0.176	0.935	2.972	0.953	2.976
49-In121	9491	3.000+01	3.380	1.020	1.012	0.971	0.976	0.985	0.926
49-In121m	9492	2.256+02	3.100	1.091	1.082	1.483	0.120	1.503	0.053
51-Sb134	9569	1.070+01	8.490	3.952	0.000	2.800	2.036	2.781	2.256
51-Sb134m	9570	8.500-01	8.400	2.954	2.094	3.780	0.000	2.284	3.272
54-Xe139	9652	4.040+01	5.020	1.787	0.928	1.702	0.760	1.002	2.239
54-Xe140	9653	1.360+01	4.060	0.881	1.362	1.181	1.210	1.204	1.149
55-Cs140	9673	6.370+01	6.050	1.931	2.131	1.649	2.300	1.429	2.791
54-Xe141	9654	1.720+00	6.000	1.571	2.270	2.345	0.776	2.048	1.489
55-Cs141	9674	2.490+01	4.980	1.377	1.825	1.912	0.800	1.276	2.135
57-La142	9710	5.550+03	4.517	0.947	2.400	0.896	2.750	0.915	2.523
55-Cs144	9677	1.001+00	8.100	2.350	3.041	3.180	0.951	2.649	2.193
57-La144	9712	4.030+01	5.300	1.511	1.937	1.461	1.824	1.338	2.091
59-Pr148	9751	1.380+02	4.800	2.044	0.300	1.648	1.221	1.653	1.165
59-Pr149	9752	1.500+02	3.000	1.158	0.251	1.158	0.126	1.137	0.180
61-Pm152	9789	2.460+02	3.470	1.439	0.288	1.310	0.288	1.385	0.115
61-Pm152m	9790	4.500+02	3.470	0.900	1.287	1.134	1.290	0.864	1.466
61-Pm154	9793	1.080+02	4.000	0.760	1.885	0.915	1.856	0.839	1.852
61-Pm154m	9794	1.680+02	4.000	1.034	1.522	0.912	1.940	0.928	1.700

[a]These nuclides have complex spectra in ENDF/B-V (and for some in ENDF/B-IV) and therefore may have incorrect average energies. The nuclides were identified by C. W. Reich, Idaho National Engineering Laboratory, Idaho Falls, Idaho in February 1984.

Table XV lists nuclides that show a significant inconsistency between average decay energies tabulated in the decay files with the values computed from the spectra. In some cases the inconsistency is between the total energy calculated from the spectra and the total Q value.

TABLE XV

NUCLIDES IN ENDF/B-V REV "0" HAVING SOME SPECTRA ERRORS[a]

Nuclide	Nuclide
35-Br- 82m	62-Sm-151
40-Zr- 93	90-Th-232
44-Ru-106	90-Th-233
46-Pd-107	91-Pa-233
47-Ag-111	92- U-237
48-Cd-109	94-Pu-237
49-In-116m	94-Pu-241
49-In-118n	96-Cm-241
50-Sn-119m	95-Am-242m
51-Sb-126n	96-Cm-243
52-Te-133m	94-Pu-244
53- I-134m	96-Cm-248
59-Pr-149	97-Bk-249
61-Pm-149	98-Cf-253
61-Pm-152m	

[a]This listing of nuclides is based on a comparison of average energies derived from individual spectra with either the total Q value or average energies for individual spectra as tabulated in the files. Nuclides showing differences greater than 15% in any component are tabulated.

C. (n,2n) Cross Sections [R. E. Schenter (HEDL), T. R. England, W. B. Wilson, and R. J. LaBauve]

Most of the fission products and a few of the actinides in ENDF/B-V do not have (n,2n) cross sections. Table XVI provides a complete set of these cross sections in the multigroup structure defined following the table. These were constructed for future use in the DANDE Code System.

TABLE XVI

N,2N CROSS SECTIONS[a]

Nuclide	Thres.	Group 1	Group 2	Group 3	Group 4	Group 5	Group 6	Group 7	Group 8	Group 9	Meth.[b]
*** Fission Products ***											
32 Ge 720	10.80	1.1880	1.1880	1.1880	0.9982	0.0859	0.	0.	0.	0.	1
32 Ge 730	6.79	1.3270	1.7494	1.7494	1.7494	1.7494	1.4665	0.0803	0.	0.	1
32 Ge 740	10.20	1.2720	1.2720	1.2720	1.2654	0.3412	0.	0.	0.	0.	1
32 Ge 760	9.45	0.7140	1.0079	1.3578	1.1220	0.7645	0.3203	0.	0.	0.	4
33 As 750	10.20	1.1562	1.1832	1.1525	1.0268	0.6546	0.1447	0.	0.	0.	4
34 Se 740	12.10	1.0060	1.0060	0.9371	0.1693	0.	0.	0.	0.	0.	1
34 Se 760	11.20	0.5967	0.7295	0.8895	0.8674	0.4236	0.	0.	0.	0.	4
34 Se 770	7.42	1.5825	1.6612	1.6612	1.6612	1.6612	1.0047	0.0020	0.	0.	1
34 Se 780	10.50	1.0977	1.1166	1.0808	0.9748	0.6667	0.0842	0.	0.	0.	2
34 Se 800	9.90	1.0408	1.2474	1.2420	1.1879	0.9891	0.3239	0.	0.	0.	2
34 Se 820	9.26	0.8304	1.2472	1.3545	1.3274	1.2129	0.6333	0.0062	0.	0.	2
35 Br 790	10.70	0.7749	0.8832	0.9591	0.8929	0.4293	0.0104	0.	0.	0.	4
35 Br 810	10.20	0.5706	0.6676	0.7837	0.7089	0.4354	0.1019	0.	0.	0.	4
36 Kr 780	11.90	0.3690	0.3568	0.3110	0.2030	0.0401	0.	0.	0.	0.	3
36 Kr 800	11.50	1.1665	1.1415	1.0417	0.7865	0.2830	0.0025	0.	0.	0.	3
36 Kr 820	11.00	1.3477	1.3366	1.2817	1.1139	0.6214	0.0385	0.	0.	0.	3
36 Kr 830	7.47	1.4131	1.4200	1.4200	1.4136	1.3972	1.2858	0.5860	0.	0.	3
36 Kr 840	10.50	1.4326	1.4625	1.4252	1.3049	0.9120	0.1144	0.	0.	0.	3
36 Kr 850	7.01	1.2704	1.3119	1.3091	1.3018	1.2771	1.1655	0.6129	0.0206	0.	2
36 Kr 860	9.85	1.3809	1.5427	1.5083	1.4094	1.1187	0.2482	0.	0.	0.	3
37 Rb 850	10.50	1.2125	1.2770	1.3225	1.1849	0.7209	0.1038	0.	0.	0.	4
37 Rb 860	8.19	1.5534	1.5534	1.5534	1.5534	1.5534	0.4435	0.	0.	0.	1
37 Rb 870	9.94	1.2110	1.2901	1.3088	1.2059	0.9938	0.5874	0.	0.	0.	4
38 Sr 840	11.80	1.6251	1.6624	1.4747	0.8357	0.2605	0.	0.	0.	0.	4
38 Sr 860	11.50	1.0900	1.0900	1.0900	0.5228	0.0036	0.	0.	0.	0.	1
38 Sr 870	8.44	1.5184	1.5184	1.5184	1.5184	1.5043	0.2844	0.	0.	0.	1
38 Sr 880	11.10	0.2497	0.2759	0.2508	0.2176	0.1119	0.	0.	0.	0.	4
38 Sr 890	6.57	1.2573	1.3068	1.3067	1.3049	1.2976	1.2587	0.9740	0.1368	0.	2
38 Sr 900	7.57	0.4730	0.8285	1.2484	1.3413	1.2970	1.0959	0.2757	0.	0.	2
39 Y 890	11.50	1.2000	1.1633	1.0051	0.8550	0.2021	0.	0.	0.	0.	4
39 Y 900	6.63	1.1947	1.7703	1.7718	1.7718	1.7718	1.5675	0.1327	0.	0.	1
39 Y 910	8.22	0.6391	0.9992	1.2659	1.2786	1.2249	1.0001	0.2532	0.	0.	2
40 Zr 900	12.00	1.1526	1.1318	0.9908	0.6303	0.1433	0.	0.	0.	0.	3
40 Zr 910	7.19	1.1640	1.1640	1.1631	1.1593	1.1450	1.0646	0.5223	0.0072	0.	3
40 Zr 920	8.64	0.8239	1.1402	1.2240	1.2034	1.1206	0.7804	0.0555	0.	0.	3
40 Zr 930	6.50	0.7901	1.1359	1.2919	1.2957	1.2838	1.2228	0.8173	0.0477	0.	2
40 Zr 940	8.23	0.6566	1.0495	1.3246	1.3333	1.2749	1.0076	0.1506	0.	0.	3
40 Zr 950	6.32	0.6320	1.0325	1.3657	1.4062	1.3984	1.3542	1.0248	0.1501	0.	2
40 Zr 960	7.84	0.4836	0.8807	1.3468	1.4409	1.4034	1.2144	0.3025	0.	0.	3
41 Nb 930	8.82	1.0456	1.1466	1.2183	1.2167	1.1006	0.5853	0.0359	0.	0.	3
41 Nb 940	7.37	1.5748	1.6682	1.6682	1.6682	1.6682	1.0453	0.0033	0.	0.	1
41 Nb 950	8.61	0.7521	1.1459	1.2878	1.2780	1.2251	0.9426	0.1174	0.	0.	2
42 Mo 920	12.60	0.6111	0.4189	0.2625	0.1286	0.0078	0.	0.	0.	0.	4
42 Mo 940	9.69	1.3434	1.3434	1.3434	1.3434	0.7289	0.0036	0.	0.	0.	1
42 Mo 950	7.37	1.0195	1.1464	1.1494	1.1463	1.1333	1.0532	0.4602	0.0013	0.	2
42 Mo 960	9.16	0.9351	1.1942	1.2153	1.1897	1.0918	0.6118	0.0124	0.	0.	2
42 Mo 970	6.82	0.8521	1.2015	1.2900	1.2896	1.2835	1.2410	0.8574	0.0375	0.	2
42 Mo 980	8.64	0.6594	1.1055	1.3365	1.3325	1.2741	0.9500	0.1042	0.	0.	2
42 Mo 990	5.74	0.4649	0.8813	1.3299	1.4050	1.4035	1.3914	1.2531	0.3976	0.	2
42 Mo1000	8.30	0.3247	0.6999	1.2794	1.4405	1.4002	1.1528	0.1694	0.	0.	2
43 Tc 990	8.58	1.6976	1.6151	1.5158	1.4255	1.2583	0.7641	0.0616	0.	0.	3
44 Ru 960	10.10	1.2860	1.2860	1.2860	1.2860	0.4096	0.	0.	0.	0.	1
44 Ru 980	10.30	1.2580	1.2580	1.2580	1.2352	0.2812	0.	0.	0.	0.	1
44 Ru 990	7.47	1.5885	1.6542	1.6542	1.6542	1.6542	0.9661	0.0010	0.	0.	1
44 Ru1000	9.67	1.0527	1.2048	1.1986	1.1603	1.0122	0.3640	0.	0.	0.	2
44 Ru1010	6.81	0.9693	1.2480	1.2810	1.2801	1.2752	1.2395	0.8802	0.0440	0.	2
44 Ru1020	9.22	0.8105	1.2268	1.3341	1.3101	1.2065	0.6641	0.0104	0.	0.	2
44 Ru1030	6.40	0.7154	1.1648	1.3906	1.3998	1.3977	1.3800	1.1819	0.2587	0.	2
44 Ru1040	8.89	0.5403	1.0294	1.4149	1.4294	1.3554	0.9336	0.0325	0.	0.	2
44 Ru1050	5.94	0.4676	1.7878	1.8684	1.8684	1.8684	1.8684	0.6255	0.0003	0.	1
44 Ru1060	8.43	0.3658	0.7835	1.3864	1.5235	1.4698	1.1581	0.1513	0.	0.	2
45 Rh1030	9.31	0.7149	0.7347	0.7587	0.7854	0.6931	0.2941	0.	0.	0.	3
45 Rh1050	9.02	0.8100	1.2599	1.3902	1.3744	1.2985	0.8704	0.0438	0.	0.	2

TABLE XVI (Cont.)[a]

Nuclide	Thres.	Group 1	Group 2	Group 3	Group 4	Group 5	Group 6	Group 7	Group 8	Group 9	Meth.[b]
46 Pd1020	10.60	1.2160	1.2160	1.2160	1.1090	0.1455	0.	0.	0.	0.	1
46 Pd1040	10.00	1.1339	1.1912	1.1699	1.1017	0.8830	0.2651	0.	0.	0.	2
46 Pd1050	7.09	1.1415	1.2667	1.2694	1 2669	1.2556	1.1885	0.7040	0.0264	0.	2
46 Pd1060	9.55	1.0561	1.3093	1.3177	1 2726	1.1109	0.5013	0.	0.	0.	2
46 Pd1070	6.55	0.9735	1.3196	1.3927	1.3924	1.3876	1.3544	1.0494	0.1543	0.	2
46 Pd1080	9.23	0.8512	1.2816	1.4264	1.3888	1.2473	0.6485	0.0095	0.	0.	2
46 Pd1100	8.81	0.6536	1.1219	1.4894	1.4958	1.3880	0.9251	0.0456	0.	0.	2
47 Ag1070	9.53	1.4459	1.4736	1.5069	1.4906	1.3428	0.6557	0.	0.	0.	3
47 Ag1090	9.18	1.3373	1.3607	1.3889	1.3795	1.2747	0.7210	0.0140	0.	0.	3
47 Ag1110	8.71	0.7625	1.2607	1.4809	1.4679	1.3867	0.9614	0.0439	0.	0.	2
48 Cd1060	10.90	1.4719	1.5295	1.5908	1.3103	0.6755	0.	0.	0.	0.	4
48 Cd1080	10.30	1.2580	1.2580	1.2580	1.2352	0.2812	0.	0.	0.	0.	1
48 Cd1100	9.86	1.1208	1.3183	1.3144	1.2768	1.1107	0.3215	0.	0.	0.	2
48 Cd1110	6.98	1.0962	1.3693	1.3860	1.3858	1.3818	1.3500	0.9489	0.0427	0.	2
48 Cd1120	9.40	0.9156	1.3612	1.4346	1.4103	1.2994	0.6550	0.0011	0.	0.	2
48 Cd1130	6.54	1.7320	1.7320	1.7320	1.7344	1.6489	1.2379	0.3407	0.	0.	3
48 Cd1140	9.05	0.6314	1.2007	1.5222	1.5184	1.4403	0.9623	0.0471	0.	0.	2
48 Cd1151	6.16	0.6844	1.8016	1.8376	1.8376	1.8376	1.8063	0.4119	0.	0.	1
48 Cd1160	8.69	0.9737	1.2846	1.5347	1.6470	1.5285	0.9043	0.	0.	0.	4
49 In1130	9.43	1.4400	1.4584	1.4849	1.4466	1.1963	0.5119	0.	0.	0.	4
49 In1150	9.03	1.9658	1.8888	1.7230	1.7584	1.2562	0.6081	0.	0.	0.	4
50 Sn1120	11.10	1.2125	1.2658	1.2882	1.1726	0.7195	0.	0.	0.	0.	4
50 Sn1140	10.30	1.2580	1.2580	1.2580	1.2352	0.2812	0.	0.	0.	0.	1
50 Sn1150	7.54	1.5945	1.6444	1.6444	1.6444	1.6444	0.9152	0.0002	0.	0.	1
50 Sn1160	9.56	1.3616	1.3616	1.3616	1.3616	0.8342	0.0085	0.	0.	0.	1
50 Sn1170	6.94	1.0556	1.4392	1.4880	1.4878	1.4845	1.4543	1.0480	0.0485	0.	2
50 Sn1180	9.33	0.9387	1.4301	1.5278	1.5019	1.3853	0.7303	0.0057	0.	0.	2
50 Sn1190	6.48	0.8340	1.3743	1.5767	1.5810	1.5797	1.5643	1.3242	0.2247	0.	2
50 Sn1200	9.11	0.6909	1.2809	1.6037	1.5953	1.5000	0.9581	0.0435	0.	0.	2
50 Sn1220	8.80	0.4662	1.0294	1.6250	1.6847	1.6314	1.2361	0.0690	0.	0.	2
50 Sn1230	5.90	0.4975	1.0374	1.6401	1.7290	1.7280	1.7179	1.5728	0.5098	0.	2
50 Sn1240	8.51	0.3164	0.7812	1.5570	1.7521	1.7176	1.4339	0.2020	0.	0.	2
50 Sn1250	5.75	0.3006	1.7540	1.8950	1.8950	1.8950	1.8950	0.8562	0.0061	0.	1
50 Sn1260	8.19	0.2016	0.5523	1.3834	1.8001	1.7893	1.5920	0.4178	0.	0.	2
51 Sb1210	9.25	1.5344	1.7037	1.7480	1.5208	1.1253	0.5091	0.	0.	0.	4
51 Sb1230	8.98	1.1685	1.2826	1.3405	1.2521	1.1244	0.6345	0.	0.	0.	4
51 Sb1240	6.45	1.0088	1.7893	1.7970	1.7970	1.7970	1.6706	0.2150	0.	0.	1
51 Sb1250	8.71	0.5500	1.1554	1.6848	1.7212	1.6742	1.3143	0.0994	0.	0.	2
51 Sb1260	6.31	0.8510	1.7987	1.8166	1.8166	1.8166	1.7412	0.2991	0.	0.	1
52 Te1200	10.30	1.2580	1.2580	1.2580	1.2352	0.2812	0.	0.	0.	0.	1
52 Te1220	10.10	1.2860	1.2860	1.2860	1.2860	0.4096	0.	0.	0.	0.	1
52 Te1230	6.94	1.4238	1.7284	1.7284	1.7284	1.7284	1.3635	0.0459	0.	0.	1
52 Te1240	9.41	1.3826	1.3826	1.3826	1.3826	0.9465	0.0183	0.	0.	0.	1
52 Te1250	6.60	0.9657	1.5021	1.6600	1.6614	1.6581	1.6304	1.3031	0.1961	0.	2
52 Te1260	9.09	1.4274	1.4274	1.4274	1.4274	1.1755	0.0598	0.	0.	0.	1
52 Te1271	6.35	0.7371	1.3426	1.7146	1.7331	1.7311	1.7143	1.4825	0.3022	0.	2
52 Te1280	8.75	0.5062	1.1065	1.7024	1.7545	1.7033	1.3131	0.0834	0.	0.	2
52 Te1291	6.08	0.5291	1.1064	1.7164	1.7960	1.7948	1.7827	1.6085	0.6255	0.	2
52 Te1300	8.39	0.3565	0.8544	1.6360	1.8154	1.7790	1.4970	0.1908	0.	0.	2
52 Te1320	8.05	0.2894	0.7030	1.5215	1.8613	1.8383	1.6203	0.4442	0.	0.	2
53 I 1270	9.15	0.9901	1.4969	1.7154	1.6332	1.3796	0.6892	0.0228	0.	0.	4
53 I 1290	8.77	0.7559	1.3977	1.7222	1.7226	1.6661	1.2511	0.0645	0.	0.	2
53 I 1300	6.58	1.1471	1.7762	1.7788	1.7788	1.7788	1.5999	0.1528	0.	0.	1
53 I 1310	8.34	0.5546	1.1660	1.7402	1.7871	1.7376	1.3801	0.1691	0.	0.	2
53 I 1350	7.78	1.5955	1.6108	1.6108	1.6108	1.6108	0.7357	0.	0.	0.	1
54 Xe1240	10.50	0.9901	1.0039	0.9887	0.9337	0.7405	0.1160	0.	0.	0.	3
54 Xe1260	10.20	1.4241	1.5144	1.5073	1.4598	1.2365	0.3491	0.	0.	0.	3
54 Xe1280	9.48	1.3679	1.7962	1.8333	1.7966	1.6401	0.8238	0.	0.	0.	3
54 Xe1290	6.91	1.3337	1.8223	1.9000	1.9000	1.8951	1.8462	1.3032	0.0388	0.	3
54 Xe1300	9.26	1.0740	1.7296	1.9210	1.9060	1.7984	0.9851	0.0165	0.	0.	3
54 Xe1310	6.60	1.0198	1.6829	1.9451	1.9500	1.9500	1.9225	1.5508	0.2311	0.	3
54 Xe1320	8.93	0.7959	1.5092	1.9439	1.9585	1.8822	1.3262	0.0740	0.	0.	3
54 Xe1330	6.58	0.7627	1.3873	1.7797	1.8008	1.7980	1.7739	1.4733	0.1969	0.	2
54 Xe1340	8.46	0.6328	1.2912	1.9311	2.0085	1.9470	1.5439	0.2048	0.	0.	3
54 Xe1350	6.48	1.0426	1.7866	1.7928	1.7928	1.7928	1.6545	0.1993	0.	0.	1
54 Xe1360	7.88	0.4218	0.8928	1.5352	1.6975	1.6661	1.4564	0.4071	0.	0.	3
55 Cs1330	9.04	1.5941	1.6027	1.6129	1.6023	1.5302	1.0537	0.0532	0.	0.	3
55 Cs1340	6.82	0.9550	1.5542	1.7676	1.7708	1.7653	1.7209	1.2148	0.0409	0.	2

TABLE XVI (Cont.)[a]

	Nuclide	Thres.	Group 1	Group 2	Group 3	Group 4	Group 5	Group 6	Group 7	Group 8	Group 9	Meth.[b]
55	Cs1350	8.86	0.8554	1.4982	1.7913	1.7853	1.7143	1.2585	0.0667	0.	0.	2
55	Cs1360	6.64	0.9028	1.5225	1.8232	1.8328	1.8273	1.7853	1.3167	0.0845	0.	2
55	Cs1370	8.38	0.6543	1.2660	1.8051	1.8491	1.8034	1.5123	0.2435	0.	0.	2
56	Ba1340	9.25	1.1808	1.6488	1.6945	1.6701	1.5476	0.8420	0.	0	0.	2
56	Ba1350	7.20	1.1942	1.6675	1.7378	1.7371	1.7313	1.6828	1.1586	0.0514	0.	2
56	Ba1360	9.23	1.0015	1.6000	1.7659	1.7472	1.6517	1.0740	0.0498	0.	0.	2
56	Ba1370	6.95	1.0740	1.6408	1.8037	1.8041	1.7982	1.7486	1.2177	0.0388	0.	2
56	Ba1380	8.54	0.4768	0.5573	1.3206	1.4996	1.5000	1.4623	0.3682	0.	0.	3
56	Ba1400	6.22	0.0140	0.0479	0.2203	0.6982	1.5349	1.8717	1.6186	0.2397	0.	2
57	La1390	8.79	1.1761	1.6978	1.8010	1.7824	1.7001	1.2328	0.0736	0.	0.	2
57	La1400	5.05	0.3824	0.8205	1.5506	1.8329	1.8387	1.8353	1.7833	1.3321	0.2387	2
58	Ce1400	9.04	0.6426	0.8390	1.0923	1.2978	1.0902	0.5304	0.	0.	0.	4
58	Ce1410	5.49	0.5925	1.1308	1.7117	1.8089	1.8083	1.8026	1.7221	1.0410	0.0122	2
58	Ce1420	7.21	1.0025	1.3068	1.6083	1.7521	1.7385	1.2060	0.4836	0.	0.	4
58	Ce1430	5.22	0.0542	0.1691	0.6210	1.4055	1.8489	1.8695	1.8389	1.4585	0.2819	2
58	Ce1440	6.92	0.0265	0.0926	0.4150	1.1581	1.8282	1.8671	1.3932	0.0510	0.	2
59	Pr1410	9.36	1.7343	1.8088	1.8546	1.7009	1.1501	0.4647	0.	0.	0.	4
59	Pr1420	5.90	0.8251	1.3925	1.7523	1.7758	1.7740	1.7619	1.6133	0.6053	0.0013	2
59	Pr1430	7.23	0.1334	0.3681	1.0523	1.7103	1.8015	1.7339	0.8805	0.0061	0.	2
60	Nd1420	9.81	1.6292	1.6931	1.6741	1.6072	1.3649	0.4168	0.	0.	0.	2
60	Nd1430	6.10	1.1100	1.5977	1.7369	1.7381	1.7358	1.7163	1.5002	0.5359	0.	2
60	Nd1440	7.83	0.2552	0.6331	1.4116	1.7641	1.7578	1.6278	0.5047	0.	0.	2
60	Nd1450	5.74	0.1851	0.4927	1.2600	1.7770	1.8110	1.8058	1.7141	0.7830	0.0041	2
60	Nd1460	7.56	0.1094	0.3306	1.0478	1.7523	1.8341	1.7499	0.8853	0.	0.	2
60	Nd1470	5.31	0.0838	0.2566	0.8648	1.6575	1.8740	1.8741	1.8370	1.3122	0.0885	2
60	Nd1480	7.33	0.0401	0.1429	0.6183	1.4946	1.8909	1.8510	1.0013	0.0087	0.	2
60	Nd1500	7.33	0.0272	0.1030	0.4976	1.3702	1.9284	1.9033	0.9934	0.0050	0.	2
61	Pm1470	7.57	0.1890	0.5281	1.3590	1.7970	1.8004	1.7053	0.7988	0.	0.	2
61	Pm1480	5.86	0.1546	0.4420	1.2313	1.8055	1.8457	1.8404	1.7372	0.6546	0.0006	2
61	Pm1481	5.86	0.1546	0.4420	1.2313	1.8055	1.8457	1.8404	1.7372	0.6546	0.0006	2
61	Pm1490	7.29	0.0743	0.2487	0.9153	1.7277	1.8733	1.8305	1.0559	0.0159	0.	2
61	Pm1510	7.66	0.0867	0.2964	1.0744	1.8514	1.9245	1.8125	0.5259	0.	0.	2
62	Sm1440	10.50	1.6807	1.7432	1.6600	1.4329	0.7143	0.0864	0.	0.	0.	4
62	Sm1470	6.33	0.4213	0.9567	1.6280	1.7370	1.7360	1.7240	1.5156	0.2826	0.	2
62	Sm1480	8.14	0.2852	0.7477	1.5636	1.7721	1.7545	1.5851	0.4466	0.	0.	2
62	Sm1490	5.85	0.5996	1.2033	1.6380	1.7827	1.7186	1.5540	1.1081	0.1962	0.0008	3
62	Sm1500	7.98	0.1324	0.4214	1.2799	1.8237	1.8348	1.7137	0.5658	0.	0.	2
62	Sm1510	5.68	0.1255	0.3902	1.1998	1.8328	1.8790	1.8773	1.8257	1.1968	0.0172	2
62	Sm1520	8.22	0.1186	0.3964	1.2855	1.8823	1.8913	1.7145	0.3312	0.	0.	2
62	Sm1530	5.93	0.2033	0.5987	1.5322	1.9326	1.9383	1.9353	1.8534	0.7662	0.0015	2
62	Sm1540	7.90	0.1196	0.4015	1.3121	1.9368	1.9541	1.8361	0.6202	0.	0.	2
63	Eu1510	7.93	1.3496	1.9457	2.1567	2.1700	2.0650	1.4792	0.1345	0.	0.	3
63	Eu1520	6.29	0.7256	1.4282	2.0934	2.2118	2.2082	2.0235	1.1042	0.1056	0.	3
63	Eu1530	8.54	0.8561	1.4641	1.9666	2.0241	1.9687	1.6092	0.3057	0.	0.	3
63	Eu1540	6.47	1.2868	1.8978	2.1744	2.2113	2.1956	1.9305	0.7621	0.0182	0.	3
63	Eu1550	7.96	0.2561	0.7529	1.7056	1.9386	1.9255	1.7695	0.5130	0.	0.	2
63	Eu1560	6.28	0.3152	0.8318	1.7368	1.9683	1.9678	1.9568	1.7452	0.3548	0.	2
63	Eu1570	7.66	0.1599	0.4803	1.3830	1.9670	1.9876	1.9197	1.0661	0.	0.	2
64	Gd1520	8.51	0.4078	1.0376	1.7833	1.8644	1.8372	1.5570	0.2150	0.	0.	3
64	Gd1540	8.61	0.4070	1.0595	1.8222	1.8993	1.8710	1.5713	0.2070	0.	0.	3
64	Gd1550	6.46	0.4437	1.0891	1.8047	1.8819	1.8813	1.8725	1.6673	0.2586	0.	3
64	Gd1560	8.53	0.3447	0.9462	1.7925	1.9098	1.8866	1.6318	0.2398	0.	0.	3
64	Gd1570	6.35	0.4303	1.0484	1.8307	1.9432	1.9422	1.9308	1.7133	0.3154	0.	3
64	Gd1580	7.93	0.2456	0.6905	1.6368	1.9665	1.9560	1.8214	0.4948	0.	0.	3
64	Gd1600	7.38	0.1162	0.3605	1.1666	1.9349	2.0152	1.9409	1.0639	0.	0.	3
65	Tb1590	8.18	0.3705	0.9757	1.8180	1.9429	1.9286	1.7707	0.5233	0.	0.	2
65	Tb1600	6.46	0.3076	0.8246	1.7398	1.9734	1.9733	1.9630	1.7522	0.3215	0.	2
66	Dy1600	8.59	0.5481	1.2702	1.8761	1.9112	1.8820	1.5951	0.2229	0.	0.	2
66	Dy1610	6.45	0.4796	1.1329	1.8620	1.9470	1.9460	1.9340	1.6946	0.2465	0.	2
66	Dy1620	8.20	0.3182	0.8588	1.7743	1.9729	1.9542	1.7661	0.4842	0.	0.	2
66	Dy1630	6.25	0.3127	0.8319	1.7574	2.0032	2.0033	1.9951	1.8161	0.4378	0.	2
66	Dy1640	7.66	0.2715	0.5879	1.3930	2.1381	2.1261	1.8156	0.6105	0.0001	0.	3
67	Ho1650	8.04	0.3291	0.8835	1.8068	2.0038	1.9896	1.8405	0.5818	0.	0.	2
68	Er1660	8.55	0.4806	1.1591	1.9010	1.9749	1.9463	1.6734	0.2500	0.	0.	2
68	Er1670	6.44	0.4902	1.1375	1.9038	2.0090	2.0075	1.9927	1.7319	0.2608	0.	2

TABLE XVI (Cont.)[a]

Nuclide	Thres.	Group 1	Group 2	Group 3	Group 4	Group 5	Group 6	Group 7	Group 8	Group 9	Meth.[b]
					*** Actinides ***						
90 Th2300	6.79	1.3284	1.4902	1.5725	1.6687	1.7767	1.8000	1.4715	0.1226	0.	3
90 Th2320	6.34	0.3476	0.4129	0.7123	1.3782	1.8444	1.9548	1.5153	0.2349	0.	3
91 Pa2310	6.81	0.8712	1.0845	1.1726	1.3159	1.4619	1.2905	0.9810	0.0817	0.	3
91 Pa2330	6.66	0.3961	0.4237	0.4572	0.5148	0.5487	0.5655	0.4944	0.0490	0.	3
92 U 2320	7.26	1.4856	1.5886	1.6003	1.7010	1.7793	1.5905	0.8430	0.0365	0.	3
92 U 2330	5.74	0.0778	0.1758	0.3714	0.5012	0.4726	0.3761	0.2707	0.1810	0.0027	3
92 U 2340	6.77	0.2020	0.2020	0.2025	0.3619	0.4560	0.3157	0.1596	0.0105	0.	3
92 U 2350	5.31	0.0141	0.0614	0.1617	0.2887	0.4273	0.4521	0.4011	0.2303	0.0178	3
92 U 2360	6.91	0.2500	0.2500	0.2509	0.5212	0.8819	0.9395	0.8034	0.1269	0.	3
92 U 2370	5.12	0.2500	0.2500	0.2500	0.3127	0.6312	1.3385	1.3276	0.7075	0.0349	3
92 U 2380	6.14	0.1461	0.1931	0.4176	0.8530	1.2997	1.4348	1.2478	0.3532	0.	3
93 Np2370	6.76	0.0080	0.0339	0.0997	0.1867	0.2414	0.2309	0.1539	0.0139	0.	3
93 Np2380	5.35	0.0100	0.0100	0.0105	0.1786	0.5254	0.7128	0.6688	0.3524	0.0035	5
94 Pu2360	7.33	0.1000	0.1000	0.1016	0.5954	0.7977	0.7217	0.3452	0.0053	0.	3
94 Pu2370	5.83	0.0500	0.0500	0.0508	0.2649	0.3651	0.3139	0.1921	0.0380	0.0001	3
94 Pu2380	6.97	0.1786	0.1492	0.1154	0.5673	1.0589	1.0408	0.5028	0.0092	0.	3
94 Pu2390	5.66	0.0089	0.0380	0.1142	0.1990	0.2356	0.2288	0.1920	0.0991	0.0016	3
94 Pu2400	6.53	0.0089	0.0380	0.1142	0.1882	0.2321	0.2280	0.1519	0.0143	0.	3
94 Pu2410	5.25	0.0310	0.0310	0.0311	0.1059	0.4211	0.5734	0.6833	0.6520	0.1029	3
94 Pu2420	6.30	0.0084	0.0296	0.1372	0.4012	0.7399	0.7974	0.6110	0.1038	0.	3
94 Pu2430	5.04	0.2000	0.2000	0.2001	0.2226	0.3653	1.2192	1.2859	1.3626	0.4654	3
94 Pu2440	5.99	0.1000	0.1000	0.1005	0.2618	0.6142	1.1128	1.4579	0.6212	0.	3
95 Am2410	6.63	0.0500	0.0501	0.0680	0.1300	0.2100	0.2021	0.1254	0.0117	0.	3
95 Am2420	5.55	0.0100	0.0100	0.0105	0.1786	0.5254	0.7128	0.6688	0.3524	0.0035	5
95 Am2421	5.46	0.0100	0.0100	0.0105	0.1786	0.5254	0.7128	0.6688	0.3524	0.0035	3
95 Am2430	6.35	0.0400	0.0400	0.0400	0.0400	0.1101	0.1400	0.0664	0.0115	0.	3
96 Cm2410	6.04	0.0050	0.0050	0.0050	0.0079	0.0103	0.0135	0.0209	0.0167	0.	3
96 Cm2420	6.94	0.0050	0.0050	0.0050	0.0094	0.0151	0.0220	0.0224	0.0015	0.	3
96 Cm2430	5.68	0.0300	0.0300	0.0301	0.0736	0.1965	0.3152	0.4792	0.4259	0.0038	3
96 Cm2440	6.77	0.0500	0.0500	0.0500	0.0901	0.4578	0.5849	0.4260	0.0329	0.	3
96 Cm2450	5.52	0.2128	0.2319	0.2496	0.2500	0.5685	0.8465	0.8481	0.6573	0.0628	3
96 Cm2460	6.34	0.	0.	0.0075	0.0393	0.5881	1.2759	0.5224	0.0323	0.	3
96 Cm2470	5.15	0.1000	0.1000	0.1000	0.1000	0.2460	0.8632	0.8167	0.8520	0.2569	3
96 Cm2480	6.18	0.1000	0.1000	0.1004	0.2175	0.5378	0.9029	0.6213	0.1002	0.	3
97 Bk2490	6.20	0.2000	0.2138	0.2577	0.3069	0.9937	1.6618	1.4613	0.5815	0.	3
98 Cf2490	5.59	0.1036	0.1506	0.1681	0.1840	0.3928	1.1617	0.9860	0.7146	0.0443	3
98 Cf2500	6.61	0.1000	0.1036	0.1363	0.1946	0.5320	1.0333	0.8802	0.2588	0.	3
98 Cf2510	5.10	0.1000	0.1025	0.1348	0.1674	0.3626	1.1586	1.0125	1.0325	0.2745	3
98 Cf2520	6.17	0.1500	0.1500	0.1500	0.1500	0.1666	0.5906	0.5300	0.2661	0.	3
98 Cf2530	5.15	0.1000	0.1000	0.1000	0.1000	0.2460	0.8632	0.8167	0.8520	0.2569	5
99 Es2530	6.45	0.2000	0.2138	0.2577	0.3069	0.9937	1.6618	1.4613	0.5815	0.	5

[a]Listed values apply for the highest energy groups in the PRS group structure:

Group	Energy Range (MeV)	
1	20.000	18.221
2	18.221	16.905
3	16.905	14.918
4	14.918	13.499
5	13.499	11.912
6	11.912	10.000
7	10.000	7.788
8	7.788	6.065
9	6.065	4.724

Threshold values are listed in MeV.

[b]Meth. refers to the origin of these cross sections:
1 refers to unpublished model based on Q-values (R. E. Schenter, Hanford Engineering Development Laboratory, Richland, Washington).
2 refers to values produced by the THRESH code.
3 refers to ENDF/B-V evaluations.
4 refers to values based on BNL-325 plots.
5 refers to values based on Q values similar to one of the above.

D Delayed Neutron Pn Values [T. R. England, W. B. Wilson, F. M. Mann (HEDL), and R. E. Schenter (HEDL)]

Part of the continuing effort described in Ref. 81 to improve the ENDF/B delayed neutron spectra requires a new evaluation of the Pn emission probabilities. Reference 82 contains an evaluation of experimental values for 77 precursors. These have subsequently been augmented with calculated values based on systematics for an additional 23 precursors. The equations used for the systematics are given in Ref. 82. We have also examined all 877 fission products in ENDF/B-V for additional precursors based on Q-values and neutron binding energies. We found a total of 262 precursors but most were not significant because of either a small fission yield, Pn value or both.

E. Status of Fission-Product and Actinide Data for ENDF/B-VI [T. R. England, P. G. Young, R. E. Schenter (HEDL), F. Mann (HEDL), and C. W. Reich (INEL)

The problems found with ENDF/B-V data, and anticipated extensions and improvements for ENDF/B-VI are summarized in Ref. 83. This was presented by P. G. Young at the March 12-16 Nuclear Energy Agency Nuclear Data Committee (NEANDC) Meeting in Tokai, Japan.

F SOURCES Calculation of TMI-2 Spontaneous-Fission and (α,n) Neutron Sources [W. B. Wilson, T. R. England, W. C. Hopkins (Bechtel Power Corp.), and R. T. Perry (Texas A & M)]

The fuel of TMI-2 is now flooded with water containing 5000 ppm boron to increase its shutdown margin; however, the signal from the source-range detector (SRD) of TMI-2 from its low exposure core ($\sim$ 3.2 GWd/tU) is currently 3-4 times that of the SRD signal of TMI-1 from an end-of-equilibrium cycle core. The higher curie inventories of spontaneously-fissioning and alpha-emitting actinide nuclides associated with higher exposure result in spontaneous-fission (SF) and $^{17,18}O(\alpha,n)$ neutron sources that increase with exposure of oxide fuel.[84] Much of the TMI-2 fuel is no longer clad, and some of it has been mechanically reduced to fine particles by the blades of coolant pumps.

The SRD signal of TMI-2, relative to that of TMI-1, is diminished by the presence of the high boron concentration in the water and the low exposure of the fuel. Fuel disruption increases the SRD signal by increasing the magnitude of the (α,n) source and, possibly, by increasing neutron multiplication. The (α,n) source of the disrupted fuel flooded with boron-rich water is composed of neutrons from $^{17,18}O(\alpha,n)$ reactions with oxygen in the fuel and water and from $^{10,11}B(\alpha,n)$ reactions.

The SF and (α,n) neutron sources of TMI-2 were produced from full-core actinide inventories calculated with CINDER-2 using a library of ENDF/B-V data[85] and following a 22-step histogram power history resolved for earlier TMI-2 fuel calculations.[86-88] These actinide inventories were used in SOURCES calculations describing the neutron production from the SF decay of actinides and (α,n) reactions of their decay alphas with $^{10,11}B$ and $^{17,18}O$. The (α,n) calculations used σ(α,n) data for $^{17,18}O$ as resolved in Ref. 89 from measured data and for ^{NAT}B as measured by Walker;[90] polynomial fits to the data of Ziegler[91] were used to describe alpha-particle stopping cross sections of the various elements.

The neutron sources were calculated for the undisturbed, clad TMI-2 oxide fuel and for the extreme limiting condition in which each alpha particle is emitted into the boron-rich water. The results of these calculations, given in Table XVII, show that the TMI-2 neutron source from actinide decay could be increased by no more than a factor of ~ 5 by complete dispersion of actinides in the boron-rich water.

Earlier inherent neutron-source survey calculations (see Ref. 84, pp. 86-87) indicate that the neutron source of the end-of-equilibirum cycle TMI-1 core should be 300-500 times that of the undisturbed low-exposure TMI-2 core. The high SRD signal of TMI-2 is not due to higher SF and (α,n) source rates and may therefore indicate a much higher neutron multiplication than that of TMI-1.

TABLE XVII

COMPARISON OF TMI-2 SPONTANEOUS-FISSION AND (α,n) NEUTRON SOURCES WITH ALL ALPHA PARTICLES ASSUMED EMITTED INTO THE OXIDE FUEL AND WITH ALL ALPHA PARTICLES ASSUMED EMITTED INTO WATER CONTAINING 5000 ppm BORON

	Core Neutron Source (n/s)	
Source	Oxide Fuel	H_2O w/5000 ppm B
$^{17}O(\alpha,n)$	6.179×10^5	3.009×10^6
$^{18}O(\alpha,n)$	7.379×10^6	3.601×10^7
$^{NAT}B(\alpha,n)$	0.	4.947×10^7
Total(α,n)	7.997×10^6	8.849×10^7
S.F.	1.163×10^7	1.163×10^7
Total	1.963×10^7	1.001×10^8

G. Gamma Fraction of Total Decay Power of Discharged BWR Fuel (W. B. Wilson, T. R. England, and R. J. LaBauve)

Planned experiments of the solid dry storage of spent BWR fuel assemblies require the knowledge of the gamma fraction (GF) of total assembly decay power. We have calculated the GF of total decay power for 4.5% enrichment fuel at three void fractions and three exposures in Grand Gulf-1 and -2, using resonance self-shielded cross sections produced by EPRI-CELL in an earlier study.[92] Also, we have calculated the GF for a Quad Cities-1 2.56% enriched fuel sample described in Ref. 88. All calculations evaluated the GF at cooling times from one week to six years. The results of the calculations are given in Table XVIII.

TABLE XVIII

EXAMINATION OF THE DEPENDENCE OF THE BWR GAMMA FRACTION OF TOTAL DECAY POWER ON INITIAL ^{235}U ENRICHMENT, DISCHARGE EXPOSURE, MODERATOR VOID, AND COOLING TIME

Unit	GG1&2	GG1&2	GG1&2	GG1&2	GG1&2	GG1&2	GG1&2	GG1&2	GG1&2	QC-1
Power Density, W/cc.	299.4	299.4	299.4	299.4	299.4	299.4	299.4	299.4	299.4	Varies
Initial 235U Enrichment, %	4.5	4.5	4.5	4.5	4.5	4.5	4.5	4.5	4.5	2.56
Discharge Exposure, GWd/tU	17.9	35.5	53.1	17.9	35.7	53.4	18.0	35.8	53.7	11.8
Moderator Void, %	0	0	0	40	40	40	70	70	70	0
Gamma Fraction of Total Decay Power @cooling times--										
1 week	.5631	.5460	.5384	.5633	.5460	.5373	.5635	.5462	.5367	.5695
1 month	.5094	.4820	.4705	.5104	.4825	.4693	.5115	.4833	.4690	.5211
2 months	.4650	.4303	.4167	.4658	.4307	.4160	.4666	.4316	.4164	.4771
3 months	.4329	.3955	.3835	.4334	.3961	.3835	.4341	.3973	.3846	.4454
6 months	.3373	.3135	.3190	.3382	.3162	.3214	.3395	.3198	.3253	.3492
1 year	.1919	.2293	.2730	.1963	.2372	.2792	.2015	.2466	.2874	.1956
1.5 years	.1601	.2293	.2872	.1669	.2397	.2945	.1746	.2516	.3038	.1588
2 years	.1728	.2536	.3138	.1807	.2647	.3208	.1897	.2775	.3297	.1694
2.5 years	.1968	.2813	.3388	.2053	.2926	.3449	.2150	.3054	.3526	.1923
3 years	.2231	.3067	.3587	.2319	.3177	.3636	.2419	.3300	.3697	.2179
3.5 years	.2482	.3276	.3727	.2570	.3379	.3761	.2669	.3493	.3803	.2429
4 years	.2701	.3430	.3809	.2786	.3525	.3828	.2882	.3629	.3851	.2652
4.5 years	.2876	.3530	.3840	.2957	.3616	.3844	.3048	.3707	.3849	.2835
5 years	.3004	.3583	.3830	.3080	.3659	.3821	.3164	.3737	.3810	.2974
5.5 years	.3090	.3598	.3791	.3159	.3663	.3770	.3235	.3728	.3744	.3071
6 years	.3141	.3585	.3733	.3202	.3640	.3700	.3271	.3693	.3661	.3131

Decay power data calculated with CINDER-2 using ENDF/B-V data and temporal self-shielded actinide cross sections from earlier EPRI-CELL calculations of Grand Gulf 1 and 2 [see Los Alamos report LA-9563-MS, NUREG/CR-3108 (February 1983), pp. 8-10, 19-20] and Quad Cities-1 [see Electric Power Research Institute report EPRI NP-2855, "Proceedings: Thermal Reactor Benchmark Calculations, Techniques, Results and Applications," (February 1983)].

Within the scope of this limited study, the following observations can be made:

1. The GF of low-exposure (12-18 GWd/tU) fuel reaches a minimum at ~ 1½ year cooling and is continuing to increase at six years cooling.
2. The GF of typical discharge exposure (~ 36 GWd/tU) fuel reaches a minimum at ~ one year cooling and a maximum at 5-5½ years cooling.
3. The GF of high exposure (~ 53 GWd/tU) fuel reaches a minimum at ~ one year cooling and a maximum at 4-4½ years cooling.
4. At cooling times less than 6 months, the GF is insensitive to moderator void and decreases with exposure.
5. At cooling times greater than six months, the GF increases with moderator void and exposure.

H. PWR Fission-Product Inventory Calculations for the ANS Special Committee on Fission-Product Source Terms (W. B. Wilson, T. R. England, and R. J. LaBauve)

An ANS Special Committee on Fission-Product Source Terms is presently working to define the characteristics of the inventory and properties of fission products liberated in hypothetical reactor accidents. On their behalf, we have performed EPRI-CELL/CINDER-2 calculations with ENDF/B-V data following 2.8% enriched fuel through equilibrium cycles at 60% duty factor in North Anna-2. These cycles each consisted of six equal 876-h up periods "u" separated by 508.8-h down periods "d," and followed by a 960-h end-of-cycle down period "D." The three equal regions at mid cycle have power histories as follows:

Region 1: ududu
Region 2: udududududuDududu
Region 3: udududududuDudududududuDududu.

The three-region and total core atom and gram inventories are listed in Table XIX, along with a comparison of unstable and stable fission products. Although all actinides eventually experience spontaneous fission or decay to the stable $^{206\text{-}208}Pb$ and ^{209}Bi, actinides existing in the time frame of this study are unstable.

TABLE XIX

CHARACTERISTICS OF MID-EQUILIBRIUM CYCLE NORTH ANNA-2 PWR INVENTORY

QUANTITY	REGION 1	REGION 2	REGION 3	TOTAL CORE
ELAPSED HOURS IN CORE	3.64560E+03	1.24056E+04	2.11656E+04	
ELAPSED FULL-POWER-HOURS	2.62800E+03	7.88400E+03	1.31400E+04	
BURNUP, ATOM % FISSION	4.36154E-01	1.29483E+00	2.14351E+00	
EXPOSURE, MWD/TU	4.21378E+03	1.26212E+04	2.10399E+04	
FISSION-PRODUCT ATOMS	5.68038E+26	1.68735E+27	2.79200E+27	5.04799E+27
UNSTABLE F-P ATOMS	1.68705E+26	4.11701E+26	6.44199E+26	1.22461E+27
ACTINIDE ATOMS	6.49352E+28	6.43773E+28	6.38263E+28	1.93139E+29
TOTAL ATOMS	6.55038E+28	6.60647E+28	6.66183E+28	1.98187E+29
FISSION-PRODUCT GRAMS	1.10458E+05	3.28466E+05	5.44420E+05	9.83343E+05
UNSTABLE F-P GRAMS	3.23460E+04	8.02047E+04	1.26634E+05	2.39185E+05
ACTINIDE GRAMS	2.56441E+07	2.54263E+07	2.52105E+07	7.62810E+07
TOTAL GRAMS	2.57546E+07	2.57548E+07	2.57549E+07	7.72643E+07
FRACTIONS: FP ATOMS/(FP+ACT ATOMS)	8.68099E-03	2.55409E-02	4.19105E-02	2.54709E-02
F-P ATOMS, UNSTABLE	2.96684E-01	2.43992E-01	2.30730E-01	2.42593E-01
F-P GRAMS, UNSTABLE	2.92837E-01	2.44180E-01	2.32604E-01	2.43236E-01

IV. CORE NEUTRONICS CODE DEVELOPMENT AND APPLICATION (R. J. LaBauve, T. R. England, D. C. George, R. E. MacFarlane, and W. B. Wilson)

We have completed a coupled Nuclear Data, Neutronics/Depletion Code System (DANDE) for neutronics calculations, and this system is now being used by the Los Alamos National Laboratory reactor design group in their reactor design calculations. A general layout of the code system is shown in Fig. 33; our approach has been to link existing, proven codes through the use of a local controller (CTL) and to transfer files via a standard interface system.[93]

In Fig. 33, the three calculational modules are designated by rectangles and the interface files by circles. At present, the cross-section processing module consists of the TRANSX code[94] operating on a fine-group cross-section library (80 groups) generated by the NJOY code[67] from the ENDF/B-V[95] basic data file. TRANSX produces neutron, photon, or coupled transport cross-section tables in the standard ISOTXS format with options for adjoint tables, mixtures, self-shielding/Doppler corrections, group collapse, cell homogenization, thermal upscatter, prompt or steady-state fission, transport corrections, elastic

removal corrections, and flexible response function edits. Weighting fluxes for group collapse derived from one-, two-, or three-dimensional diffusion or discrete ordinates core model calculations done in the core calculational module can be transferred directly to TRANSX via the standard RZFLUX file. In principle, the CTL controller could be used to update the microscopic cross sections of the principal nuclides during a depletion run; but, as we have not done this to date, this path is not indicated in Fig. 33.

At present, in the core calculational module, we are using the DIF3D diffusion code[96] (both finite differences and nodal options) and the TWODANT[97] and TWOHEX[98] discrete ordinates transport codes. Our largest problems (e.g., three-dimensional HEX-Z, DIF3D 1/3 core model of the FTF in 13 planes and 80 groups) can only be run on our largest Cray machine (1.8-M word storage). Such problems run in about 12 minutes. The running times for two-dimensional problems using the Sn codes are comparable to those for three-dimensional problems with the diffusion code.

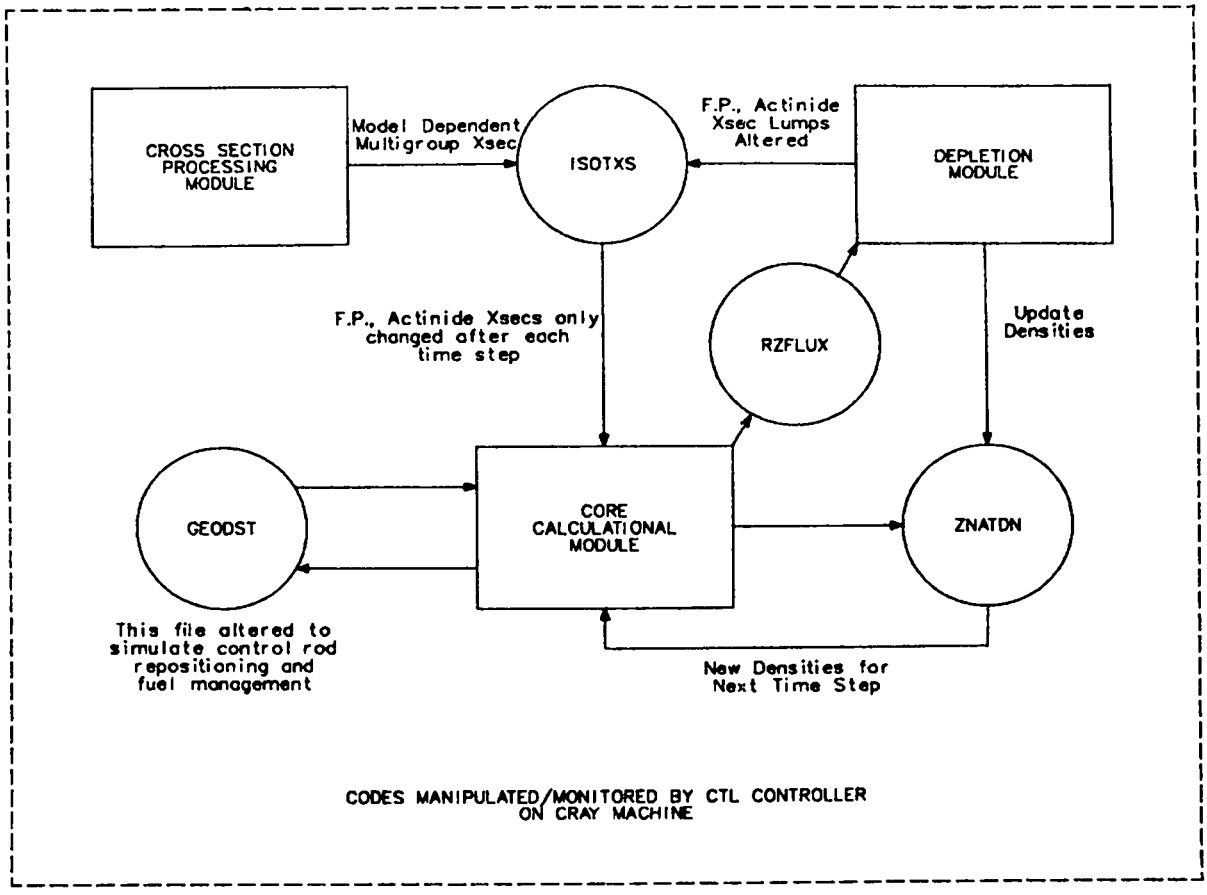

Fig. 33. Code system for neutronics calculations.

The depletion module is a modified version of the CINDER-2 code[99] that we are calling CINDER-3. This code does summation calculations over the various fission-product and actinide chains and provides updated nuclear densities for the principal nuclides and groups the remaining actinides and fission-products into lumps. In fact, the capability also exists for updating all the microscopic cross sections for the lumps at each time step, but thus far we are only updating the capture cross sections.

As an example of the flexibility of the CTL controller in manipulating and monitoring this code system, consider the problem of control rod repositioning to keep a fairly level k_{eff} during a depletion run. The model used in this example is the core of a carbide version of a modular breeder reactor, currently being studied at Los Alamos. This model consists of eight rings of hexagonal assemblies in 11 vertical planes; 8-group cross sections were used in the DIF3D one-sixth core, HEX-Z calculations. The hypothetical power history chosen for the problem was four periods of 200 days at full power, the first three of which were followed by 100 days at shutdown (total time of 1100 days) and depletion was calculated for Driver-1, Driver-2, radial- and axial-blanket regions in time steps of 100 days. The CTL Controller examined k_{eff} after each time step; and, if this fell below a certain allowed value, it repositioned the outer control assembly bank a predetermined amount. In this manner, k_{eff} stayed between 1.000 and 1.035. A parallel problem was run in which the control assemblies were not repositioned and depletion was calculated using an average power (70% of full). A comparison of the behavior of the peak/average power for the two runs is shown in Fig. 34, illustrating the necessity of the more detailed calculation. The CRAY running time for a single time step averaged about 40 seconds, giving a total running time of about 7½ minutes for each problem.

The DANDE code was also applied in the calculation of the High Power Characterizer experiment (HPC) of the Large Core Code Evaluation Working Group (LCCEWG) benchmark problem No. 5 in the FFTF reactor.[100] The core layout for FFTF/HPC is shown in Fig. 35.

The ISOTX nuclear data file, which we have designated as ISOMANA, used in the benchmark calculations was that supplied by F. Mann of Hanford Engineering Development Laboratory, as specified in the benchmark write-up. An additional nuclear data library, supplied by HEDL, contained reaction cross sections used to calculate specified reaction rates. Unfortunately, the HEDL ISOTXS library did not contain data for threshold reactions explicitly--these were lumped in

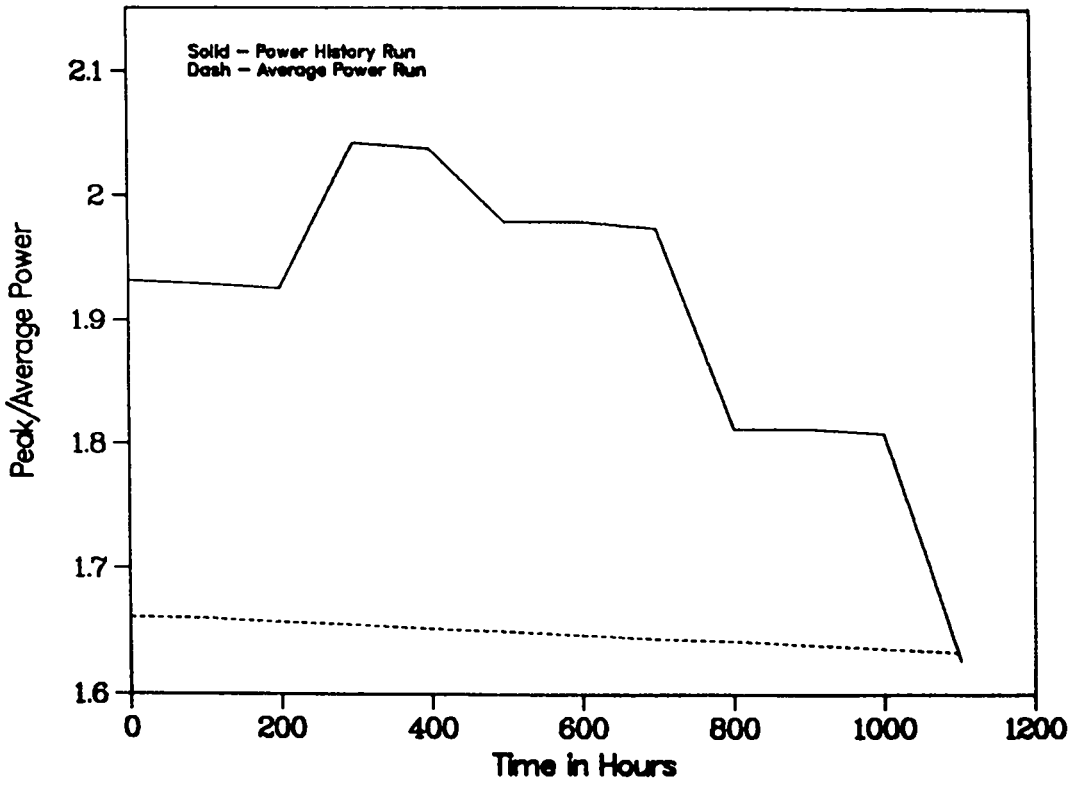

Fig. 34. Effect on peak/average power ratio in Driver-2.

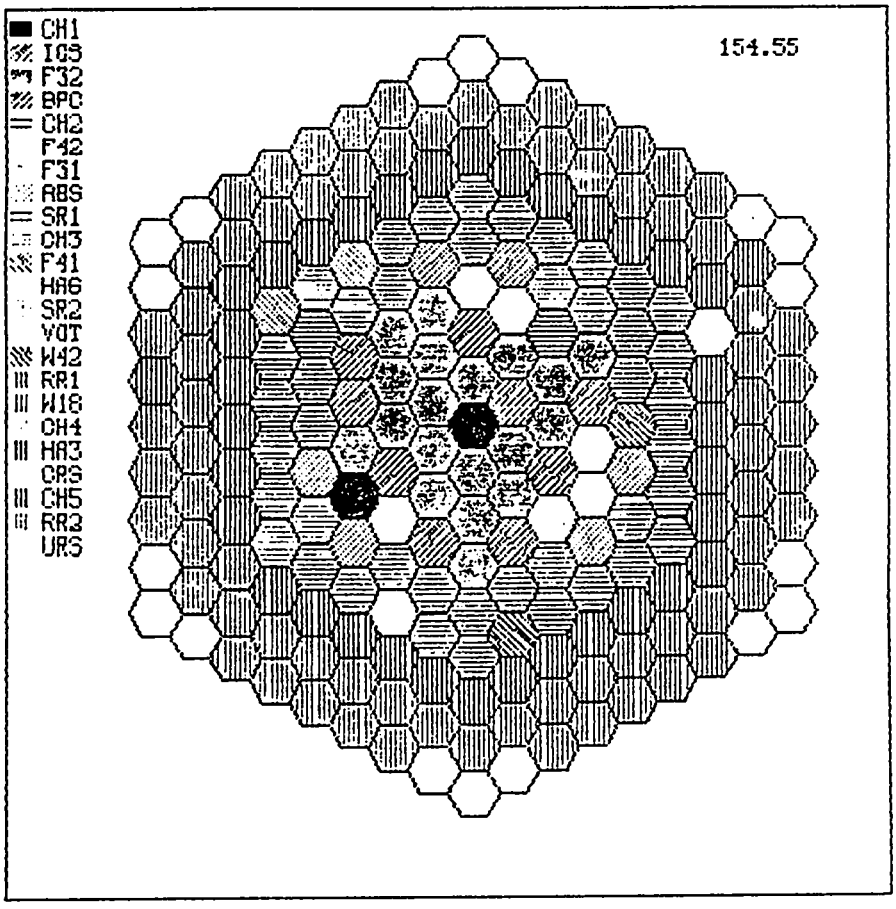

Fig. 35. FFTF/HPC full core plan at Z = 154.55. Control assemblies designated by ABS; safety assemblies by BPC.

an "absorption" cross section--which were required in our depletion module (Fig. 33). As a result, we had to run all depletion leading up to the HPC run using our ISOTXS file (ISO12A).

The depletion calculation consisted of two 10-day runs of all fueled assemblies except the characterizers plus a single 8-day run of all fueled assemblies including the characterizers. The Ring 3 safety rods were banked in the withdrawn position and the Ring 5 control rods were banked at the half-way out position, 19.1" withdrawn, for all runs. The nodal option of DIF3D was used as the core calculational module (Fig. 33) with the full-core, hexagonal-Z model of the FFTF/HPC as input. As stated above, the Los Alamos data library was used for the depletion runs; beginning-of-cycle (BOC) and end-of-cycle (EOC) calculations were repeated using the HEDL ISOTXS file.

The k_{eff} at BOC using ISO12A was 0.98935; at EOC it was 0.98006, a loss of about 1% in k. This is to be compared with 0.98572 and 0.97567, respectively, for runs with ISOMANA. In the depletion calculations using ISO12A, a $\Delta k/k$ loss of 0.0679 was observed after the first 20-day run. Using the HEDL determined value of β_{eff} = 0.00318 for the FFTF gives a value of 10.69¢/day reactivity loss. This compares very favorably with the HEDL reported value of 10.75¢/day. Incidentally, using the number of fissions from the CINDER-3 output and values of $\bar{\nu}_d$ and $\bar{\nu}_t$ derived from ENDF/B-V for the various fissioning nuclides, we determined a value of β = 0.00349.

Also, as stated in the benchmark specifications, the control assembly bank was withdrawn 2.6 cm during the 8-day characterizer run. Our $\Delta k/k$ calculated loss for this period was 0.0026, indicating a rod worth of 1 milli-k/cm; this is the value we calculate for the control assembly bank at mid core.

REFERENCES:

1. P. W. Lisowski, R. E. Brown, J. C. Gursky, S. D. Howe, N. Jarmie, and G. L. Morgan, "Cross Sections for the ^{6}Li(t,n)2α Reaction," Bull Am. Phys. Soc. 29, 748 (1984).

2. G. M. Hale and G. D. Doolen, "Cross Sections and Maxwellian Reaction Rates for Polarized d+d Reactions," Los Alamos National Laboratory report LA-9971-MS (February 1984).

3. H. M. Hofmann and D. Fick, "Fusion of Polarized Deuterons," to be published in Phys. Rev. Lett. (1984).

4. G. M. Hale and P. W. Keaton, "Cross Sections and Reaction Rates for Polarzed Fusion, I. Formalism," G. M. Hale, G. D. Doolen, and D. C. Dodder, "Cross Sections and Reaction Rates for Polarized Fusion, II. Numerical Results for $\vec{d}+\vec{t}$ and $\vec{d}+\vec{d}$," Los Alamos National Laboratory report LA-9971 (February 1984).

5. P. G. Young and E. D. Arthur, "GNASH: A Preequilibrium-Statistical Nuclear Model Code for Calculations of Cross Sections and Emission Spectra," Los Alamos Scientific Laboratory report LA-6947 (November 1977).

6. E. D. Arthur and P. G. Young, "Evaluated Neutron-Induced Cross Sections for ^{54,56}Fe to 40 MeV," Los Alamos Scientific Laboratory report LA-8626-MS (ENDF-304) (December 1980).

7. D. Wilmore and P. E. Hodgson, "The Calculation of Neutron Cross Sections from Optical Potentials," Nucl. Phys. 55, 673 (1964).

8. F. D. Becchetti, Jr., and G. W. Greenlees, "Nucleon-Nucleus Optical Model Parameters," Phys. Rev. 182, 1190 (1969).

9. W. F. McGill, R. F. Carlson, T. H. Short, J. M. Cameron, J. R. Richardson, I. Slaus, W. T. H. van Oers, J. W. Verba, D. J. Margaziotis, and P. Doherty, "Measurements of the Proton Total Reaction Cross Section for Light Nuclei between 20 and 48 MeV," Phys. Rev. C 10, 2237 (1974).

10. P. P. Singh, R. E. Malmin, M. High, and D. W. Devins, "Optical Model Analysis of Alpha-Particle Scattering from ^{24}Mg," Phys. Rev. Lett 23, 1124 (1969).

11. W. Zobel, F. C. Maienschein, J. H. Todd, G. T. Chapman, "Gamma-Rays from Bombardment of Light and Intermediate Weight Nuclei by 16 to 160 MeV Protons and 59 MeV Alpha Particles," Nucl. Sci. Eng. 32, 392 (1968).

12. G. M. Crawley and G. T. Garvey, "Inelastic Scattering in the 2s-1d Shell. II. Odd-A Nuclei," Phys. Rev. 167, 1070 (1968).

13. E. D. Arthur, Comp., "Applied Nuclear Data Research and Development, April 1, 1982-September 30, 1982," Los Alamos National Laboratory report LA-9647-PR (1983).

14. B. B. Back, O. Hansen, H. C. Britt, and J. D. Garrett, "Fission of Doubly Even Actinide Nuclei Induced by Direct Reactions," Phys. Rev. C 9, 1924 (1974).

15. E. D. Arthur, "Use of the Statistical Model for the Calculation of Compound Nucleus Contributions to Inelastic Scattering on Actinide Nuclei," Proc. Specialists Meeting on Fast Neutron Scattering on Actinide Nuclei, Paris, November 23-25, 1981 [NEANDC-158"U" (1982)], p. 145.

16. E. D. Arthur, "Calculation of ^{239}Pu Neutron Inelastic Cross Sections," K. H. Böckhoff, Ed., Proc. Int. Conf. Nucl. Data Sci. Technol., Antwerp, Belgium, September 6-10, 1982 (D. Reidel Publ. Co., Dordrecht), p. 556 (1983).

17. C. L. Dunford, "A Unified Model for Analysis of Compound Nucleus Reactions," Atomics International report AI-AEC-12931 (1970).

18. E. N. Shurshikov, M. F. Filchenkov, Yu. F. Jaboray, A. I. Khovanovich,"Nuclear Data Sheets for A=238," Nuclear Data Sheets 38, 277 (1983).

19. D. K. Olsen, G. L. Morgan, J. W. McConnell, "Measurement of ^{238}U(n,n'γ) Cross Sections," Proc. Int. Conf. Nucl. Cross Sections for Technol., Oct. 22-26, 1979, Knoxville, Tenn. (NBS Special Publication 594, 1980), p. 677.

20. D. W. S. Chan, J. J. Egan, A. Mittler, E. Sheldon, "Analyses of Fast Neutron Inelastic Scattering Cross Sections to Higher (Vibrational) States of ^{232}Th and ^{238}U. 1 Standard Formalism," Phys. Rev. C 26, 841 (1982).

21. Ti-Qun Shao, "Fast Neutron Inelastic Scattering Cross Sections of ^{238}U," Ph.D. Thesis, Univ. of Lowell, Lowell, Mass, 1983 (unpublished).

22. D. G. Madland and P. G. Young, "Neutron-Nucleus Optical Potential for the Actinide Region," Proc. Int. Conf. on Neutron Phys. and Nucl. Data for Reactor and Other Applied Purposes, Harwell, U.K., September 25-29, 1978 (published by the Organization for Economic Cooperation and Development, Paris, France), p. 349.

23. A. Mittler, G. P. Couchell, W. A. Schier, S. Ashar, J. H. Chang, and A. T. Y. Wang, "Neutron Inelastic Scattering Cross Sections of ^{238}U via (n,n'γ)," Proc. Int. Conf. Nucl. Cross Sections for Technol., Oct. 22-26, 1979, Knoxville, Tenn. (NBS Special Publication 594, 1980), p. 680.

24. E. D. Arthur, Comp., "Applied Nuclear Data Research and Development: October 1, 1982-March 31, 1983," Los Alamos National Laboratory report LA-9841-PR (August 1983).

25. L. Mewissen, F. Poortmans, E. Cornelis, G. Vanpraet, A. Angeletti, G. Rohr, H. Weigmann, "Neutron Resonance Parameters for ^{237}Np," Nucl. Sci. Eng. 70, 155 (1979).

26. G. Haouat, J. Lachkar, Ch. Lagrange, J. Jary, J. Sigaud, and Y. Patin, "Neutron Scattering Cross Sections for ^{232}Th, ^{233}U, ^{235}U, ^{238}U, ^{239}Pu, and ^{242}Pu between 0.6 and 3.4 MeV," Nucl. Sci. Eng. 81, 491 (1982).

27. L. W. Weston, "Neutron Capture Cross Section of ^{237}Np," Nucl. Sci. Eng. 79, 184 (1981).

28. H. J. Bak, B. Strohmaier, M. Uhl, "Model Calculations of the ^{237}Np Fission Cross Sections for E_n = 0 to 20 MeV," Journal of the Korean Nucl. Soc. 13, 207 (1981).

29. S. Bjørnholm and J. E. Lynn, "The Double Humped Fission Barrier," Rev. Mod. Physics 52, 725 (1980).

30. H. Derrien, J. P. Doat, E. Fort, D. Lafond, "Evaluation of ^{237}Np Neutron Cross Sections in the Energy Range from 10^{-5} keV to 14 MeV," Cadarache report INDC(FR)-42/2 (1980).

31. E. D. Arthur, Comp., "Applied Nuclear Data Research and Development: April 1, 1983-September 30, 1983," Los Alamos National Laboratory report LA-10069-PR (June 1984).

32. J. W. Meadows, "The Fission Cross Section of ^{237}Np Relative to ^{235}U from 0.1 to 9.4 MeV," Nucl. Sci. Eng. 85, 271 (1983).

33. J. K. Dickens, T. A. Love, and G. L. Morgan, "Gamma-Ray Production due to Neutron Energies Between 2.0 and 20 MeV; Tabulated Differential Cross Sections," Oak Ridge National Laboratory report ORNL-4864 (1973).

34. F. G. Perey, "Optical-Model Analysis of Proton Elastic Scattering in the Range of 9 to 22 MeV," Phys. Rev. 131, 745 (1963).

35. D. L. Lessor and R. E. Schenter, "Neutron Spectra from (α,n) Reactions in Plutonium Compounds Calculated from Hauser-Feshbach Theory," Battelle Pacific Northwest Laboratories report BNWL-B-109 (1971).

36. P. Axel, "Electric Dipole Ground State Transition Width Strength Function," Phys. Rev. 126, 671 (1962).

37. D. M. Brink, "Individual Particle and Collective Aspects of the Nuclear Photo Effect," Nucl. Phys. 4, 215 (1957).

38. F. Ajzenberg-Selove and C. L. Busch, "Energy Levels of Light Nuclei H= 11-12," Nucl. Phys. A 336, 1 (1980).

39. F. Ajzenberg-Selove, "Energy Levels of Light Nuclei A = 13-15," Nucl. Phys. A 360, 1 (1981).

40. G. L. Morgan and E. Newman, "The Au(n,xγ) Reaction Cross Section for Incident Neutron Energies between 0.2 and 20.0 MeV," Oak Ridge National Laboratory report ORNL-TM-4973 (1975).

41. D. M. Hetrick and C. Y. Fu, "GLUCS: A Generalized Least-Squares Program for Updating Cross Section Evaluations with Correlated Data Sets," Oak Ridge National Laboratory report ORNL/TM-7341 (1980).

42. Experimental data provided from the CSISRS compilation by the National Nuclear Data Center, Brookhaven National Laboratory, Upton, N.Y.

43. W. P. Poenitz, J. F. Whalen, and A. B. Smith, "Total Neutron Cross Sections of Heavy Nuclei," Nucl. Sci. Eng. 78, 333 (1981).

44. D. C. Larson, "ORELA Measurements to Meet Fusion Energy Neutron Cross Section Needs," Proc. Symp. Neutron Cross Sections from 10 to 50 MeV, Brookhaven National Laboratory, Upton, N.Y., May 12-14, 1980 (BNL-NCS-51245), V. I, p. 277.

45. D. G. Foster, Jr., and D. W. Glasgow, "Neutron Total Cross Sections, 2.5-15 MeV: I. Experimental," Phys. Rev. C 3, 576 (1971).

46. S. F. Mughabghab, ENDF/B-V Data File for ^{197}Au (MAT 1379), described in BNL-NCS-17541 (ENDF-201), R. Kinsey, Ed., National Nuclear Data Center, Brookhaven National Laboratory, Upton, N. Y. (July 1979).

47. P. Schwandt, H. O. Meyer, W. W. Jacobs, A. D. Bacher, S. E. Vigdor, M. D. Kaitchuck, and T. R. Donoghue, "Analyzing Power of Proton-Nucleus Elastic Scattering between 80 and 180 MeV," Phys. Rev. C 26, 55 (1982).

48. P. Schwandt, "SNOOPY VIII - Optical Potential Model for Elastic Scattering Analysis," Indiana University Cyclotron Facility report no. IUCF 82-3, September 15, 1982.

49. J. Raynal, "Optical-Model and Coupled-Channel Calculations in Nuclear Physics," International Atomic Energy Agency report no. IAEA-SMR-9/8, Vienna, 1972.

50. M. Franey, "RELOM Instructions," University of Minnesota unpublished report, May 1984.

51. R. J. LaBauve and D. G. Madland, "Comparisons of Measured and Calculated Integral Cross Sections for the Thermal Fission of ^{235}U," Trans. Am. Nucl. Soc., 41, 565 (1982).

52. R. J. LaBauve and D. G. Madland, "Comparisons of Thermal Fission Spectrum Representations with Microscopic and Integral Experimental Measurements," Proc. of Conf. on Thermal Reactor Benchmark Calculations, Techniques, Results, and Applications, Brookhaven National Laboratory, EPRI NP-2855, pp. 4.1-4.5 (1983).

53. R. J. LaBauve and D. G. Madland, "Use of Integral Cross-Section Measurements in Evaluating the ^{252}Cf Spontaneous Fission Neutron Spectrum," Trans. Am. Nucl. Soc. 44, 538 (1983).

54. D. G. Madland and J. R. Nix, "New Calculation of Prompt Fission Neutron Spectra and Average Prompt Neutron Multiplicities," Nucl. Sci. Eng. 8, 213 (1982).

55. J. A. Grundl, "A Study of Fission-Neutron Spectra with High Energy Activation Detectors. Part II: Fission Spectra," Nucl. Sci. Eng. 31, 191-206 (1968).

56. D. Abramson and C. Lavelaine, "Comparisons of ^{235}U and ^{239}Pu Fast Neutron Fission Spectra," compiled by J. M. Adams in Proc. of Specialist Meeting on Inelastic Scattering and Fission Neutron Spectra, Harwell, U.K. April 14-16, 1975.

57. E. D. Arthur, P. G. Young, D. G. Madland, and R. E. MacFarlane, "Evaluation of n + ^{239}Pu Nuclear Data for Revision 2 of ENDF/B-V," Los Alamos National Laboratory report LA-9873-MS (ENDF 336) (October 1983).

58. Minutes of the May 12, 1983 meeting of the Cross Section Evaluation Working Group (CSEWG), compiled by S. Pearlstein, National Nuclear Data Center, Brookhaven National Laboratory, Encl. 3, p. 5 (unpublished).

59. W. P. Poenitz and T. Tamura, "Investigation of the Prompt-Neutron Spectrum for Spontaneously-Fissioning ^{252}Cf," Proc. Int. Conf. on Nuclear Data for Science and Technology, Antwerp, Belgium, 1982, Reidel, Dordrecht (1983), p. 465.

60. K. Kobayashi, I. Kimura, and W. Mannhart, "Measurement and Covariance Analysis of Californium-252 Spectrum Averaged Cross Sections," J. Nucl. Sci. and Tech. 19, No. 5, pp. 341-351 (1982).

61. D. G. Madland and J. R. Nix, "Prompt Fission Neutron Spectra and Average Prompt Neutron Multiplicities," presented at the Specialists' Meeting on Yields and Decay Data of Fission Product Nuclides, Brookhaven National Laboratory, Upton, New York, October 24-27, 1983 (proceedings to be published).

62. J. W. Boldeman, D. Culley, and R. J. Cawley, "The Fission Neutron Spectrum from the Spontaneous Fission of ^{252}Cf," Trans. Am. Nucl. Soc., 32, 733 (1979).

63. J. Grundl and C. Eisenhauer, "Fission Rate Measurements for Materials Neutron Dosimetry in Reactor Environments," Proc. of the First ASTM-EURATOM Symposium on Reactor Dosimetry, Petten (Holland), 1975.

64. C. Kalbach and F. M. Mann, "Phenomenology of Continuum Angular Distributions I. Systematics and Parameterization," Phys. Rev. C 23, 112 (1981).

65. R. E. MacFarlane, "TRANSX-CTR: A Code for Interfacing MATXS Cross-Section Libraries to Nuclear Transport Codes for Fusion Systems Analysis," Los Alamos National Laboratory report LA-9863-MS (February 1984).

66. D. W. Muir and R. J. LaBauve, "COVFILS: A 30-Group Covariance Library Based on ENDF/B-V," Los Alamos National Laboratory report LA-8733-MS (ENDF-306) (March 1981).

67. R. E. MacFarlane, D. W. Muir, and R. M. Boicourt, "The NJOY Nuclear Data Processing System, Vol I.: User's Manual," Los Alamos National Laboratory report LA-9303-M (ENDF 324)(May 1982).

68. R. E. MacFarlane, D. W. Muir, and R. M. Boicourt, "The NJOY Nuclear Data Processing System, Vol. II: The NJOY, RECONR, BROADR, HEATR, and THERMR Modules," Los Alamos National Laboratory report LA-9303-M (ENDF 324) (May 1982).

69. P. G. Young and L. Stewart, "Evaluated Data for n+^{9}Be Reactions," Los Alamos Scientific Laboratory report LA-7932-MS (ENDF-283) (July 1979).

70. D. W. Muir, R. E. MacFarlane, and R. M. Boicourt, "Multigroup Processing of ENDF/B Dosimetry Covariances," Proc. 4th ASTM-EURATOM Symp. on Reactor Dosimetry, Gaithersburg, Maryland, March 22-26, 1982, NUREG/CP-0029 (CONF-820321), P. 655 (1982).

71. S. A. W. Gerstl, "SENSIT: A Cross-Section and Design Sensitivity and Uncertainty Analysis Code," Los Alamos National Laboratory report LA-8498-MS (August 1980).

72. Mark J. Embrechts, "SENSIT-2D: A Two-Dimensional Cross-Section Sensitivity and Uncertainty Analysis Code," Los Alamos National Laboratory report LA-9515-MS (October 1982).

73. R. E. MacFarlane, E. D. Arthur, R. B. Kidman, R. J. LaBauve, and D. G. Madland, "Effects of Revisions to the ENDF/B-V ^{239}Pu Evaluation on Fast Critical Assemblies," Trans. Am. Nucl. Soc. 44, 540 (June 1983).

74. "ENDF-202, Cross Section Evaluation Working Group Benchmark Specifications," Brookhaven National Laboratory report BNL-19302 (ENDF-202) (November 1974, with various later revisions).

75. R. B. Kidman, "Los Alamos Benchmarks: Calculations Based on ENDF/B-V Data," Los Alamos National Laboratory report LA-9037-MS (ENDF-318) (November 1981).

76. D. W. Muir, "Analysis of Central Worths and Other Integral Data from the Los Alamos Benchmark Assemblies," Los Alamos National Laboratory report LA-10230-MS (ENDF-340) [to be published (1984)].

77. R. Kinsey, Ed., "ENDF-102, Data Formats and Procedures for the Evaluated Nuclear Data File, ENDF/B-V," Brookhaven National Laboratory report BNL-NCS-50496 (ENDF-102) (revised by B. A. Magurno, November 1983).

78. V. J. Orphan, N. C. Rasmussen, and T. L. Harper, "Line and Continuum Gamma-Ray Yields from Thermal-Neutron Capture in 75 Elements," General Atomic report GA-10248 (July 1970).

79. R. E. MacFarlane, "Energy Balance of ENDF/B-V," Trans. Am. Nucl. Soc. 33, 681 (1979).

80. T. R. England, W. B. Wilson, R. E. Schenter, and F. M. Mann, "ENDF/B-V Summary Data for Fission Products and Actinides," Electric Power Research Institute report NP-3737 (December 1984); Los Alamos document LA-UR-83-1285 (ENDF 332).

81. T. R. England, W. B. Wilson, R. E. Schenter, and F. M. Mann, "Aggregate Delayed Neutron Intensities and Spectra Using Augmented ENDF/B-V Precursor Data," Nucl. Sci. Eng. 62, pp. 139-155 (October 1983).

82. F. M. Mann, M. Schreiber, R. E. Schenter, and T. R. England, "Evaluation of Delayed Neutron Emission Probabilities," Nucl. Sci. Eng. 87, pp. 418-431 (1984).

83. P. G. Young, "Status of Recent Nuclear Model Code Comparisons Organized by the Nuclear Energy Agency Data Bank," Los Alamos informal document LA-UR-84-1046 (to be published in proceedings of the 24th Nuclear Energy Agency Nuclear Data Committee Meeting, Tokai-mura, Japan, March 1984).

84. G. E. Bosler, J. R. Phillips, W. B. Wilson, R. J. LaBauve, and T. R. England, "Production of Actinide Isotopes in Simulated PWR Fuel and Their Influence on Inherent Neutron Emission," Los Alamos National Laboratory report LA-9343 (July 1982).

85. W. B. Wilson, T. R. England, R. J. LaBauve, "Formation and Testing of ENDF/B-V Based Fission-Product and Actinide Data Libraries for CINDER-2," In P. G. Young, Comp., "Applied Nuclear Data Research and Development: July 1-September 30, 1981," Los Alamos National Laboratory report LA-9262-PR (March 1982).

86. T. R. England and W. B. Wilson, "TMI-2 Decay Power: LASL Fission-Product and Actinide Decay Power Calculations for the President's Commission on the Accident at Three Mile Island," Los Alamos Scientific Laboratory report LA-8041-MS (October 1978, Revised March 1980).

87. T. R. England and W. B. Wilson, "TMI-2 Fission-Product Elemental and Isotopic Inventories," Los Alamos National Laboratory report LA-9622 (January 1983).

88. W. B. Wilson, R. J. LaBauve, and T. R. England, "Calculations of Spent Thermal Reactor Fuel Nuclide Inventories and Comparisons with Measurements," in Proceedings: Thermal Reactor Benchmark Calculations, Techniques, Results, and Applications, Electric Power Research Institute Proc. EPRI NP-2855 (February 1983).

89. R. T. Perry and W. B. Wilson, "Neutron Production from (α,n) Reactions and Spontaneous Fission in ThO_2, UO_2, and $(U,PU)O_2$ Fuels," Los Alamos Scientific Laboratory report LA-8869-MS (June 1981).

90. R. L. Walker, "The (α,n) Cross Section of Boron," Phys. Rev. 76, 144 (1949).

91. J. F. Ziegler, Helium Stopping Powers and Ranges in All Elemental Matter, Vol. 4 of The Stopping and Ranges of Ions in Matter series (Pergamon Press, New York, 1977).

92. W. B. Wilson, T. R. England, R. J. LaBauve, "Extended Burnup Calculations for Operating Reactor Reload Reviews," Los Alamos National Laboratory report LA-9563-MS (NUREG/CR-3108) (February 1983).

93. R. D. O'Dell, "Standard Interface Files and Procedures for Reactor Physics Codes, Version II," Los Alamos National Laboratory report LA-6941-MS (September 1977).

94. R. J. Barrett and R. E. MacFarlane, "The MATXS-TRANSX System and the CLAW-IV Nuclear Data Library," Proc. Int. Conference Nuclear Cross Sections for Technology, Oct. 22-26, 1979, Knoxville, Tenn. (NBS Special Publication 594, 1980), p. 213.

95. R. Kinsey, comp., "ENDF-201: ENDF/B Summary Documentation," Brookhaven National Laboratory report BNL-NCS-17541 (ENDF 201), 3rd Ed. (ENDF/B-V) (1979).

96. R. D. Lawrence, "The DIF3D Neutronics Option for Two- and Three-Dimensional Theory Calculations in Hexagonal Geometry," Argonne National Laboratory report ANL-831 (March 1983).

97. Ray E. Alcouffe, Forrest W. Brinkley, Duane R. Marr, R. Douglas O'Dell, "User's Guide for TWODANT: A Code Package for Two-Dimensional, Diffusion-Accelerated, Neutral-Particle Transport," Los Alamos National Laboratory report LA-10049-M, Rev. 1 Manual (October 1984).

98. Wallace F. Walters, Forrest W. Brinkley, Duane R. Marr, "User's Guide for TWOHEX: A Code Package for Two-Dimensional, Neutral-Particle Transport in Equilateral Triangular Meshes," Los Alamos National Laboratory report LA-10258-M Manual (October 1984).

99. W. B. Wilson, T. R. England, R. J. LaBauve, M. E. Battat, D. W. Wessol, and R. T. Perry, "Status of CINDER and ENDF/B-V Based Libraries for Transmutation Calculations," in Proc. Int. Conf. Nuclear Waste Transmutation, July 22-24, 1980, p. 653, The University of Texas at Austin, (March 1981).

100. R. M. Wu, R. B. Rothrock, K. D. Dobbin, and J. A. Rawlins, "The Large Core Code Evaluation Working Group Benchmark Problem 5," Hanford Engineering Development Laboratory (December 1983).

☆ U.S. GOVERNMENT PRINTING OFFICE 1985—576-034/20004

Printed in the United States of America
Available from
National Technical Information Service
US Department of Commerce
5285 Port Royal Road
Springfield, VA 22161
Microfiche (A01)

Page Range	NTIS Price Code	Page Range	NTIS Price Code	Page Range	NTIS Price Code	Page Range	NTIS Price Code
001-025	A02	151-175	A08	301-325	A14	451-475	A20
026-050	A03	176-200	A09	326-350	A15	476-500	A21
051-075	A04	201-225	A10	351-375	A16	501-525	A22
076-100	A05	226-250	A11	376-400	A17	526-550	A23
101-125	A06	251-275	A12	401-425	A18	551-575	A24
126-150	A07	276-300	A13	426-450	A19	576-600	A25
						601-up	A99

*Contact NTIS for a price quote.

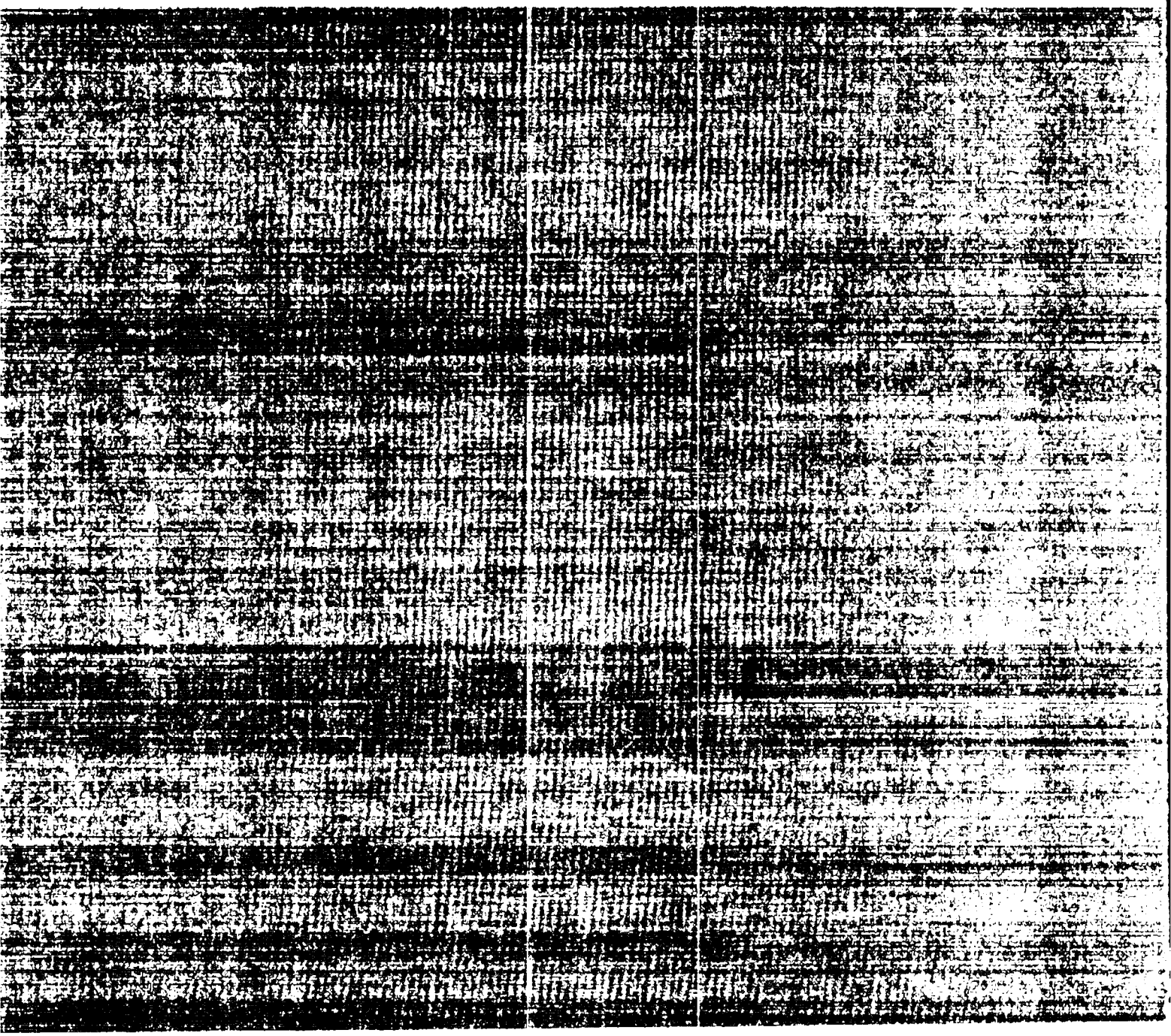

Los Alamos